Study of the bubble behavior in alkaline water electrolysis

Hoedemakers, Inge M.E.

Award date:
2021

EINDHOVEN UNIVERSITY OF TECHNOLOGY

Department of Chemical Engineering
Sustainable Process Technology Research Group

Study of the bubble behavior in alkaline water electrolysis

MSc Thesis

Inge Hoedemakers

Date: 11-12-2020
Graduation supervisor: prof. dr. ir. J. van der Schaaf
External committee member: dr. ir. K. Buist
Daily supervisor: PDEng. ir. R. Lira Garcia Barros
Committee Member: dr. ir. M.T. de Groot

Abstract

Hydrogen is used in many chemical industries like the ammonia and methanol production. Hydrogen can be produced in a sustainable way through alkaline water electrolysis. In this process an electrochemical cell is filled with electrolyte (KOH) and direct current is applied so that hydrogen and oxygen are produced. To reduce the Ohmic resistance, it is important to understand the bubble behavior in the electrochemicel cell. Therefore, this project aims to visualize and analyze the bubble size distribution of the corresponding gas volume in the outlet of the electrochemical cell and find a correlation between the bubble size distribution and process variables, i.e. current density, temperature, electrolyte concentration and superficial inlet velocity.

To reach this goal the bubbles at the outlet of the (zero-gap) electrochemical cell (with a round hole staggered perforated Nickel plates as electrodes) are visualized using a photographic method. Therefore it is possible to measure and quantify bubbles bigger than a bubble diameter of $120\mu m$ with a MATLAB script. By analysing different pictures the bubble size distribution is obtained. To determine the effect of the process conditions on the bubble size distribution experiments are carried out at different conditions, namely 30 to 200 $\frac{A}{m^2}$, 20 and 50 °C, 5 and 20 wt% and at no flow and at 0.048 $\frac{m}{s}$ superficial inlet velocity.

A bimodal distribution is found at a current density of $50\frac{A}{m^2}$ with one peak in gas volume of bubbles with a diameter between 120 and $200\mu m$ and one peak in gas volume of bubbles with a diameter between 200 and $400\mu m$. The bubbles of the latter peak are caused by the electrode geometry (perforated plate) in a zero-gap configuration. Furthermore, at an increase in current density, the number of bubbles with a smaller diameter than $200\mu m$ increases, especially for the 20 wt% KOH which becomes a unimodal distribution at current densities higher than $70\frac{A}{m^2}$. It is recommended to find a visualisation technique with a higher resolution so that the bubbles smaller than a bubble diameter of $120\mu m$ can be detected, which gives more inside in bubble behavior of the smaller bubbles and the size of the gas-liquid separator.

Contents

1 | Introduction

Hydrogen is being used in many chemical industries such as the ammonia and methanol production [1]. Furthermore, hydrogen is one of the most promising energy carriers for the future [2]. Therefore, hydrogen is also used for energy storage and, for example, this energy can be used as fuel for car engines. Currently, most hydrogen is produced from fossil fuels, because the production costs by using fossil fuels are much lower than alternatives [3]. However, a disadvantage of using fossil fuel is the large amount of CO_2 which is simultaneously produced. Moreover, fossil fuel is not renewable. An alternative to produce hydrogen in a more sustainable way is the alkaline water electrolysis process (see Figure 1.1). In this process the electrochemical cell is filled with electrolyte (mainly diluted KOH or NaOH [4]) and direct current is applied to produce hydrogen and oxygen. This direct current can be obtained from a sustainable energy source like wind turbines or solar panels [5]. However, to compete with the fossil fuel, the efficiency of 25% has to be increased [3].

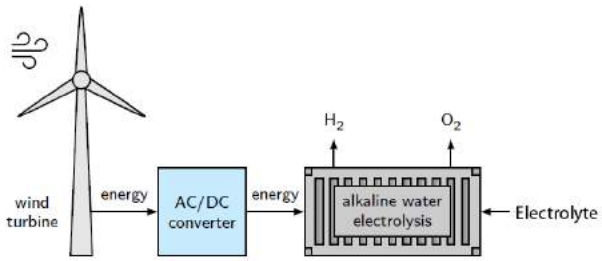

Figure 1.1: *Schematic drawing of the alkaline water electrolysis process powered by a wind turbine [6].*

1.1 Process design

A schematic drawing of the alkaline water electrolysis process is shown in Figure 1.2. In the electrochemical cell the conversion of water into hydrogen and oxygen takes place. When the electrolyte is supersaturated with hydrogen or oxygen, gas bubbles are formed which need to be separated via a gas-liquid separator. Therefore, the gas-liquid mixtures leave the electrochemical cell at the top via the outlet device and are transported via a tube to the gas-liquid separators. The gas leaves at the top of the gas-liquid separator and at the bottom the electrolyte is recirculated by the pump to the electrochemical cell. The design of the gas-liquid separator is dependent on the bubble size distribution.

For a better understanding of this research, the design of the electrochemical cell is explained in more detail. When the electrolyte enters the electrochemical cell the electrolyte will be equally distributed over the electrodes via an inlet device. The electrochemical reactions take place at the electrodes. To enhance the conductivity, diluted KOH is used as electrolyte since the conductivity of KOH is higher than the conductivity of NaOH [6]. Hydrogen is formed (see Equation 1.1), while oxygen is formed at the anode (see Equation 1.2). This results in an overall conversion of 2 mol water into 1 mol oxygen and 2 mol hydrogen (see Equation 1.3) [6].

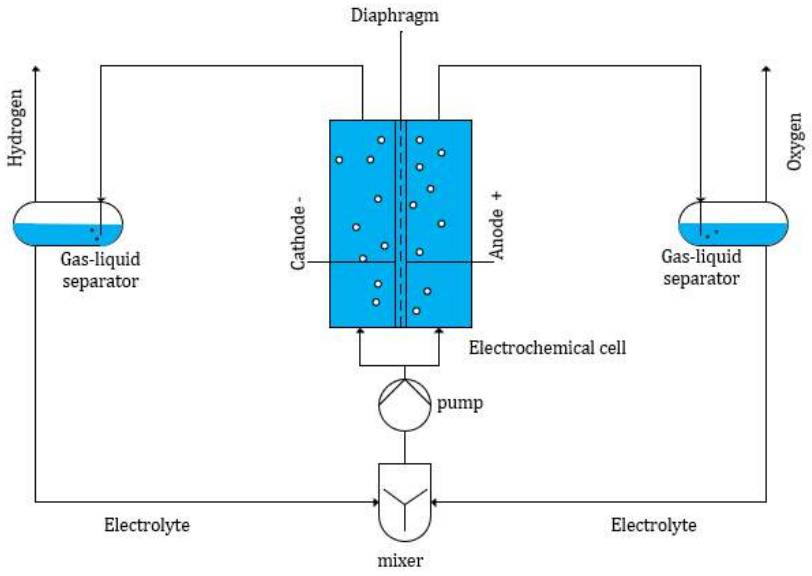

Figure 1.2: *Schematic drawing of the alkaline water electrolysis process.*

$$Cathode : 4H_2O(l) + 4e^- \rightarrow 2H_2(g) + 4OH^-(aq) \tag{1.1}$$

$$Anode : 4OH^-(aq) \rightarrow O_2(g) + 2H_2O(l) + 4e^- \tag{1.2}$$

$$Overall : 2H_2O(l) \rightarrow O_2(g) + 2H_2(g) \tag{1.3}$$

The electrodes are separated by a diaphragm to prevent the formation of the highly flammable mixture of oxygen and hydrogen [7]. Because of safety reasons only 2 mol % H_2 may be present in the $electrolyte - O_2$ mixture [8, 9].

To run these reactions, power has to be supplied to the electrodes. To make sure that the gas production is constant, a constant current is set and the required voltages are dependent on the resistance in the system. To have a high efficiency, the resistance of the system has to be as low as possible. The conventional and the zero gap assembly are two different cell designs (see Figure 1.3) [6]. In the conventional design the Ohmic resistance is dependent on the electrode resistance, the electrolyte resistance and the diaphragm resistance, while in the zero-gap the electrodes are pressed to the diaphragm which reduces the electrolyte resistance. So the zero-gap configuration is the most promising to increase the efficiency.

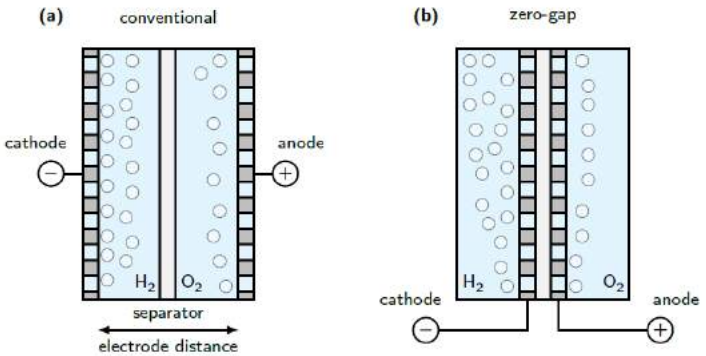

Figure 1.3: *Conventional and the zero-gap configuration in the electrochemical cell designs [6]. In the conventional configuration the ions flow through the electrolyte-gas mixture and the diaphragm, while in the zero-gap configuration the ions flows only through the diaphragm.*

An electrode could be made of different materials like noble metals or nickel. Nickel is good corrosion resistant and is not that expensive compared to noble metals [10]. Therefore, nickel based electrodes are currently used in the alkaline water electrolysis [11, 12]. In a zero gap configuration the electrode needs an open space to make it possible that the evolved gas bubbles can be removed from the electrolysis gap [4]. In industrial electrolysis a perforated plate is most often used as electrodes [13]. The size of the hole of the perforated plate has to be larger than the average gas bubble diameter to prevent gas clogging [14].

1.2 Bubble behavior in alkaline water electrolysis

The bubble behavior in the electrochemical cell affects the energy efficiency of the process [15]. By the presence of a non-conductive gas bubble in between the electrodes, the resistance increases. To reduce this effect, it is important to understand the bubble behavior in the electrochemical cell.

In literature, the bubble size distributions have already been determined at different process conditions [7, 16, 17]. The alkaline water electrolysis process normally operates in the industry at a temperature between 50 and $80°C$, a concentration about $30wt\%$, a liquid superficial velocity about $1\ \frac{mm}{s}$ and a current density about $2000\frac{A}{m^2}$ [4]. In Table 1.1 an overview of the measured bubble sizes are shown with their corresponding conditions. Janssen et al. [17] and Zhang et al. [16] measured the average bubble size and the maximum bubble size respectively, in a conventional assembly. In the conventional assembly the Ohmic resistance is dependent on the electrode resistance, the electrolyte resistance and the diaphragm resistance, while in the zero-gap the electrodes are pressed to the diaphragm which reduces the electrolyte resistance [6]. Therefore, Haug et al. have measured the average bubble diameter in the zero-gap configuration [7].

Based on these measurements it is found that:

- At current densities above $300\frac{A}{m^2}$, the average bubble size decreases at an increasing current density. At current densities below $< 300\frac{A}{m^2}$, the bubble size increases at a increase in current density.
- At an increase in concentration the bubble size decreases.
- At an increasing temperature the bubble diameter seems to increase.
- By increasing the liquid superficial velocity, the bubble diameter decreases according to Janssen et al., while Haug et al. did not measure any difference.
- The effect of the type of gas seems to be unclear. Since Zhang et al. measured almost no difference between the hydrogen and oxygen bubbles, Janssen et al. measured bigger oxygen bubbles compared to the hydrogen bubbles and Haug et al. measured smaller oxygen bubbles compared to the hydrogen bubbles.

Moreover, Janssen et al. state that oxygen bubbles coalesce more easy than hydrogen bubbles. This should lead to less fluctuation in hydrogen bubble size compared to the oxygen bubble size [17]. Furthermore, the solubility of gas decreases as the temperature increases and as the KOH concentration increases [7].

Table 1.1: Literature based bubble size distributions with their corresponding conditions [7, 16, 17].

Parameters	Concentration	Temperature	Velocity	Current density	Bubble diameter		Assembly electrode	Electrode type
					H2	O2		
source \units	*wt%*	*°C*	$\frac{mm}{s}$	$\frac{A}{m^2}$	μm	μm		
Zhang et al.	2.8	22	0	3	590	600	Conventional	Nickel plate
				6	1090	1080		
	2.8	22	0	6	1080	-	Conventional	Nickel plate
	5.4				500	-		
	10.3				360	-		
	19.1				240	-		
Janssen et al.	5.4	30	0	500	52	64	Conventional	Nickel plate
				1000	30	56		
				2000	-	42		
	5.4	30	300	500	34	42	Conventional	Nickel plate
				1000	24	58		
				2000	11.8	54		
	5.4	30	0	2000	-	34	Conventional	Nickel plate
		60			-	36		
		80			-	38		
	0.6	30	0	2000	45.4	60.6	Conventional	Nickel plate
	5.4				18.2	25.6		
	10.3				21.2	27.2		
	23.1				20.4	15		
Haug et al.	28.6	80	1	100	200	100	Zero-gap	Nickel mesh
				300	200	100		
				2000	115	100		
	28.6	80	3	100	170	100	Zero-gap	Nickel mesh
				300	210	100		
				2000	115	100		

1.3 Scope and outline of the thesis

All measured sizes of bubbles are measured in a bubble diameter ranging from 38 to $1080\mu m$. However, besides the process conditions the bubble size seems to be dependent on the cell assembly. Therefore, in this research the bubble size distributions,additional to the research of Haug et al., the temperature and concentration effect are determined in a zero-gap configuration.

Moreover, since the bubble size distribution is not yet well known, in literature there are almost no studies of a design of a gas-liquid separator. Therefore, based on the found bubble size distribution in this research, the design of the gas-liquid separator is determined. Since the KOH concentration reduces the coalescence [18], it is assumed that the bubble size distribution could be determined at the outlet of the electrochemical cell.

This leads to the following project goals:

- Visualize and determine the bubble size distribution at the outlet of the (zero-gap) electrochemical cell.
- Correlate the bubble size distribution to current density at different temperatures, KOH concentrations and liquid superficial velocities.
- Determine the size of the gas-liquid separator dependent on the bubble size distribution at the outlet of the electrochemical cell.

The remainder of this study is organized as follows: Chapter 2 presents the theory about the bubble generation in electrolysis, the bubble rising velocity and the design of the gas-liquid separator are explained. Moreover, the bubble detachment radius of the electrode surface, the rising velocity and the design of the gas-liquid separator are predicted based on literature. In Chapter 3 the methodology of visualizing and detecting the bubble size distribution is explained. More over the experiments are explained to evaluate the assumption for designing the gas-liquid separator. In Chapter 4 the results are shown and discussed. Finally Chapter (Chapter 5) summarized the main conclusions of this research and it provides suggestions for future research.

2 | Theory

In this chapter a theory is provided that presents the bubble behavior in the electrochemical cell and design of the gas-liquid separator. In Section 2.1 theories of bubble detachment on a vertical electrode are described. Moreover, the sizes of detached bubbles are predicted. In Section 2.2 the steady state rising velocity are described and predicted. In Section 2.3 the theory of designing a gas-liquid separator is explained.

2.1 Bubble generation in electrolysis

To understand the bubble size distribution at the outlet of the electrochemical cell, it is important to understand the behavior of bubble detachment (see Section 2.1.1). When this is explained the bubble sizes are predicted (see Section 2.1.2).

2.1.1 General bubble formation and detachment principle

The formation of gas bubbles on the electrode can be explained in three different phases: the nucleation phase, growth phase and detachment phase (see Figure 2.1) [16]. In the alkaline water electrolysis process the produced gas dissolves in the electrolyte close by the electrode if the electrolyte is not totally saturated with gas. The dissolved gas is transported to the bulk electrolyte by mass diffusion and convection [15]. In the case that the electrolyte close by the electrode is supersaturated, bubbles start nucleating at the electrode surface. When a bubble is nucleated, the bubble can grow by diffusion of dissolved gas or by coalescence.

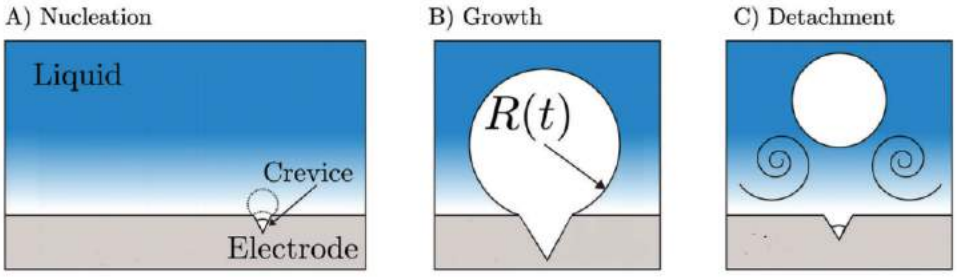

Figure 2.1: *Different phases of bubble formation at the (horizontal) electrode [19]. (a) Nucleation: the gas formation dissolves in the electrolyte until the electrolyte is supersaturated. At a supersaturated electrolyte, the bubble start nucleating. (b) Bubble grow: a bubble grows due to coalescence or by diffusion of dissolved gas. (c) Detachment: When the forces balance acting on a bubble is unequal to zero, the bubble will detach.*

However, the bubble size at the outlet of the electrochemical cell is dependent on the bubble detachment from the electrode. In Figure 2.2a a bubble attached to a vertical electrode is shown. The flow is in the x-direction. In Figure 2.2b the main forces which are applied to the bubble are shown. A bubble

can detach or lift when the sum of forces in the x-direction or in the y-direction is unequal to zero [16]. When a bubble is lifted, the advancing angle (α) and the receding angle (β) change (see Figure 2.2c). The advancing angle increases, while the receding angle decreases when a bubble detaches. These angles could be calculated as follows:

$$\alpha = \theta + \theta' \tag{2.1}$$

$$\beta = \theta - \theta' \tag{2.2}$$

Where (θ) is the contact angle in $[rad]$ and θ' is the deviation of the contact angle in $[rad]$.

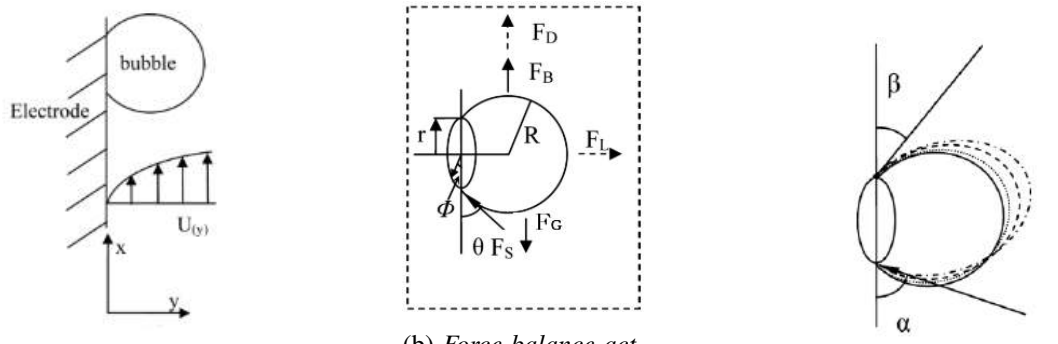

(a) *Bubble attached to electrode surface with liquid flow in the x-direction*

(b) *Force balance acting on a attached bubble in no flow and flow condition.*

(c) *Advancing and receding angle*

Figure 2.2: *Bubble detachment of a bubble from the electrode surface [16].*

For the estimation of the bubble size of a detached bubble it is assumed that the bubble detaches due to the fact that the sum of forces in the x-direction is unequal to zero [16]. Therefore, the forces which are acting in the x-direction are explained in more detail. Moreover, the theory consider the bubble detachment behavior in a conventional assembly of the electrochemical cell.

- *Gravitational force*
  The gravity force (F_g) pulls the bubble down. The force is equal to gravity acceleration (g) in $[\frac{m}{s^2}]$ multiplied by the mass of the gas bubble (m_b) in $[kg]$. Since the bubble is a truncated sphere, the mass of the bubble can be calculated by the volume of the bubble, with a bubble radius (R) in $[m]$ and the density of the gas (ρ_g) in $[\frac{kg}{m^3}]$. The formula of the gravitational force is shown in Equation 2.3 [20].

$$F_g = m_b g = \frac{4}{3}\pi R^3 \frac{(1 + cos\theta)^2(2 - cos\theta)}{4}\rho_g g \tag{2.3}$$

- *Buoyancy force*
  The buoyancy force works in the opposite direction as the gravitational force. As shown in Equation 2.4, the buoyant force is the gravity acceleration multiplied by the mass of displaced liquid (m_l) in $[kg]$ [21]. Since the bubble is a truncated sphere, the mass of the displaced liquid can be calculated by the volume of the bubble and the density of the liquid (ρ_l) in $[\frac{kg}{m^3}]$ [20].

$$F_b = m_l g = \frac{4}{3}\pi R^3 \frac{(1 + cos\theta)^2(2 - cos\theta)}{4}\rho_l g \tag{2.4}$$

- *Tension force*
  The tension force is the contact area multiplied by the surface tension, the sinus of the advancing and receding angle and a correction factor. In Figure 2.2b it is shown that the force acts in the x- and y-direction. The equation in the x-direction is shown in Equation 2.5 [22].

$$F_{s,x} = 2r\sigma_{sur}\frac{\pi(\alpha-\beta)}{\pi^2-(\alpha-\beta)^2}(sin\alpha + sin\beta) \tag{2.5}$$

  Where r is the circular contact radius of the bubble with the electrode in $[m]$, σ_{sur} is the surface tension between the electrolyte and the gas in $[\frac{N}{m}]$. This force is among others dependent on the temperature and concentration due to the change in surface tension [16]. The circular contact radius of the bubble is estimated as follow [16, 23]:

$$r = Rsin\theta \tag{2.6}$$

- *Drag force*
  The drag force works in the opposite direction of the relative velocity of the bubble. So this force is only present when there is a liquid flow present or when the bubble is moving. The force is equal to the friction factor multiplied by the area of the bubble, half of the liquid density and the square of the relative velocity. In Equation 2.7 the definition of the drag force is shown.

$$F_d = \frac{1}{2}\pi R^2(1-\frac{(\theta - cos\alpha sin\theta)}{\pi})\rho_l v_l^2 f \tag{2.7}$$

  Where f is the friction factor. This friction factor is dependent on the flow regime as shown in Figure 2.3.

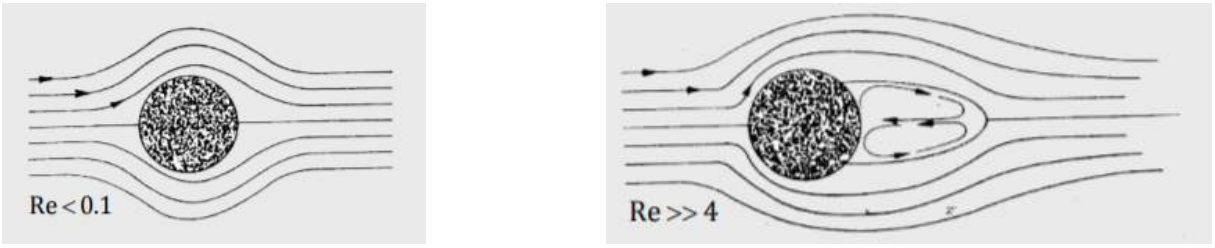

(a) Low Reynolds number (b) High Reynolds number

Figure 2.3: *Flow regime around a spherical shape. At a Reynolds number higher than 4 the friction factor will be lower due to the eddy motion in the wake of a sphere. [24]*

At flows with a high Reynolds number ($Re >> 4$) eddy motion is present behind the spherical bubble, which decreases the friction factor. Therefore, the dimensionless Reynolds number is important to calculate. The Reynolds number is defined in Equation 2.8, where v_l is the average liquid velocity in $[\frac{m}{s}]$, μ_l is the viscosity of liquid in $[Pas]$ and d_{cell} is the depth of the electrochemical cell in $[m]$.

$$Re = \frac{\rho_l v_l d_{cell}}{\mu_l} \tag{2.8}$$

For a Re < 0.1 the Stokes law is valid and the friction factor can be estimated by $\frac{24}{Re}$. At a Reynolds number of 1 a force is predicted about 10% too low due to the Stokes law [21]. For a Reynolds number above 1 a significant unsteady eddy motion in the wake of a sphere is present which is shown in Figure 2.3. Therefore, for Reynolds numbers of 1 up to 6000 the correlation for the friction is shown in equation 2.9. At a Reynolds number between $5x10^2$ and 10^5 a friction value

of 0.44 is valid.

$$f = (\sqrt{\frac{24}{Re}} + 0.5407)^2 \tag{2.9}$$

By solving the force balance for a no flow condition (see Equation 2.10) the bubble detachment radius could be estimated by equation 2.11.

$$0 = -F_g + F_b - F_s \tag{2.10}$$

$$R = \sqrt{\frac{6sin(\theta)\sigma_{sur}\frac{(\alpha-\beta)}{\pi^2-(\alpha-\beta)^2}(sin(\alpha)+sin(\beta))}{(1+cos(\theta)^2(2-cos(\theta))g(\rho_l-\rho_g)}} \tag{2.11}$$

With presence of flow, the Fd also becomes an important force. The receding and advancing angle are assumed to be equal to a no flow condition. By solving the force balance (see Equation 2.12) the bubble size of a bubble which will be detected soon in the future can be estimated by equation 2.13.

$$0 = -F_g + F_b - F_s + F_d \tag{2.12}$$

$$\begin{aligned} R &= \frac{-b + -\sqrt{(b^2-4ac)}}{2a} \\ &Where \\ a &= \frac{4}{3}\pi\frac{(1+cos\theta)^2(2-cos\theta)}{4}(\rho_l-\rho_b)g \\ b &= \frac{1}{2}\pi(1-\frac{(\theta-cos\alpha sin\theta)}{\pi})\rho_l v_l^2 f \\ c &= -2sin\theta\sigma_{sur}\frac{\pi(\alpha-\beta)}{\pi^2+(\alpha-\beta)^2}(sin\alpha+sin\beta) \end{aligned} \tag{2.13}$$

2.1.2 Prediction bubble detachment principle in alkaline water electrolysis

In this research the influences of current density, temperature, concentration, superficial inlet velocity and gas type are investigated for a zero-gap configuration. In this section the bubble sizes are predicted by assuming that the behavior of the bubbles at a zero-gap configuration is equal to the behavior at a conventional configuration. For predicting the bubble detachment radius contact angle, the surface tension and the deviation of the contact angle are found in literature (see Table 2.1).

Table 2.1: *Assumed values for estimation of the bubble detachment [16].*

	θ [°]	θ' [°]	σ [$\frac{N}{m}$]
5wt% O_2	50	4	0.0785
5wt% H_2	43	4	0.0785
20wt% O_2	50	1.5	0.0864
20wt% H_2	43	1.5	0.0864

The surface tension is dependent on the KOH concentration and temperature. In literature the temperature effect on the surface tension for the electrolyte is not known, therefore the bubble size at higher

temperatures could not be estimated. However, for pure water the surface tension decreases at a higher temperature [25]. This same behavior is expected for the electrolyte solution. A higher surface tension should lead to a decrease in bubble size.

The contact angle of a bubble at a vertical nickel plate is not known in literature. For a Platinum electrode the average contact angle for hydrogen and oxygen is respectively 43 and 50 ° [26]. Therefore, in the calculation of the bubble size it is assumed that the angles are the same for a Nickel electrode.

The advancing and receding angle could differ max 10 °of the average contact angle [27]. Zhang et al. assumed these value condition based on earlier research. Based on the literature the expected average bubbles sizes are estimated. Since the contact angle is not sure, in Figure 2.4 the contact angle is varied which results in different bubble detachment radius.

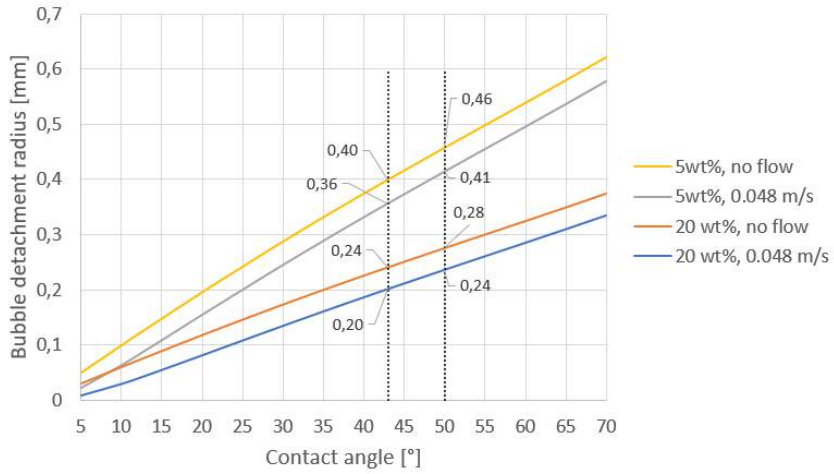

Figure 2.4: *The influence of the contact angle on the bubble detachment radius. According to literature the contact angle is equal to 43 and 50 °for hydrogen and oxygen respectively.*

In Figure 2.5 the force balance is shown for the hydrogen bubbles at flow condition. It is shown that the gravitational force has almost no influence.

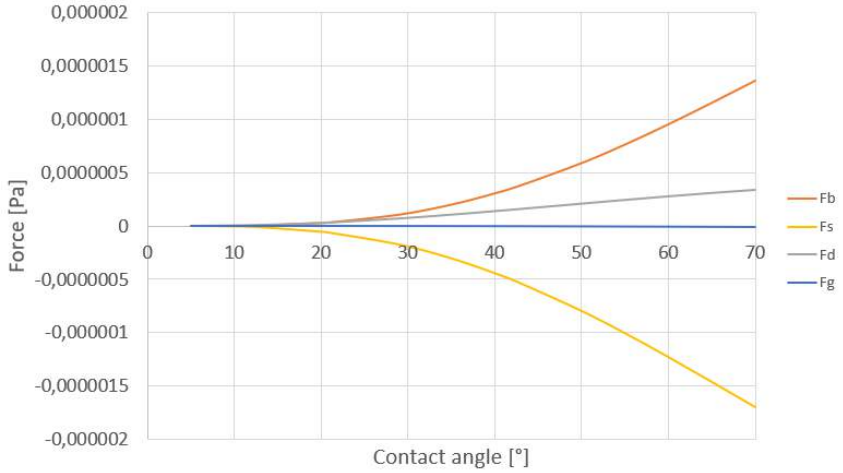

Figure 2.5: *The influence of the deviation of the contact angle on the force balance for the bubble detachment of the hydrogen bubbles at flow condition.*

2.2 Bubble rising velocity

In Section 2.2.1 the theory is explained of the bubble rising velocity. In Section 2.2.2 the expected bubble rising velocity is determined.

2.2.1 General bubble rising velocity

When a bubble detaches from the electrode, the bubble accelerates until the bubble reach a steady state bubble rising velocity. The steady state bubble rising velocity is important to determine the design of the gas-liquid separator. Big bubbles cause high rising velocity and as a result of this the gas-liquid separator can be designed smaller. To understand the bubble rising velocity a balance of forces is set-up as shown in Figure 2.6, where d_b is the bubble diameter in $[m]$. Only three forces are taken into account to calculate the steady state bubble rising velocity. During the steady state rising velocity state, there is no acceleration anymore, so the total sum of forces (F_g, F_b and F_d) is equal to zero. These forces are already explained in Section 2.1.1.

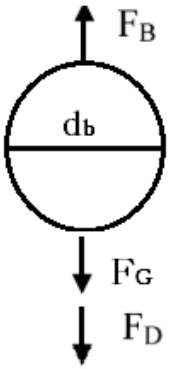

Figure 2.6: *Forces acting on a gas bubble.*

The shape of the bubble is important in order to determine the motion of the bubbles [28]. The shape could be considered based on the Grace Diagram [28], which is available in Appendix A and visualized by the camera. In this calculation it is assumed that bubbles are spherical. Since the bubbles are spherical, the forces are shown in Equation 2.14, 2.15 and 2.16.

$$F_g = m_b g = \frac{1}{6}\pi d_b^3 g \rho_g \tag{2.14}$$

$$F_b = m_l g = \frac{1}{6}\pi d_b^3 g \rho_l \tag{2.15}$$

$$F_d = \frac{1}{4}\pi d_b^2 \frac{1}{2}\rho_l v_{rel}^2 f \tag{2.16}$$

The determination of the friction factor (f) can be found in Section 2.1.1. The Reynolds number is defined in Equation 2.17, where v_{rel} is the relative velocity of the bubble in $[\frac{m}{s}]$ and μ_l is the viscosity of liquid in $[Pas]$.

$$Re = \frac{\rho_l v_{rel} d_b}{\mu_l} \tag{2.17}$$

Combining these three forces (Equation 2.18) leads to the formula of the relative rising velocity given in Equation 2.19.

$$F_{total} = F_b - F_g - F_d \tag{2.18}$$

$$v_{rel} = \sqrt{\frac{4d_b g(\rho_l - \rho_g)}{3f\rho_l}} \tag{2.19}$$

2.2.2 Prediction bubble rising velocity in alkaline water electrolysis

Based on the properties of the gas and liquid the relative bubble rising velocity is predicted (see Figure 2.7). The influence of the gas type and the temperature on the rising velocity are neglectable. Moreover, since it is assumed that there is no bubble interaction, the effect of current density is also not taken into account. It is found that a higher concentration KOH results in a higher rising velocity.

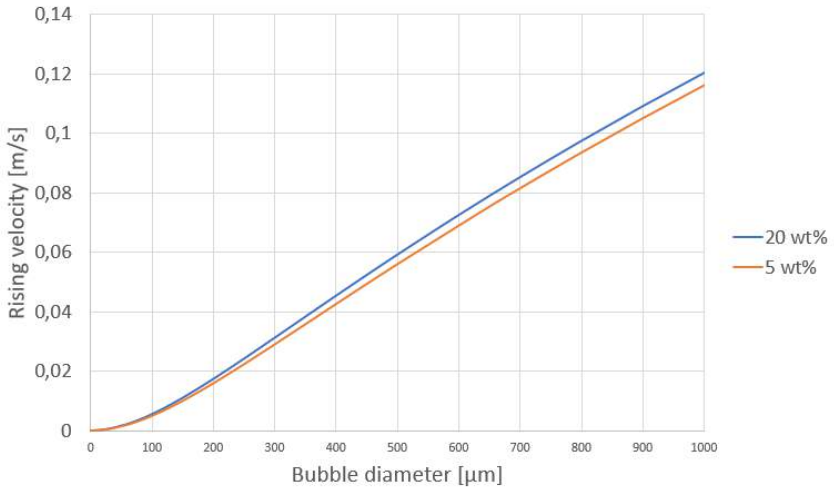

Figure 2.7: *The relative bubble rising velocity dependent on the bubble diameter at 5wt% and 20 wt%.*

2.3 Design gas-liquid separator

At atmospherical condition the separator is most often designed horizontally or vertically [29, 30]. In this section the sizing of a horizontal and vertical gas-liquid separator is discussed.

2.3.1 Sizing horizontal separator

In Figure 2.8 a schematic drawing of a horizontal gas-liquid separator is shown. The gas-electrolyte mixture enters the gas-liquid separator in the liquid part. Here, the gas bubbles rise with a rising velocity to the surface and leave the separator at the top. The electrolyte leaves at the bottom of the gas-liquid separator. It is important that the residence time of the liquid is long enough so that the bubble can rise to the surface before the liquid leaves the separator.

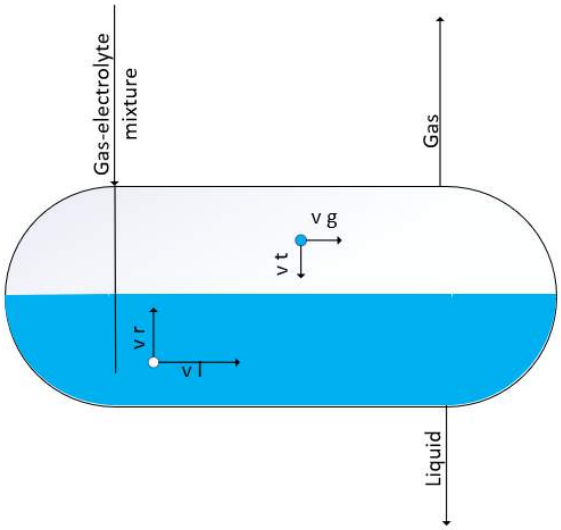

Figure 2.8: *A schematic drawing of the horizontal gas-liquid separator. The gas-electrolyte mixture enters the gas-liquid separator in the liquid. The gas bubbles rise to the gas-phase and leave at the top, while the electrolyte leaves at the bottom.*

The bubble rising velocity can be calculated with Equation 2.19. This equation is explained in detail in Paragraph 2.2. The calculation of the minimum necessary liquid residence time ($\tau_{l,necessary}$) in $[s]$ is shown in Formula 2.20.

$$\tau_l, necessary = \frac{h^* D}{v_r} \tag{2.20}$$

Where the maximum rising distance of gas bubbles is the relative liquid height (h^*) multiplied by the diameter of the separator D in $[m]$. Furthermore, for the bubble rising velocity the diameter of the smallest bubble has to be determined.

The actual residence time of the liquid ($\tau_{l,actual}$) in $[s]$ can be estimated by the volumetric liquid flow (Q_l) in $[\frac{m^3}{s}]$, the flow area of liquid A_l in $[m^2]$ and the length of the separator L in $[m]$ as shown in Formula 2.21.

$$\tau_l, actual = \frac{L}{v_l} = \frac{L}{\frac{Q_l}{A_l}} = \frac{L}{\frac{Q_l}{\frac{\pi D^2}{4} A^*}} \tag{2.21}$$

For the volumetric liquid flow it is assumed that this does not change and is equal to the inlet volumetric liquid flow. The liquid area is calculated by multiplying the total flow area (A_{ves}) in $[m^2]$ by the relative

liquid area (A^*). The relative liquid area is derived from the relative liquid height ($h*$). This is explained in Figure 2.9.

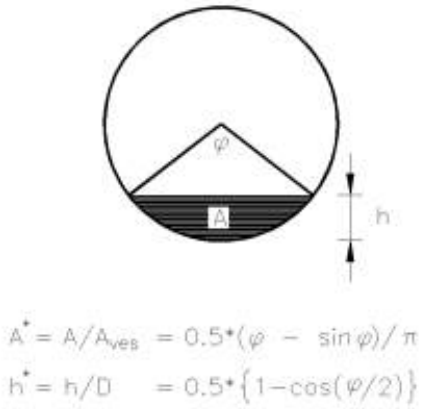

Figure 2.9: *Correlation relative height and relative liquid area [31].*

In Figure 2.9 the liquid height(h) is in [m] and ϕ is the angle [$^\circ$].

The minimum size of the gas-liquid separator can be found when the necessary residence time is equal to the actual residence time. However, when a bubble reaches the liquid surface, it breaks the liquid film and it forms jet droplets as shown in Figure 2.10. In this way some liquid droplets go into the gas phase and fall back in the liquid phase. However, below, the phenomenon is explained.

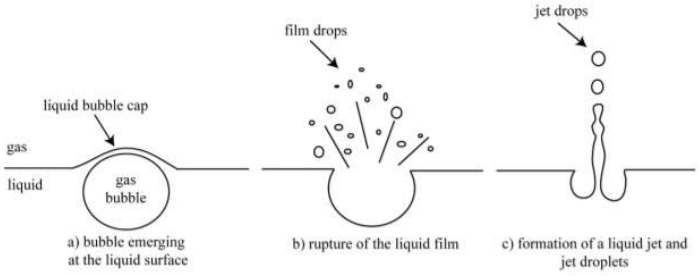

Figure 2.10: *Bursting gas bubble at the surface area [32].*

To remove the liquid droplets from the gas phase, the residence time of the gas has to be long enough so that the liquid droplets settle again. The necessary residence time ($\tau_{g,necessary}$) in [s] and the actual residence time ($\tau_{g,actual}$) in [s] can be estimated by Formula 2.22 and 2.23.

$$\tau_{g,necessary} = \frac{h^* D}{v_t} \tag{2.22}$$

$$\tau_{g,actual} = \frac{L}{v_g} = \frac{L}{\frac{Q_g}{A_g}} = \frac{L}{\frac{Q_g}{\frac{\pi D^2}{4} A^*}} \tag{2.23}$$

The possible dimensions of the gas-liquid separator are found when the actual residence time is equal or longer than the necessary residence time. For a horizontal gas-liquid separator a typical $\frac{L}{D}$ ratio is between 2.5 and 5 [29].

2.3.2 Sizing vertical separator

At low gas fractions a vertical gas-liquid separator is commonly used. In this paragraph the sizing of this vertical separator is discussed. A schematic drawing of a vertical gas-liquid separator is shown in Figure 2.11 . Equal to the horizontal gas-liquid separator, it is important that the residence time of the liquid is long enough so that the bubble can rise to the surface before the liquid leaves the separator.

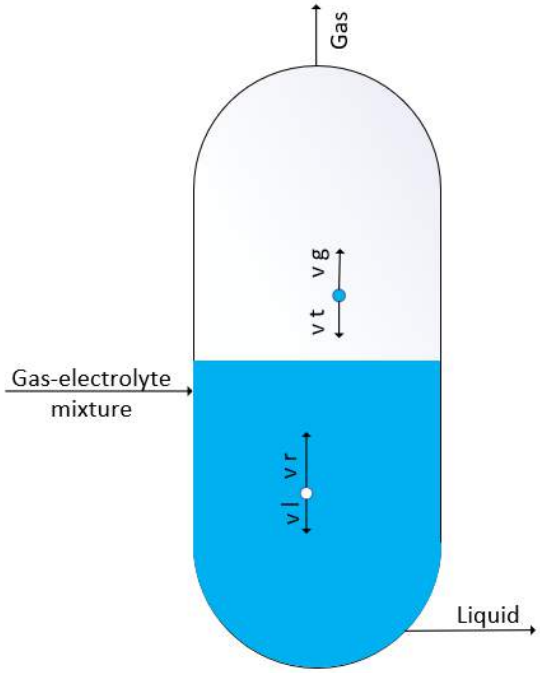

Figure 2.11: *Schematic drawing of a vertical gas-liquid separator. The gas-electrolyte mixture enters in a liquid phase. The gas bubbles rise to the top and leave while the electrolyte leaves at the bottom.*

In this example the inlet is just below the liquid level. The necessary residence time of the liquid has to be long enough so that the bubbles in the mixture can rise to the liquid surface. This can be calculated by Formula 2.24.

$$\tau_{l,necessary} = \frac{L(h_l - h_i)}{v_r - v_l} = \frac{L(h_l - h_i)}{v_r - \frac{Q_l}{\frac{\pi}{4}D^2}} \tag{2.24}$$

Where h_i is the relative inlet height and h_l is the relative liquid height. For the bubble rising velocity Equation 2.19 can be used. The minimum actual residence time of the liquid can be calculated by formula 2.25 .

$$\tau_{l,actual} = \frac{L(h_i)}{v_l} = \frac{L(h_i)}{\frac{Q_l}{\frac{\pi}{4}D^2}} \tag{2.25}$$

For the minimum size of the gas-liquid separator, the actual liquid residence time is at least equal to or higher than the necessary liquid residence time. The liquid height and the height of the inlet depends on the droplet formation which is shown in Figure 2.10. For a vertical gas-liquid separator a typical $\frac{L}{D}$ ratio is between 2 and 4 [29, 33].

2.3.3 Design gas-liquid separator in the alkaline water electrolysis

To determine design of the gas-liquid separator, some assumptions are made:

- The theoretical rising velocities which are discussed in Section 2.2.2 are assumed to be correct.
- The inlet of the gas-liquid separator is in the liquid phase. For the vertical gas-liquid separator a relative liquid height of 0.4 is assumed.
- The size of liquid droplets is not yet known and therefore this behavior is not taken into account during this research. To prevent that the droplets leave the system, a h =0.5
- The $\frac{L}{D}$ ratios are determined to reduce the separator volume. Therefore the horizontal gas-liquid separator a $\frac{L}{D}$ ratio of 5 is chosen, while in the vertical gas-liquid separator a $\frac{L}{D}$ ratio of 2 is chosen.
- The liquid flow is assumed at $10\frac{l}{h}$.

In Figure 2.12 the bubble diameter is plotted over correlated required volume of the gas-liquid separator. Since the total volume of a horizontal gas-liquid separator is always lower than the vertical gas-liquid separator it is assumed that the gas-liquid separator is horizontal.

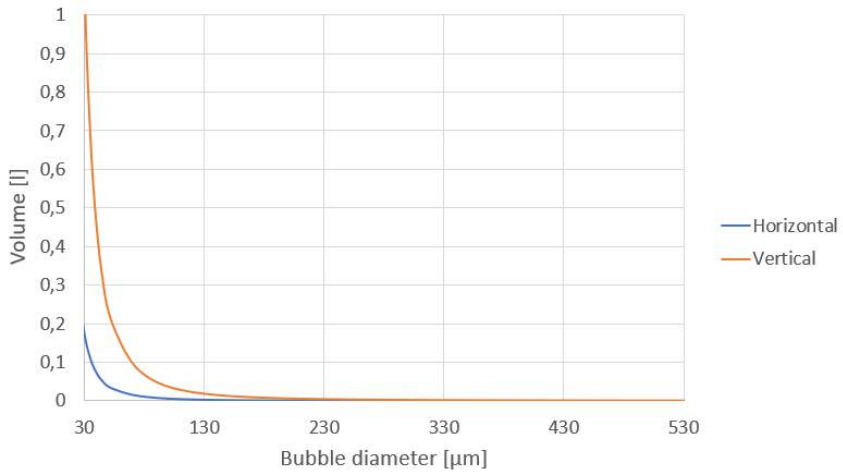

Figure 2.12: *Theoretical volume difference between a horizontal and vertical gas-liquid separator.*

Therefore, during this research the gas-liquid separator is designed horizontally. In Figure 2.13 the bubble diameter is shown with the corresponding length of the gas-liquid separator.

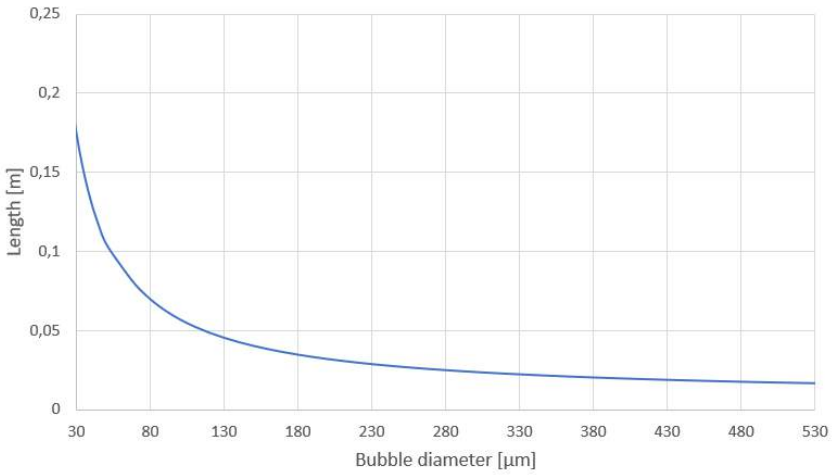

Figure 2.13: *The theoretical size of the gas-liquid separator based on the minimum bubble diameter.*

3 | Methodology

For this research the TU/e set-up is used, which is discussed in detail in Section 3.1. In Section 3.2 the method for the determination of the bubble size distribution is discussed. In Section 3.3 the method for the determination of the bubble rising velocity and the effect of the barrier in the outlet device are discussed.

3.1 Set-up

In this section the set-up is explained in more detail, which is shown in Figure 3.1. In the electrochemical cell the reactions take place and, at the top, the gas-liquid mixtures leave the cell and are transported to the gas-liquid separators. The gas-liquid mixtures enter the separators in the liquid phase. The gas bubbles rise to the top and leave the separator, while the liquid leaves the separator at the bottom. The liquid recirculates to the inlet of the electrochemical cell via the pump. To visualise the bubbles, a Dedocool light source is placed in the position of the back of the electrochemical cell. The light goes through the diaphragm (The diaphragm is the porous membrane between the electrodes) and the high speed camera records the shadows of the bubbles.

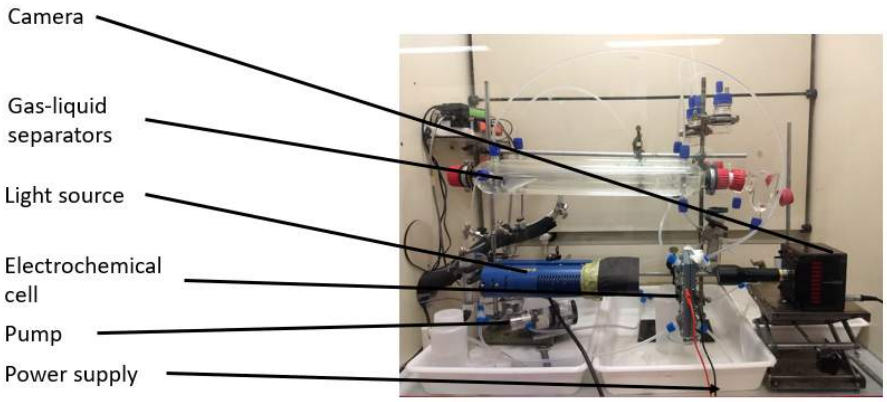

Figure 3.1: *Set-up*

Electrochemical cell
The electrochemical cell is printed by a 3D printer using Acrylonitrile Butadiene Styrene (ABS). The cell is made up of the inlet part, the electrode part, the outlet part and the sealing part. All these parts are discussed separately in detail in Appendix B. Because of limitations due to corrosion a maximum concentration of $30wt\%$ KOH can be used. Because of the compatibility of ABS with KOH, a maximum temperature of 70 °C can be reached [34].

The electrolyte enters the electrochemical cell at the bottom on both cell sides. In the inlet part the liquid is equally distributed over the surface of the electrodes. At the electrode some electrolyte is converted to

gas. This electrolyte-gas mixtures leave the electrochemical cell via the outlet part. The sealing prevents leakages in the cell. Unfortunately due to a damaged electrochemical cell, there was still a small leakage. As shown in Figure 3.2a, a gas window is placed to make the visualisation possible.

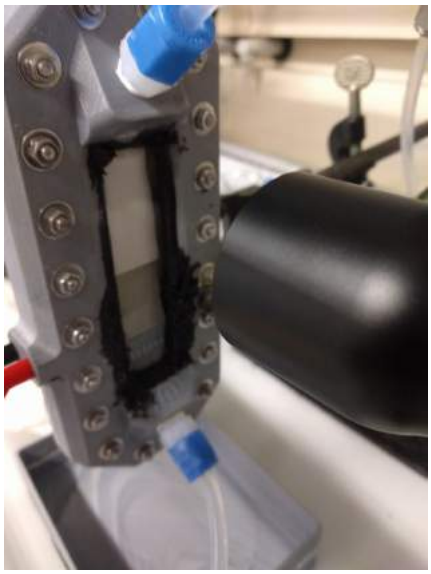

(a) *Design of the 3D printed electrochemical cell.*

(b) *Place of visualisation of the bubbles indicated by a squared blue rectangle.*

(c) *Change in outlet device (with additional barrier)*

Figure 3.2: *Several designs of the 3D printed electrochemical cell. The design which is shown in (a) and (b) is used to visualise the bubble size distribution. The design which is shown in (c) is used to show the effect of the barrier in the outlet device on the bubble size distribution.*

Gas-liquid separator

For the gas-liquid separator a horizontal vessel is used with a jacket. Via this jacket the electrolyte can be heated to reach the desired temperature via a water bath which is connected to this separator. To prevent that oxygen and hydrogen are still present in the electrolyte which is recirculated to the cell, the use of a gas-liquid separator with a diameter of $5.5cm$ and a length of $44cm$ is adopted. The $\frac{L}{D}$ of 5 (according literature) is increased to 8 to be sure that no high flammable mixture is formed.

Pump

By using the pump a flow rate up to $30\frac{l}{h}$ per electrode side can be reached, which is equal to a superficial inlet velocity of $1.4\frac{m}{s}$. However, to operate close to the industrial conditions, a liquid flow should be used about $0.001\frac{m}{s}$. Unfortunate, at these low velocities the pump cannot deliver a continuous flow.

Power supply

Direct current is applied on the electrodes of the electrochemical cell using a power supply. Since the current density is important for this research an application of a constant current at the electrodes is adopted. The model of the power supply is Velleman LABPS3005DN. This power supply can deliver a maximum current of $5A$ which is correlated to a nominal current density of $5000\frac{A}{m^2}$.

Visualisation

In the set-up the use of back-lighting is adopted. A Dedocool light is used as light source. To record the bubbles several camera types and lenses were available. The 'FASTCAM Mini AX200 with the Edmund Optics Telecentric Lens 2.0X TML-HP' is used instead since this one has the highest resolution per millimetre, namely 100 pixels per mm. Furthermore, the magnification is fixed. The lens has a magnification of 2 times.

A shutter time of $\frac{1}{1000}s$ is used. At a longer shutter speed the pictures of a moving object could become more blurry, than at a shorter shutter speed [35]. For a shorter shutter speed, more light is necessary to

prevent underexposure which could cause noise in the pictures.

The frame rate (number of frames per second) depends on the purpose of the picture. This is mentioned separately in each section. In Appendix C the parameters of the set-up for visualisation are discussed in more detail.

Electrolyte
The electrolyte is prepared by dissolving KOH pellets in demineralized water. The concentration of the electrolyte solution is determined by the electrical conductivity and the density. During the experiments it was noticed that the bubble size increased when the solution was used during a longer period. This is explained in more detail in Appendix D. Because of this behavior, every solution is refreshed after two consecutive days of use.

3.2 Bubble size distribution

The bubble size distribution is determined by the photographic method by using the experimental set-up. The minimum frame rate of $50fps$ is used. The area in which the bubble size distribution is measured is indicated with a blue rectangle in Figure 3.2b. The pictures of the bubbles are analysed by a MATLAB script. In Section 3.2.1 the MATLAB script is explained. In Section 3.2.2 the experimental conditions are shown.

3.2.1 Bubble detection

By using MATLAB a picture can be analysed and the bubble size distribution can be determined. There was already an in-house MATLAB script [36] which could be used for detecting the bubble size distribution. In this script the largest bubble needs to be selected and then the script will shrink this bubble and search for bubbles with the same pixels of the shrunken bubble. Unfortunately, in this research it is not possible to use this script because this script only detects bubbles with zero overlap, when in this research bubbles have a big overlap. Therefore, in this research another MATLAB script is developed, which detects circular bubbles with the MATLAB function 'imfindcircles' [37].

In this research a MATLAB script is developed to detect bubbles with a minimum bubble diameter of 12 pixels. In this case this is correlated to a bubble diameter of $120\mu m$. Smaller bubbles cannot be detected by the MATLAB script because of the accuracy [37]. The MATLAB script is developed by using the image processing toolbox in MATLAB. The script is shown in Appendix E. The MATLAB script is built up out of several parts and each part is discussed separately. The line numbers ($ln.$) are referring to the lines in this script.

- **Before the bubble detection**
  Before the bubbles are detected ($ln.2 - 146$) the process variables are defined ($ln.2 - 20$), the selected main folder with the subfolders with the series of pictures ($ln.24-76$) and their correlated process parameters are loaded ($ln.78 - 91$), the time step in between the analysed pictures is determined based on the superficial inlet velocity and the size of the picture to prevent double detection of the same bubble($ln.96 - 103$) and the sensitivity which is necessary to set for the bubble detection ($ln.106 - 146$) is defined. The time step and the height sensitivity are explained in more detail:

  - *Time step in between analysed pictures*
    The superficial inlet velocity in the electrochemical cell is used to set the time step in between the analysed pictures. This prevents that bubbles are double detected($ln.96 - 103$). So the time step is calculated by taking the length of the picture ($ln.96 - 99$) divided by the superficial inlet velocity. In case of no flow condition, the time step of $1s$ (and so 50 frames)

is assumed based on the rising velocity of a bubble with a bubble diameter of $120\mu m$. To be sure that no bubbles were detected twice, the bubble rising velocity is tracked manually. For some reason, the actual liquid rising velocity is lower than the expected rising velocity at a flow of $10\frac{l}{h}$(see Appendix F). This causes that some bubbles are double detected, however, this double detection seems to have no influence on the bubble size distribution. Therefore, the time step is used based on the superficial inlet velocity.

- *Sensitivity*
  To use the 'imfindcircles' function it is important to define the sensitivity. The sensitivity has to be set at a value so that most of the bubbles are correctly detected ($ln.106 - 146$). The height of the sensitivity value dependents on:
  * The amount of bubbles. To analyse a picture with a lot of bubbles, the sensitivity has to be higher compared to a picture with only a few bubbles.
  * The size of bubbles. It was noticed that some bigger bubbles were a bit blurry, which resulted in more bubble detections for only one real bubble. In this case only the biggest bubble detection were preserved. To prevent that the bubbles were overestimated the smaller bubbles had a higher sensitivity compared to the bigger bubbles.

- **Bubble detection and adjustments**
  The bubbles were detected in this part of the script ($ln.149 - 173$). The output of the detection is the radius and the location of the centre of the bubbles. The minimum radius is $6pixels$ which is correlated to a bubble diameter of $120\mu m$. As a consequence, bubbles with a smaller diameter were not detected. As already explained: the bigger bubbles became a bit blurry. This caused multiple detections of bubbles at the same place. Therefore, when a bubble is detected at the same picture at the same place multiple times, only the biggest bubble is selected ($ln.180 - 200$). A few bubble were stuck in the surface of the diaphragm, therefore, these bubbles were deleted when they were detected at least in two of the three analysed pictures before ($ln.202 - 263$). The detection of the first 19 pictures of a series of at least 145 pictures are saved in order to check later ($ln.272 - 310$). Finally, the results of a series are gathered in vectors ($ln.318 - 324$).

- **Export the results**
  After all expected pictures had been analysed, the results were gathered in a table ($ln.331 - 343$). This was done for each subfolder, until all the folders were analysed.

In Figure 3.3 an example is shown of the bubble detection. In this figure it is shown that there are also bubbles with a bubble diameter smaller $120\mu m$. Therefore some pictures are analysed by hand. Due to limited resolution of the pictures a minimum bubble diameter of $30\mu m$ could be measured. In Appendix G an example of the bubble detection is shown and discussed in more detail.

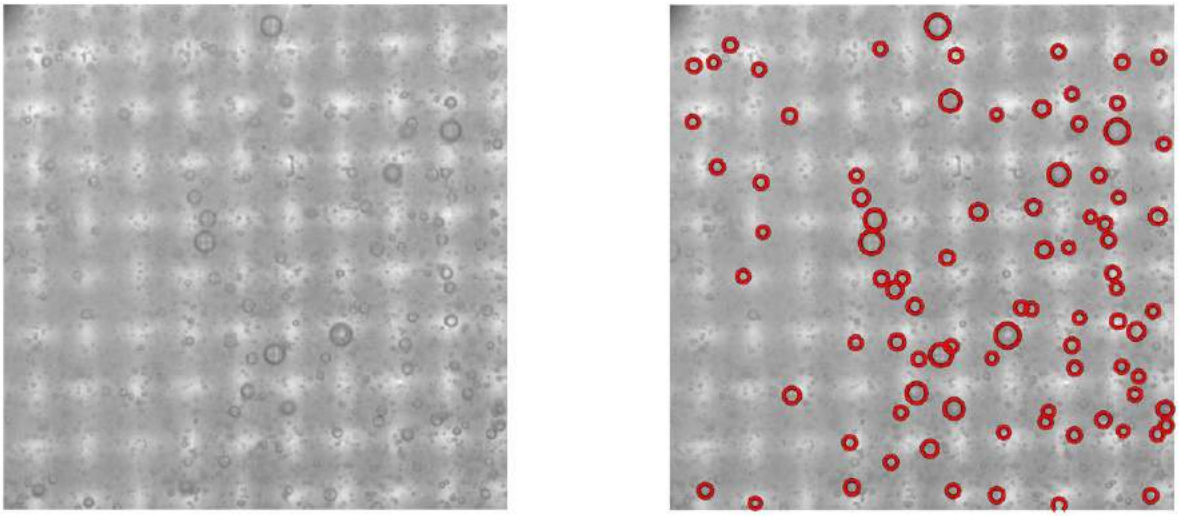

Figure 3.3: *Bubble detection at 20 wt%, 20 °C, no flow and* $50\frac{A}{m^2}$.

The MATLAB script generates tables with the bubble detection per analysed picture. These tables are converted to the normalized bubble size distribution and to the gas fraction.

- **Normalized bubble size distribution**
  The total number of bubbles per diameter for the total series analysed pictures is summed and divided by the total number of analysed pictures. The number of bubbles in a picture depends on the value of current density and the superficial velocity. To be able to compare the varies results more easily, the graphs are normalized. Normalization means two steps:
  - Firstly, the bubble size distribution based on the number of bubbles is converted to a bubble size distribution based on volume. This is done because bigger bubbles have a bigger volume compared to the smaller bubbles.
  - Secondly, the volume per diameter is divided by the total volume per picture.

  The result is a normalized bubble size distribution based on volume.
- **Gas fraction**
  The gas fraction is calculated based on the total measured gas volume at an analysed picture divided by the corresponding electrochemical cell volume. This electrochemical cell volume is equal to the dimensions of the pictures multiplied by the depth of the cell side.

3.2.2 Experimental conditions

For determining the bubble size distribution the extreme conditions are tested to see the effect of the changes in the conditions, as shown in Table 3.1. The maximum operated temperature is limited to $50°C$, to prevent an increase in leakages. The range of operated current density is limited: The lower limitation is caused by a too low gas volume to find a correlation. The upper limit is caused by the difficulties in analysing because of the relatively high gas volume. This is explained in more details in Appendix H. Since the hydrogen gas volume is almost twice as high as the oxygen volume due to the reaction stoichiometry, the operated current density for hydrogen bubbles is also almost twice as low as the operated current density for oxygen bubbles. The temperature of the system is checked before starting the experiment. The concentration of the electrolyte is checked before use by conductivity and density measurements. The liquid flow rate is calibrated by measuring the liquid volume for a specific period of time.

Table 3.1: *Experimental conditions for determining the bubble size distribution dependent on the type of gas.*

	Oxygen bubbles	Hydrogen bubbles
Current density [$\frac{A}{m^2}$]	50, 70, 100, 200	30, 50, 70, 100
Temperature [$^{\circ}C$]	20, 50	20, 50
Concentration [$wt\%$]	5, 10, 20	5, 10, 20
Superficial inlet velocity [$\frac{m}{s}$]	0, 0.048	0, 0.048

To make sure that the hydrogen and oxygen bubbles can be compared with each other, the same electrochemical cell side is used and the cathode and anode sides are switched. To validate the results the measurements were planned to be done in triplicate. In between the experiments the electrochemical cell is re-opened, the electrode is washed with iso-propanol and the same electrode is replaced in the cell. In Appendix I an overview is shown of the experiments which were done to determine the bubble size distribution. A few experiments are missing. There are several reasons for this:

- In Experiment 1 the range of the current densities were not yet know since the bubble behavior was different than expected, because of the change over bubble behavior in the electrolyte over time (see Appendix D). Therefore, the experiments were done without all the conditions.
- Some files became corrupted, with the result that the picture could not be analysed anymore.

Moreover, a few experiments are excluded form this research. The reason for this are summed below:

- The limited current densities.
- Only tests with a diaphragm activation of at least 3 days are used during this experiment, since it was noticed that at a shorter activation time measured gas fraction became much lower (see Appendix J and K).
- An increase in leakages of the cell results in a lower measured gas volume. Therefore, the following results are excluded: 'Experiment 3 20wt% and 20 °C for O_2' and 'Experiment 3 5wt% and 50 °C for O_2' (see Appendix L).

Moreover, despite the poor detection of bubbles at current densities higher than $200\frac{A}{m^2}$ experiments are also done at 500, 700 and $1000\frac{A}{m^2}$ to check if the same bubble size distribution was found.

For analysing the picture a time step of 50 frames (this corresponds to $1s$) is used at no flow conditions and a time step of 8 (this corresponds to $0.16s$) frames is used at a superficial inlet velocity of $0.048\frac{m}{s}$.

It was noticed that the bubble size distribution was bimodally distributed. Since Chandran et al. found a modal distribution of the bubbles [38] in a conventional assembly, the behavior at the (zero-gap) electrode is investigated. At low current densities, there are less bubbles present which reduce the chance of coalescence. Therefore, at low current densities the bubble behavior is recorded at a frame rate of $50fps$. At higher current densities the chance of coalescence is bigger and therefore, a frame rate of $1000fps$ is used so that the exact behavior can be detected.

3.3 Design the gas-liquid separator

The theoretical bubble rising velocity is used to size the gas-liquid separator. In Section 3.3.1 the experiment is explained to measure the experimental rising velocity. In this way, the theoretical rising velocity could be compared to the experimental rising velocity. The bubble size distribution at the outlet of the gas-liquid separator is used to determine the size of the gas-liquid separator. In Section 3.3.2 the coalescence effect caused by the barrier in the outlet device is tested.

3.3.1 Bubble rising velocity

To analyse the bubble rising velocity, in the area indicated with a blue rectangle shown in Figure 3.2b the bubble rising velocity is measured. This is done with a high speed camera with a frame rate of $1000 fps$. To prevent interaction between the bubbles itself, a low current density of 10 and $30 \frac{A}{m^2}$ is used for the hydrogen and oxygen side respectively. These results are compared to the expected velocities based on literature.

3.3.2 Effect of barrier in outlet device

The outlet device of the electrochemical cell is designed based on the industrial design [39]. To indicate the effect of the barrier at the outlet, an extra barrier is added at the middle of the outlet device (see Figure 3.4).

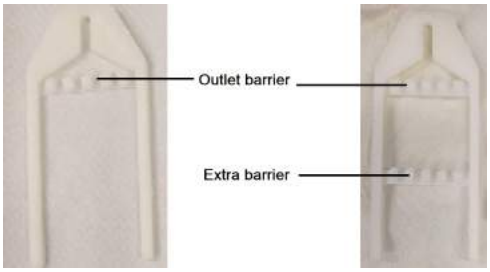

Figure 3.4: *On the left side the design of the outlet device is shown and on the right side the design with an extra barrier is shown.*

In Figure 3.2c the design is shown in the electrochemical cell. It is expected that due to coalescence of smaller bubbles at the barrier, the average bubble size after the barrier increases compared to before. To analyse this behavior the bubble size distributions are measured before and after the barrier. Since the coalescence happens more easily when more bubbles are present (but too many bubbles make the visualisation difficult) current densities of $30 \frac{A}{m^2}$ and $50 \frac{A}{m^2}$ are used.

4 | Results and discussion

In this chapter an overview of the results is provided. The focus is on the bubble size distribution at 20wt% and no flow conditions, because these conditions are the closest to industrial conditions. To compare the results with the model the focus is on the conditions of $50\frac{A}{m^2}$ and 20°C. In Section 4.1 the results of the bubble size distribution are discussed. In Section 4.2 the results based on sizing the gas-liquid separator are discussed in more detail.

4.1 Bubble size distribution

One of the goals of this research was to determine the bubble size distribution at the outlet of the electrochemical cell. The bubble size distribution is described in Section 4.1.1. In addition, the effect of current density, type of evolved gas, temperature, concentration and superficial inlet velocity on the (normalized) bubble size distribution are discussed in Sections 4.1.2, 4.1.3, 4.1.4, 4.1.5, 4.1.6 respectively. In Section 4.1.7 the measured gas production is discussed.

4.1.1 Description of the bubble size distribution

In Figure 4.1 the normalized bubble size distribution is shown for hydrogen bubbles at $50\frac{A}{m^2}$, 20 °C, 20wt% and no flow condition. A bimodal distribution is found. The 'first peak' with a bubble diameter between 120 and $200\mu m$ and the 'second peak' with a bubble diameter between 200 and $400\mu m$ and there are some bubbles with a bubble diameter larger than $400\mu m$. This similar behavior is found for the bubble size distributions at different conditions (at $50\frac{A}{m^2}$) (see Appendix M). To describe the distribution more accurately, a Poisson and a binormal distribution are tested (see Appendix N). However, for this distribution it was not really possible to find a correct model. The first peak is hard to fit due to the unknown height and shape of the bubbles with a bubble diameter smaller than $120\mu m$. The bubbles with a bubble diameter larger than $200\mu m$ are caused by the gap between the electrode and the diaphragm and coalescence at the holes of the electrode. This behavior explains the long tail of the second peak on the right side. Moreover, it could also be noticed that there is less volume measured at a bubble diameter around $200\mu m$. A possible explanation for this could be that at this bubble size the bubbles are becoming stuck in the gap of the electrode and the diaphragm. When the bubbles start growing, the bubbles can move again to the holes of the electrodes.

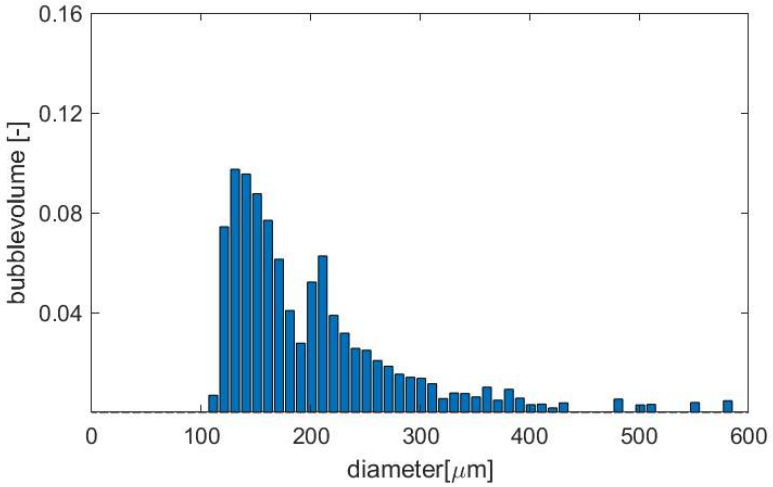

Figure 4.1: *Normalized bubble volume distribution for the hydrogen bubbles at* $50\frac{A}{m^2}$, $20°C$, $20wt\%$ *and no flow condition.*

First peak

The first peak is probably caused by the bubble detachment which is discussed in section 2.1.2. The theoretical model was expecting a bubble detachment diameter of $480\mu m$. This is almost four times higher than the found bubble diameter. A possible explanation could be that the contact angle found in literature is not valid for a nickel electrode. To find a bubble diameter of $130\mu m$, which is the mode value of the first peak, the contact angle would be around $11°$. Moreover, the theory consider a flat plate electrode in the conventional configuration, while in this research a zero-gap configuration is used. This could have influence on the forces acting the attached bubbles on the electrode surface.

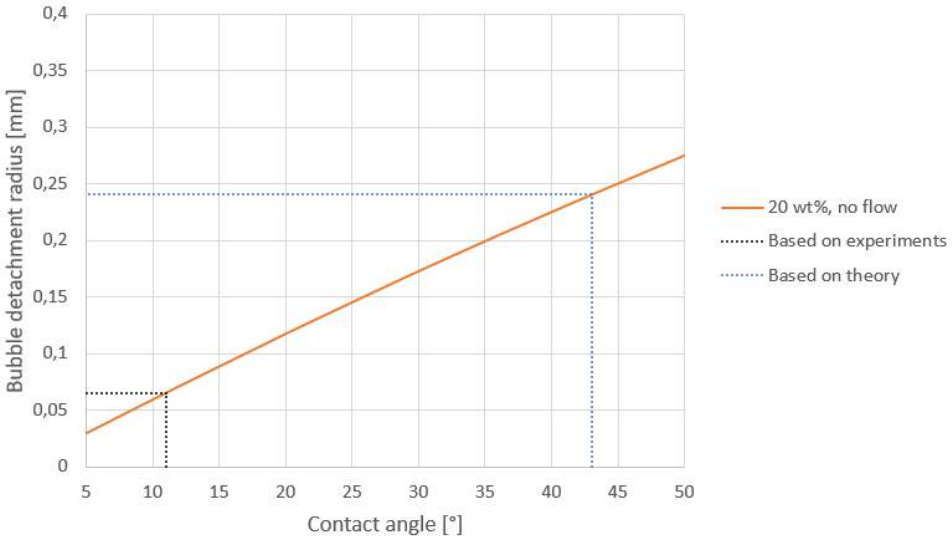

Figure 4.2: *The contact angle dependency on the bubble detachment radius. At a bubble detachment radius of* $65\mu m$ *a contact angle of 11 °is found, while the theoretical contact angle is equal to 43 °.*

However, it has to be taken into account that the mode value of the peak could also be smaller than a bubble diameter of $130\mu m$ since bubbles with a diameter smaller than $120\mu m$ can not be measured.

Second peak

It is found that the bubbles with a bubble diameter between 200 and $300\mu m$ are caused by bubble growth of bubbles in the electrode hole after the bubble with a bubble diameter about 200 μm leave the gap between the electrode and the diaphragm. This is shown in Figure 4.3a. The bubble which is formed has a diameter of $230\mu m$. Bubbles with a bubble diameter above the $300\mu m$ are bubble which are stuck in the electrode hole. Most of the time these bubbles leave when they coalesce. An example is shown in Figure 4.3b. Bubble 1 and 2 on the left side of the figure have a bubble diameter of 230 and $250\mu m$, respectively. When they coalesce a bubble is formed with a bubble diameter of $310\mu m$. Bubbles are also measured with a bubble diameter larger than $400\mu m$. These bubbles do immediately leave the electrode hole after coalescence. This behavior is shown in Figure 4.3c. In this case the smaller bubble with a diameter of $240\mu m$ coalesce with a bubble with a diameter of $590\mu m$ and forms a bubble with a diameter of $690\mu m$.

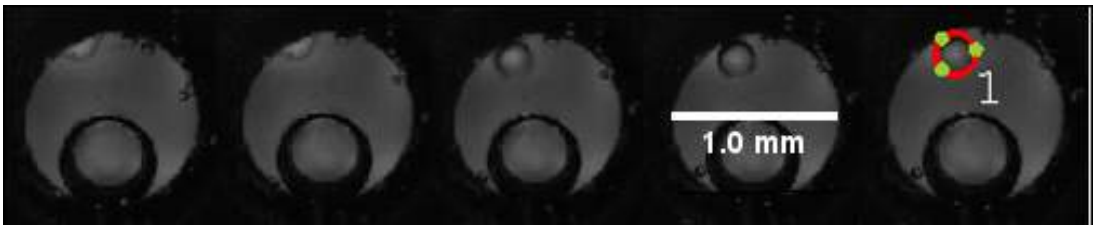

(a) *To identify bubbles with a bubble diameter between* 200 *and* $300\mu m$. *In the left the bubble is partly visible behind the electrode. A few frames later the bubble goes to the hole as shown in the right.*

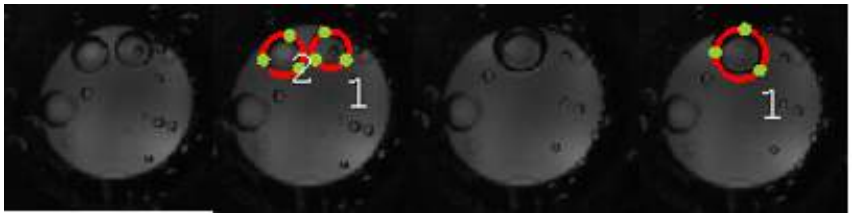

(b) *To identify bubbles with a bubble diameter between* 300 *and* $400\mu m$. *A bubble is stuck in the electrode hole and leaves when it coalesce with another bubble.*

(c) *To identify bubbles with a minimum bubble diameter of* $400\mu m$. *The bubble coalesce multiple time before it leaves the electrode hole.*

Figure 4.3: *Bubble behavior at the electrode to identify the bubbles with a bubble diameter bigger than* $200\mu m$.

This phenomenon of the second peak could also explain why in a previous research this bimodal distribution is not found [38]. The difference in the research is the zero-gap configuration. According to Figure 4.3 the second peak is caused by the gap in between the electrode and the diaphragm.

For future research it is recommended to vary the electrode-diaphragm gap to be sure that the second peak is caused by the (close to) zero-gap assembly. The gap could be varied and monitored by 3D printing of several plastic pieces which could be placed between the electrode and the diaphragm.

4.1.2 Effect of current density

Based on the theoretical model discussed in Section 2.1.2, it is expected that the size of the bubbles do not change. However, in the previous research it is found that the size of the bubbles increase below a current density of $300\frac{A}{m^2}$. The normalized bubble size distributions for hydrogen at 20 wt% KOH, 20°C and no flow conditions are shown in Figure 4.4. In Appendix M all the distributions are shown with simular results.

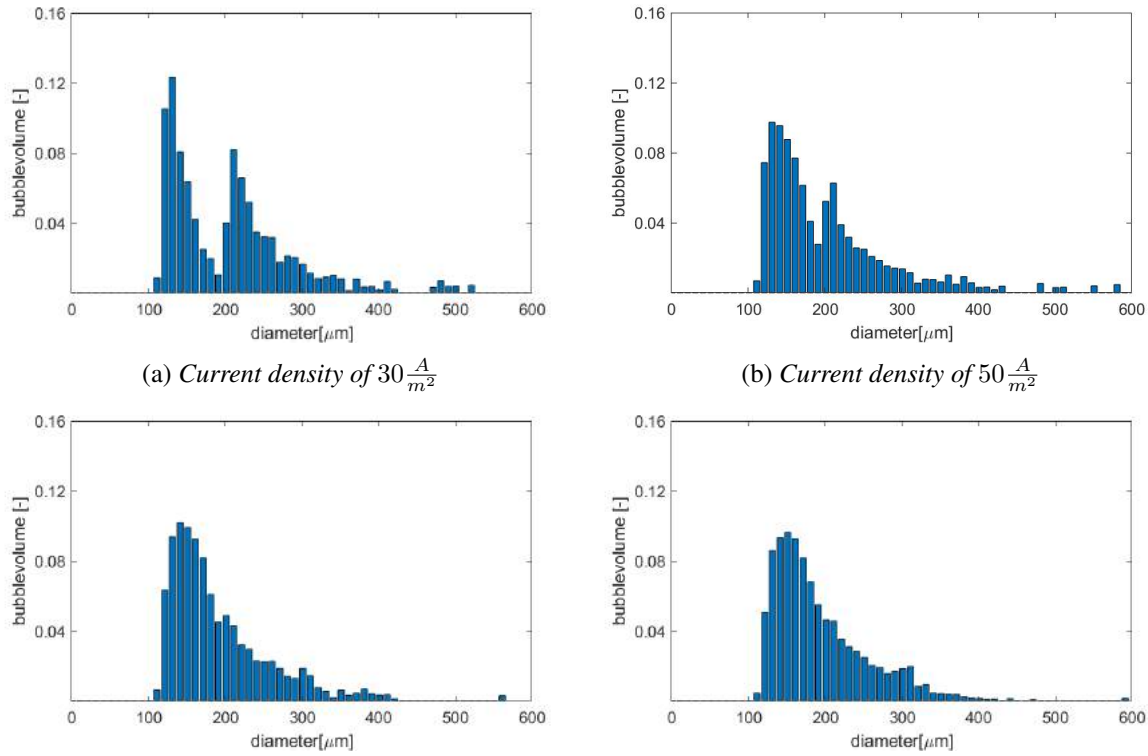

(a) *Current density of* $30\frac{A}{m^2}$

(b) *Current density of* $50\frac{A}{m^2}$

(c) *Current density of* $70\frac{A}{m^2}$

(d) *Current density of* $100\frac{A}{m^2}$

Figure 4.4: *The effect of current density on the normalized bubble size distribution for the hydrogen bubbles at* $20°C$, $20wt\%$ *and no flow condition.*

As already discussed in Section 4.1.1 a bimodal distribution is obtained at a current density of $50\frac{A}{m^2}$. However, at an increase in current density the bimodal distribution turns into a unimodal distribution. This phenomenon happens because the volume of the second peak does not change as much as the first peak (see Figure 4.5). This can be explained by the limited space at the electrode. Moreover, it could be noticed that at a higher current density more bubbles of $200\mu m$ are detected. So probably at higher current densities less bubbles are stuck between the electrode-diaphragm gap due to the higher gas production. The same phenomenon is happening for the bubbles at current densities higher than $200\frac{A}{m^2}$ (see Appendix O). So increasing the current density the bubble volume of the first peak increases.

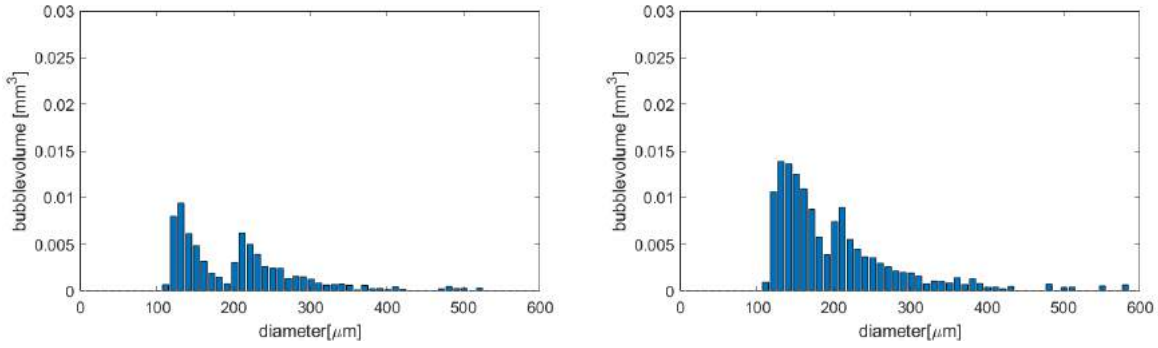

(a) *Current density of* $30\frac{A}{m^2}$ (b) *Current density of* $50\frac{A}{m^2}$

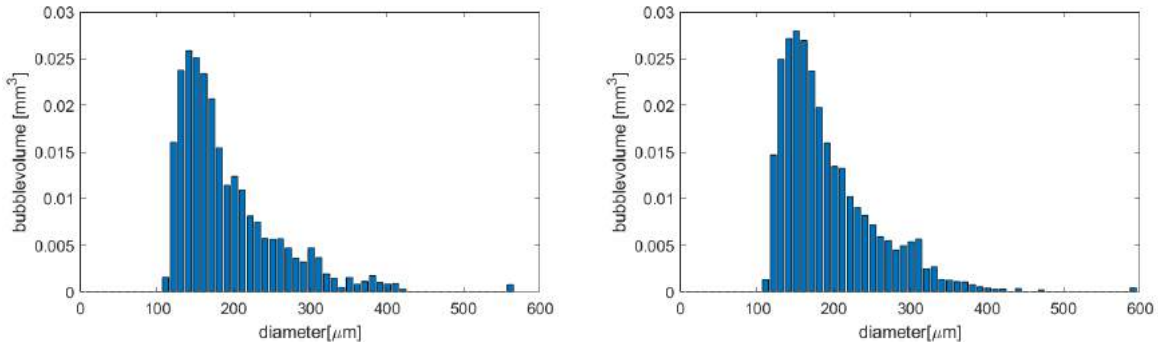

(c) *Current density of* $70\frac{A}{m^2}$ (d) *Current density of* $100\frac{A}{m^2}$

Figure 4.5: *The effect of current density on the bubble size distribution for the hydrogen bubbles at* $20°C$*,* $20wt\%$ *and no flow condition.*

The bubbles with a bubble diameter smaller than $120\mu m$ are analysed manually at current densities of $30\frac{A}{m^2}$ and $50\frac{A}{m^2}$, as shown in Figure 4.6. This figure shows that the current density seems to have almost no influence on the normalized bubble size distribution of the bubbles with a bubble diameter between 30 and $120\mu m$. The measured gas fraction of these smaller bubbles is around 0.25 of the total measured gas volume. This is a substantial quantity of gas.

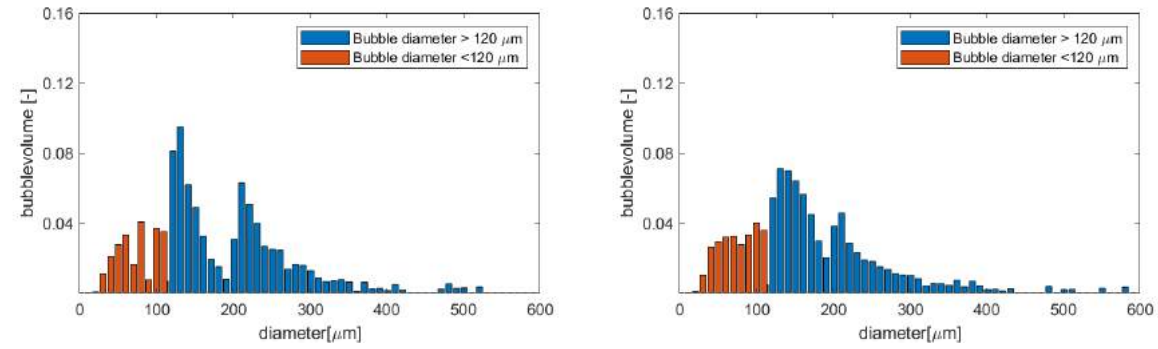

(a) *Current density of* $30\frac{A}{m^2}$ (b) *Current density of* $50\frac{A}{m^2}$

Figure 4.6: *The current density effect on the overall normalized bubble size distribution for hydrogen bubbles at* $20°C$*,* $20wt\%$ *and no flow condition.*

4.1.3 Effect of type evolved gas

Based on the bubble detachment calculations, it was expected that the hydrogen bubbles were smaller than the oxygen bubbles. In Figure 4.7 the normalized bubble size distribution for hydrogen and oxygen are shown. No significant difference is measured between the sizes of the hydrogen and oxygen bubbles. However, it could be notice that for the first peak of the hydrogen bubble size distribution is wider compared to the first peak of the oxygen bubble size distribution. This is in contrary to literature, which indicates that the hydrogen bubbles were more consist measured compared to the oxygen bubbles [17]. On the other hand, Haug et al. measured narrower distribution for the oxygen bubbles compared to the hydrogen bubbles at low current densities [7].

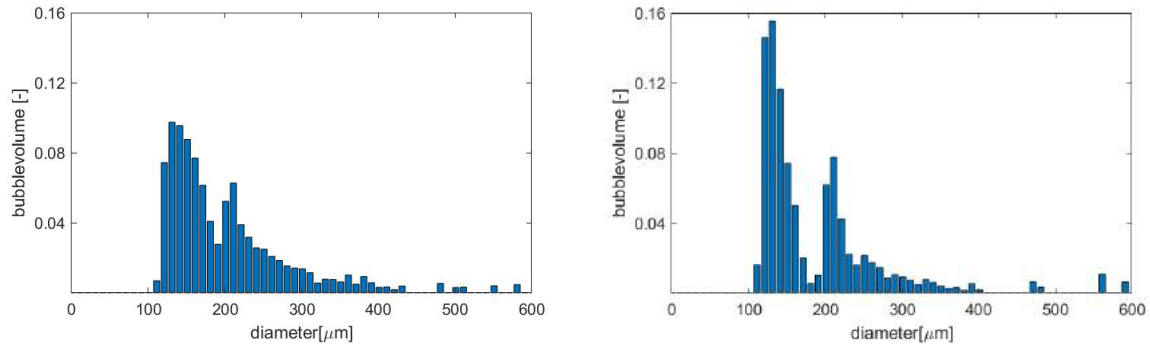

(a) Hydrogen bubbles (b) Oxygen bubbles

Figure 4.7: *The effect of gas type on the normalized bubble size distribution at* $50\frac{A}{m^2}$, $20°C$, $20wt\%$ *and no flow condition.*

Although the MATLAB script does not count bubbles smaller than $120\mu m$, an indication of the bubble size distribution of bubbles with a bubble diameter between 30 and $120\mu m$ is given (see Figure 4.8). The results of bubbles with a bubble diameter smaller than $120\mu m$ are combined with the obtained bubble size distribution via the MATLAB script. In this case a volume fraction over the total measured gas volume of 0.21 is found for oxygen, while there is a volume fraction of 0.26 found for hydrogen. However, since this gas fractions are only based on one picture of the hydrogen and oxygen production, it is not possible to make a conclusions. However, it seems to be that the gas type has hardly an influence on the sizes of the bubbles. This is contrary to the expectations of the theoretical calculation. A possible explanation would be that the contact angle of oxygen and hydrogen are the same.

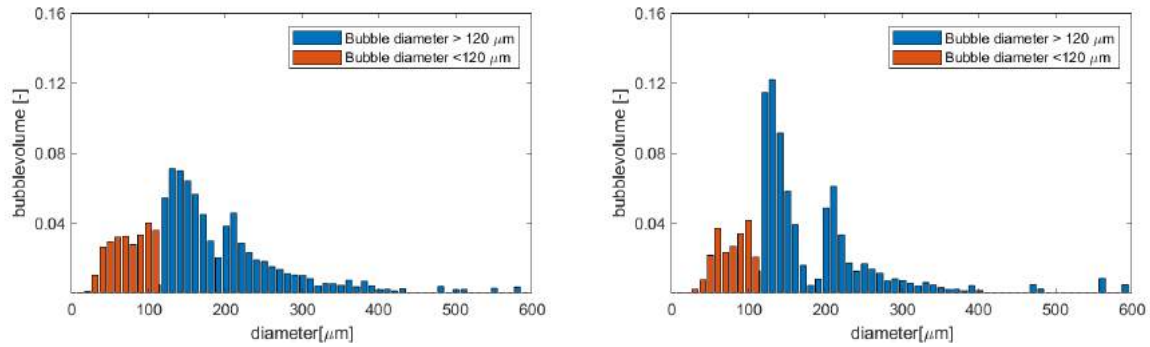

(a) *Hydrogen bubbles* (b) *Oxygen bubbles*

Figure 4.8: *The effect of gas type on the normalized bubble size distribution at* $50\frac{A}{m^2}$, $20°C$, $20wt\%$ *and no flow condition.*

4.1.4 Effect of temperature

The temperature is one of the process parameters which is investigated. It was expected that the bubble diameter should decrease at a higher temperature based on the expected surface tension. The normalized bubble size distribution at 20 and 50°C are shown in Figure 4.9. In this figure the results are shown for the hydrogen bubbles at $20wt\%$, $50\frac{A}{m^2}$ and no flow condition. It shows that the temperature hardly influences the normalized bubble size distribution. This is also found for different conditions, which are shown in Appendix M.

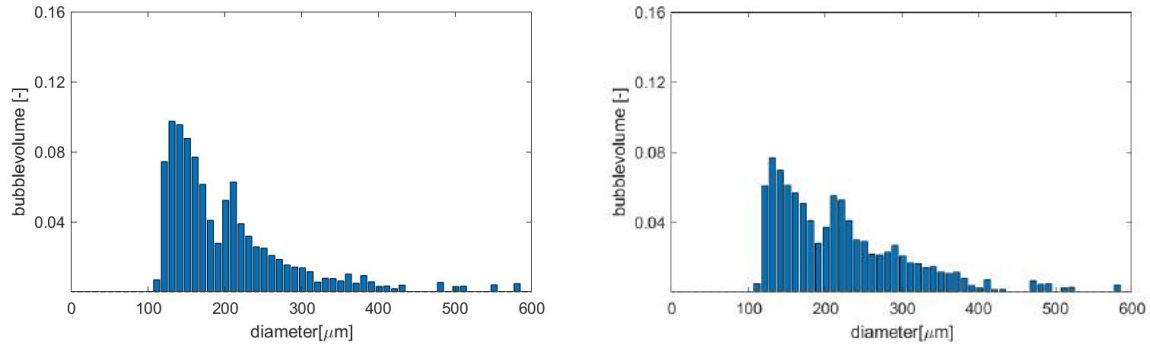

(a) *Temperature of* $20°C$ (b) *Temperature of* $50°C$

Figure 4.9: *The effect of temperature on the normalized bubble size distribution for hydrogen bubbles at* $50\frac{A}{m^2}$, $20wt\%$ *and no flow condition.*

Moreover bubbles with a diameter smaller than $120\mu m$ seem to be comparable. So no significant difference is measured by the temperature difference. A possible explanation for this would be that the surface tension does not change that significant at the different temperatures.

4.1.5 Effect of concentration

It was expected that the bubble diameter would decrease as the concentration increases based on the surface tension and the deviation of the contact angle. The normalized bubble size distribution for 5 and $20wt\%$ are shown in Figure 4.10. The bubble size distribution at 5wt% turns from a bimodal distribution into an unimodal distribution at a current density of $100\frac{A}{m^2}$, while at 20 wt% the distribution turns into an unimodal distribution at a current density of $70\frac{A}{m^2}$. The coalescence behavior could explain this behavior since, according to literature [18], at a higher KOH concentration the chance of coalescence decreases. It is expected that in the case of more coalescence, the bubbles stuck at the diaphragm-electrode gap, could grow more easily. So, at current densities lower than $100\frac{A}{m^2}$ the bubbles are smaller at 20 wt% are smaller than at 5 wt%.

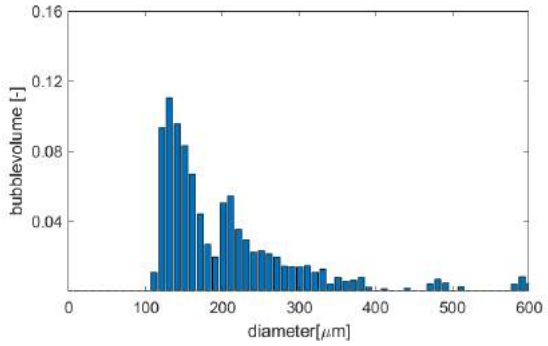

(a) *KOH concentration of* $5wt\%$ *(*$50\frac{A}{m^2}$*)*

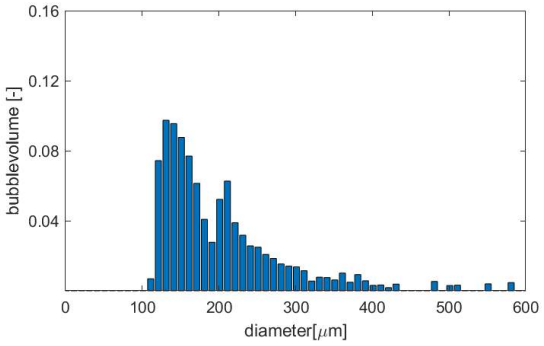

(b) *KOH concentration of* $20wt\%$ *(*$50\frac{A}{m^2}$*)*

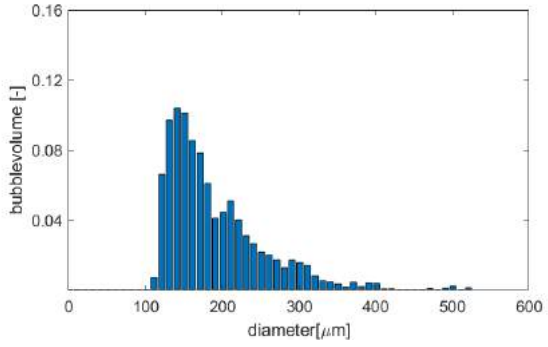

(c) *KOH concentration of* $5wt\%$ *(*$70\frac{A}{m^2}$*)*

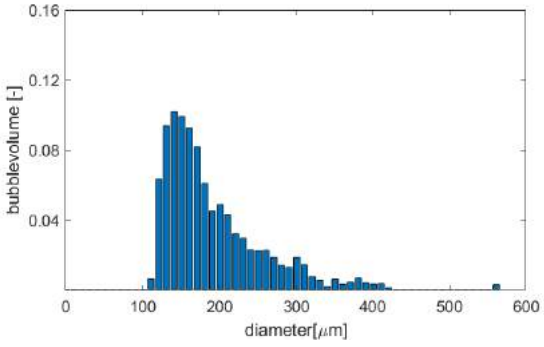

(d) *KOH concentration of* $20wt\%$ *(*$70\frac{A}{m^2}$*)*

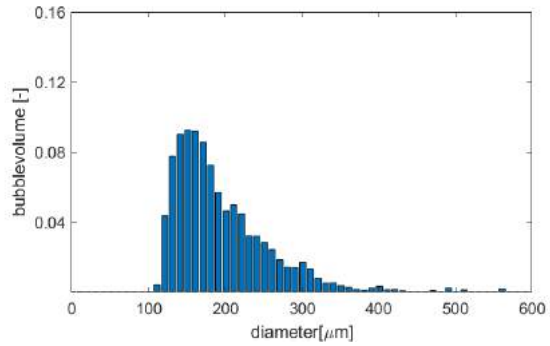

(e) *KOH concentration of* $5wt\%$ *(*$100\frac{A}{m^2}$*)*

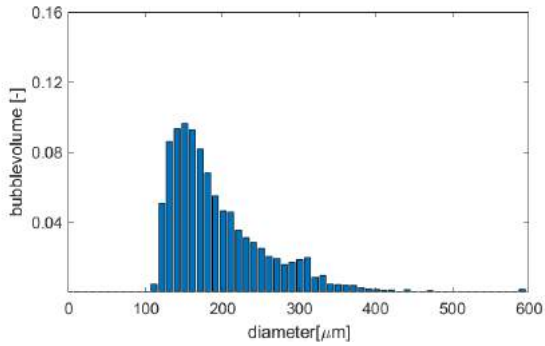

(f) *KOH concentration of* $20wt\%$ *(*$100\frac{A}{m^2}$*)*

Figure 4.10: *The effect of KOH concentration on the normalized bubble size distribution for hydrogen bubbles at* $20°C$ *and no flow condition*

The bubble with a bubble diameter smaller than $120\mu m$ seems to be comparable. However, based on the measurements of the MATLAB script, at current densities lower than $100\frac{A}{m^2}$, the bubbles at 20 wt% were smaller than the bubbles at 5wt% as expected according the theoretical modal. However, at $100\frac{A}{m^2}$ and probably higher current densities, the distribution is similar. A possible explanation for this would be that the deviation of the contact angle should not be different for the different concentrations.

4.1.6 Effect of superficial inlet velocity

The superficial inlet velocity effect on the normalized bubble size distribution is investigated. It was expected that the bubble diameter should decrease as there is a flow present based on the bubble theoretical bubble detachment phenomenon. However, there is no significant difference in mode values measured between no flow and $0.048\frac{m}{s}$ electrolyte flow, as shown in Figure 4.11. It is noticed that the results of the flow conditions are not very consistent (see Appendix M).

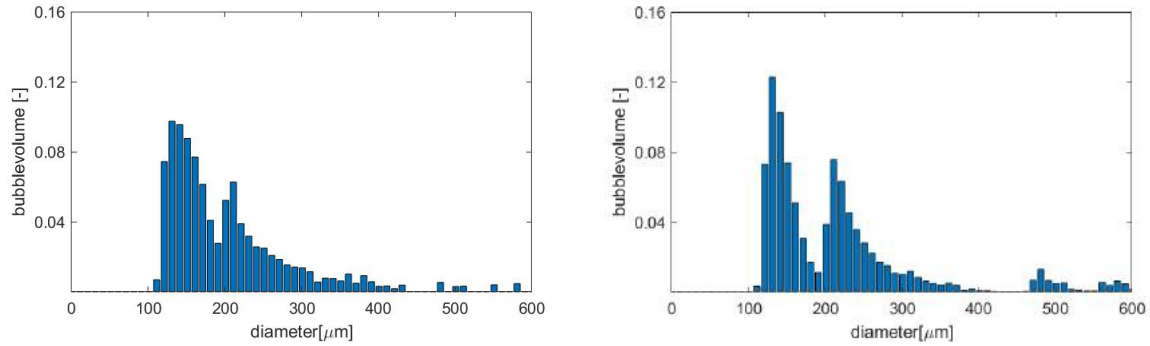

(a) *No flow condition* (b) $0.048\frac{m}{s}$ *superficial velocity*

Figure 4.11: *The superficial inlet velocity effect on the normalized bubble size distribution for hydrogen bubbles at* $50\frac{A}{m^2}$, $20°C$ *an* $20wt\%$.

It is noticed that the gas fraction of the first peak compared to the total gas fraction at a no flow condition, there is more gas volume in the first peak (bubbles with a diameter between 120 and $200\mu m$) compared to the flow condition. This indicates that the size of the bubbles become bigger in a flow condition compared to a no flow condition. This is contrary to the expectation. A possible explanation could be the limiting bubble detection for small bubbles. The video footage shows that there are smaller bubbles, however those cannot be measured by the MATLAB script or by hand due to the lack of resolution.

4.1.7 Gas production

The gas fraction is calculated based on the found bubble size distribution. It is expected that the gas fraction should increase in a linear way with the current density. The duplicate results for 5wt%, 20°C and no flow conditions are shown in Figure 4.12. The gas fractions in duplicate are close to each other. However, since the liquid velocity is varying in the elctrochemical cell in a no flow condition (see section 4.2.1) the gas fraction is not a reliable parameter. So in this section the findings are shown, however no conclusion are made based on these results.

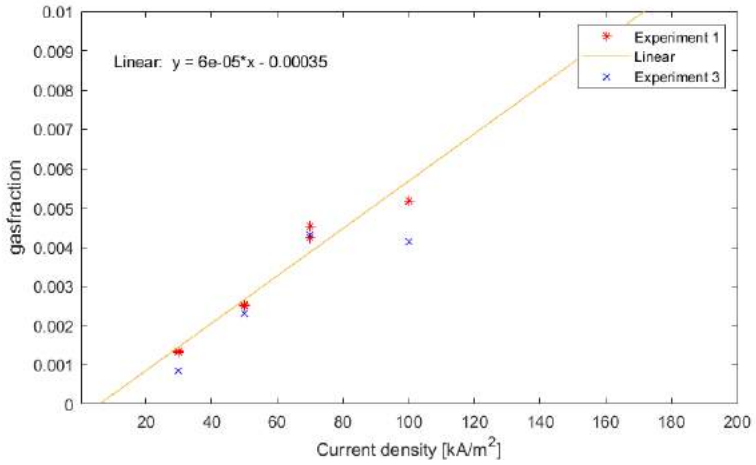

Figure 4.12: *The gas fraction in duplicate over the current density at* $20°C$*,* $20wt\%$ *and no flow condition. The linear regression line is based on experiment 1.*

Despite the gas fraction depending on the dimensions of the electrochemical cell, the measured gas fraction is too low compared to the results of Haug et al. They measured a gas fraction of 0.1 for the hydrogen bubbles at a current density around $100\frac{A}{m^2}$ for 28.6 wt% at $80°C$ [7]. This is 20 times higher than the measured gas fraction. A possible reasons for this could be that the gas fraction is not equal over the width of the electrochemical cell. If this were the case: a lot of gas bubbles slip via the sides of the electrochemical cell (the area where the bubble size distribution is not measured) and the real gas fraction would be higher than the measured gas fraction.

According literature the solubility of the gases decreases as the temperature increases and as the KOH concentration increases [7]. At a lower solubility, it is expected that more gas volume is measured. This is also measured for the concentration difference in the current research (see Figure 4.13). However, the temperature effect seems to have the opposite effect (see Figure 4.14).

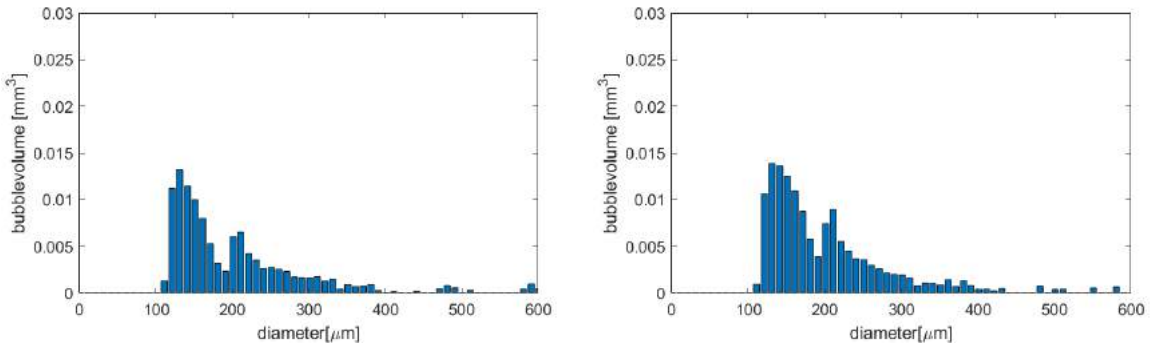

(a) *KOH concentration of* $50wt\%$ (b) *KOH concentration of* $20wt\%$

Figure 4.13: *Concentration effect on the gas volume.*

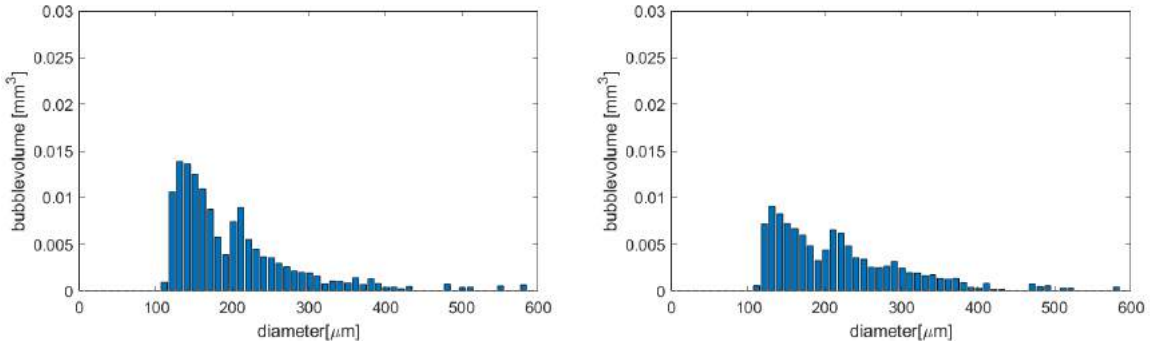

(a) *Temperature of* $20°C$ (b) *Temperature of* $50°C$

Figure 4.14: *Temperature effect on the gas volume.*

4.2 Design gas-liquid separator

One of the goals in this research is to find the optimal design of the gas-liquid separator. The results are discussed in this section. In Section 4.2.1 the theoretical bubble rising velocity is compared with the experimental data. In Section 4.2.2 the effect of the outlet barrier is shown. In Section 4.2.3 the estimation of the size of the gas-liquid separator is shown.

4.2.1 Rising velocity

The rising velocity is determined theoretically and experimentally. The results for hydrogen bubbles at 20 °C and 20 wt% are shown in Figure 4.15. The theoretical rising velocity matches relatively well with the experimental rising velocity. The theoretical values are a bit lower than the experimental results. This could be explained by the liquid flow which is caused by the gas lifting effect. The more gas bubbles are formed, the more liquid is pushed up by the bubbles, which results in a higher liquid flow. Since the gas bubble flow is not constant, the liquid flow is also not constant. This result is also found for 20 °C, 5wt% and no flow condition which is shown Appendix P.

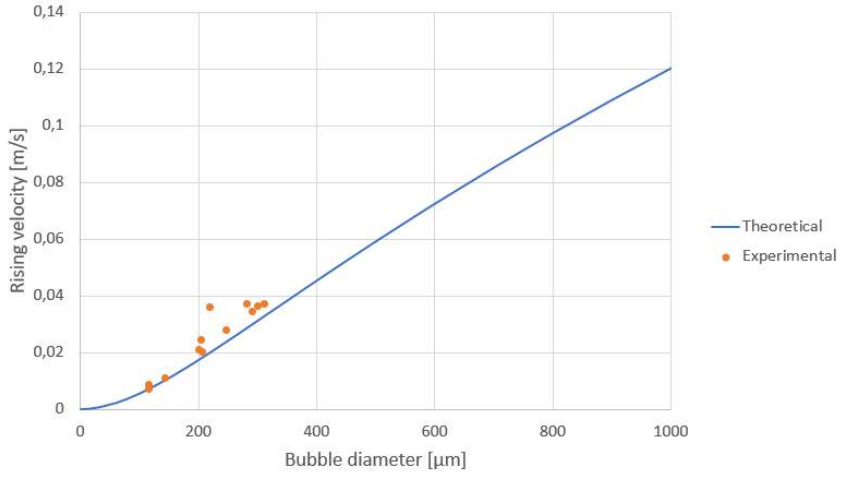

Figure 4.15: *The theoretical bubble rising velocity compared to the experimental rising velocity at* $20°C$ *and* $20wt\%$.

4.2.2 Effect of the barrier at the outlet device

The bubble size distribution is also measured before and after the outlet device at 20 °C, 20wt% and no flow condition. This is investigated for the hydrogen and oxygen bubbles at 30 and $50\frac{A}{m^2}$. The results of the hydrogen bubbles at a current density of $30\frac{A}{m^2}$ are shown in Figure 4.16. Before the barrier there are more bubbles with a diameter between 120 and $200\mu m$ compared to the bubbles after the barrier. This shows that at 20 wt% still coalescence happens. Under different conditions comparable results are obtained. These are shown in Appendix Q. Since there is coalescence happening at the outlet device, it is found that the size of the bubbles in the electrochemical cell are smaller than the size of the bubbles at the inlet of the gas-liquid separator. Therefore, it is recommended for sizing the gas-liquid separator to analyse the bubble size distribution at the inlet of the gas-liquid separator.

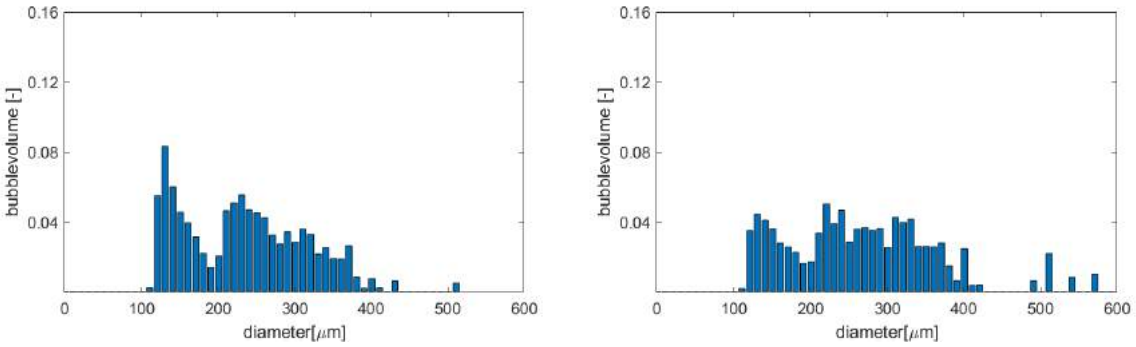

(a) *Before the outlet device* (b) *After the outlet device*

Figure 4.16: *Effect of barrier in the outlet device on the normalized bubble size distribution for the hydrogen bubbles at* $50\frac{A}{m^2}$, $20°C$, *20 wt% and no flow condition.*

4.2.3 Sizing the horizontal gas liquid separator

In this section the required size of the gas-liquid separator is estimated. First, the found bubble size distribution is converted to a reversed accumulative gas volume over the minimum bubble diameter (see Figure 4.17). This is only done for the hydrogen side, since there is no significant difference measured between the hydrogen and oxygen bubbles.

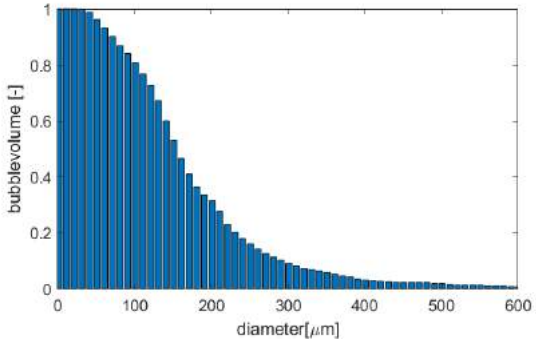

Figure 4.17: *The reversed accumulated gas fraction over the bubble diameter for hydrogen bubbles (bubble diameter of* $30\mu m$ *to* $600\mu m$*) at* $50\frac{A}{m^2}$, $20wt\%$, $20°C$, *and no flow condition. This graph is made based on the bubble size distribution shown in Figure 4.6b.*

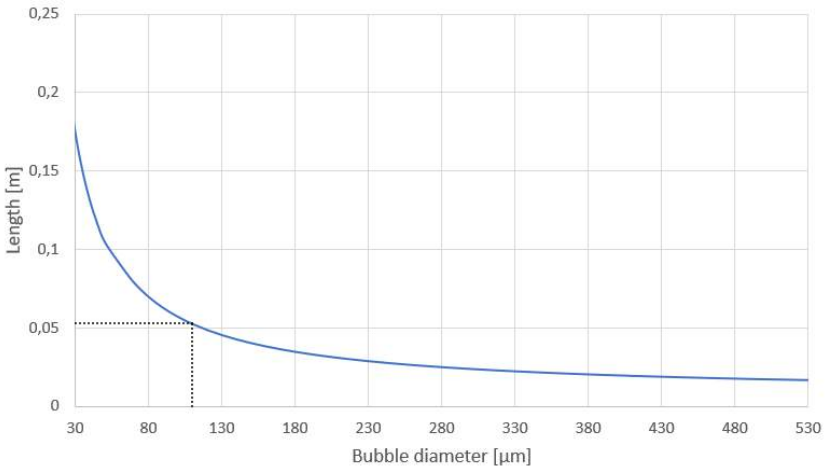

Figure 4.18: *The theoretical size of the gas-liquid separator based on the minimum bubble diameter with a* $\frac{L}{D}$ *ratio of 5. To remove a bubble of* $110\mu m$ *the size of the required length of the gas-liquid should be at least* $5cm$*.*

In the current process design it is important to remove the gases completely from the electrolyte before both streams of the electrolytes are combined and recycled to the electrochemical cell. When not all of the gases are removed a high flammable mixture could be obtained over time. In the case of removing all the gases the gas-liquid separator has to be oversized. In Figure 4.17 it has already been shown that for both gases bubbles with a minimum bubble diameter of $30\mu m$ are measured. In this case a separator length of $18cm$ is needed (see Figure 4.18). However, the bubbles could be smaller and so the minimum size of the gas-liquid separator should become bigger since the minimum bubble diameter which could be measured is equal to a bubble diameter of $30\mu m$.

Another option could be that the H_2-liquid and the O_2-liquid mixtures are not combined by adding an extra pump in the system. In this case the gas-liquid separators could become smaller. For example when $80volume\%$ has to be removed from the liquid mixture, for the removal of both the oxygen and hydrogen the separators have to have a length of $5cm$. But for a proper estimation of the gas volumes, it is important to better understand the bubble behavior of the bubbles with a bubble diameter smaller than $120\mu m$.

5 | Conclusion and Recommendations

The focus of this research was to get a better understanding of the bubble behavior in the electrochemical cell. In this way the resistance in the electrochemical cell could be understood better and the design of the gas-liquid separator could be estimated. In this chapter the final conclusions are given with some recommendations for further research.

5.1 Conclusion

In this research the bubble size distribution of bubbles with a minimum bubble diameter of $120\mu m$ are visualised and analysed by a MATLAB script. This has led to the following conclusions:

- A bimodal bubble size distribution is found at a current density of $50\frac{A}{m^2}$ with a volume peak of bubbles with a bubble diameter between 120 and $200\mu m$ and a volume peak of bubbles with a bubble diameter between 200 and $400\mu m$ is found.
- The (close to) zero-gap configuration of the electrochemical cell causes an extra volume peak of bubbles with a bubble diameter between 200 and $400\mu m$ due to the presence of a small gap between the electrode and the diaphragm and the electrode holes.
- Increasing the current density, the number of hydrogen bubbles with a smaller diameter than $200\mu m$ increases, especially for the 20 wt% which becomes a unimodal distribution at current densities higher than $70\frac{A}{m^2}$. The temperature have no significant influence affect.
- There is no significant difference measured between the size of the hydrogen and oxygen bubbles.
- The effect of the superficial inlet velocity cannot be determined because of the lack of resolution of the pictures. Bubbles smaller than $120\mu m$ should be quantified for a better understanding of this effect.

Moreover, based on the bubble size distribution, the design of the gas-liquid separator could be estimated:

- The required size of the (horizontal) gas-liquid separator is larger than the estimated gas-liquid size based on the measured bubble size distribution due to coalescence of the small bubbles before the gas-liquid mixture enters the gas-liquid separator.
- To estimate the size of the gas-liquid separator, the resolution of the pictures has to be increased.

5.2 Recommendations

In this research it is found that the bubble volume that could not be measured is around 20 to 30 volume percentage. It is recommended for future research to improve the visualisation technique. The current

high speed camera has a resolution of 1 megapixel and a lens with a magnification of 2 times is used. One option to improve the visualisation is to use a high speed camera with a higher resolution and to use the same lens. Another option is to use a lens with a higher magnification. In both cases the bubbles with a smaller diameter can be measured with the MATLAB script of this project. The advantages of measuring the smaller bubbles would be:

- To explain the bubble size distribution in more detail.
- The effect of the current density, gas type, superficial inlet velocity, temperature and KOH concentration on the smaller bubbles could be investigated.
- The size of the gas-liquid separator could be estimated. However, in this research, the bubble size distribution is determined inside the electrochemical cell. After measuring the bubble size, the bubble could grow due to coalescence. Therefore, it is recommended to investigate the bubble size distribution also at the inlet of the gas-liquid separator. This prevents the gas-liquid separator is oversized. It is also recommended to check the experimental rising velocity at the gas-liquid separator. In this case the flow caused by air lifting, does not influence the rising velocity anymore.

To understand the bubble detachment better, it could be interesting to investigate the contact angle of the bubble with the electrode. In the current research it expected that the volume peak of bubbles with a bubble diameter between 120 and $200\mu m$ could be explained by the force balance of the bubble detachment. In this case the contact angle for a bubble diameter of $130\mu m$ should be between 7 to 20 $^\circ$. If the experimental data does not match with the theoretical data, it would also be good to investigate the advancing, receding angle and bubble contact area radius since these values are assumed.

It is found that the gas volume peak with a bubble diameter between 200 and $300\mu m$ is caused by the gap in between the electrode and the diaphragm. For future research it would also be interesting to investigate if the location of the peak is dependent on the gap in between the electrode and the diaphragm. This gap could be monitored by 3D printing a piece which could be placed in between. Moreover, it could be investigated if the hole density of the perforated plates influence the location of the volume peak.

It is recommended for further research to use a conductivity meter in the process. The advantages of this conductivity meter would be:

- By using the bubble size distribution, the gas fraction could be measured. To check if all the bubbles are measured, it would be good to measure the gas fraction in different way. This could be done by placing the conductivity meter at the outlet of the electrochemical cell.
- In this research it is found that the KOH concentration changes over time. By adding a conductivity meter, the change in conductivity and so the change in KOH concentration could be monitored.

Furthermore, it would be interesting to investigate the behavior of the diaphragm in detail. During this research it was noticed that the bubble behavior is different when the diaphragm is soaked in the electrolyte for a shorter time. In this case the bubbles were stuck at the electrode. It is recommended to investigate this behavior in more detail.

List of Symbols

Symbols

d_b	Diameter gas bubble	m
d_{cell}	Depth cell	m
g	Gravity acceleration	$\frac{m}{s^2}$
h	Liquid height	m
i	Current	A
n	Number of electrons	$mole^-$
m_b	Mass of the gas bubble	kg
m_l	Mass of the liquid	kg
r	Circular contact radius of the bubble	m
v_g	Gas velocity	$\frac{m}{s}$
v_l	Liquid velocity	$\frac{m}{s}$
v_r	Rising velocity	$\frac{m}{s}$
v_{rel}	Relative velocity of the bubble	$\frac{m}{s}$
v_t	Liquid droplet settling velocity	$\frac{m}{s}$
A_l	Flow area of the liquid	m^2
A_{ves}	Total flow area of the vessel	m^2
D	Diameter gas-liquid separator	m
F	Faraday constant	$\frac{sA}{mol}$
F_b	Bouyancy force	Pa
F_d	Drag force	Pa
F_g	Gravitational force	Pa
$F_{s,x}$	Surface tension force (x-direction)	Pa
L	length of the separator	m
Mn_g	Molar mass of the gas component	$\frac{kg}{mol}$
Q_l	Volumetric flow rate	$\frac{m^3}{s}$
Q_{v_g}	Volumetric gas production	$\frac{m^3}{s}$
R	Radius gas bubble	m

Greek symbols

α	Advancing angle	rad
β	Receding angle	rad
θ	Contact angle	rad
θ'	Deviation of the contact angle	rad
λ	Mean	μm
μ_g	Gas viscosity	Pas
μ_l	Liquid viscosity	Pas
ρ_l	Density liquid	$\frac{kg}{m^3}$
ρ_g	Density gas	$\frac{kg}{m^3}$
σ_{sur}	Surface tension	$\frac{N}{m}$
σ	Standard deviation	μm
$\tau_{g,actual}$	Actual residence time of the gas	s
$\tau_{g,necessary}$	Necessary residence time of gas	s
$\tau_{l,actual}$	Actual residence time of the liquid	s
$\tau_{l,necessary}$	Necessary residence time of liquid	s

Dimensionless number

f	Friction factor
h^*	Relative liquid height
h_i	Height of the inlet
h_l	Liquid height
A^*	Relative surface area
Re	Reynolds number

Abbreviations

fps	frames per second
$ln.$	line
TU/e	Technical University Eindhoven

Bibliography

[1] H. A. Jakobsen, *Chemical Reactor Modeling*, 2nd ed. Trondheim: Springer, 2014.

[2] A. Kerkhof, "Towards a hydrogen economy," *The Electricity Journal*, vol. 18, no. 6, pp. 63–76, 2005.

[3] M. Mohamedali, A. Henni, and H. Ibrahim, "Hydrogen Production from Oxygenated Hydrocarbons: Review of Catalyst Development, Reaction Mechanism and Reactor Modeling," in *Hydrogen Production Technologies*, Canada, 2017, ch. 1, pp. 1–76.

[4] F. Hine, *Electrode Processes and Electrochemical Engineering*. New York: Springer Science & Business Media, 1985.

[5] G. Gahleitner, "Hydrogen from renewable electricity: An international review of power-to-gas pilot plants for stationary applications," *International Journal of Hydrogen Energy*, vol. 38, no. 5, pp. 2039–2061, 2013. [Online]. Available: http://dx.doi.org/10.1016/j.ijhydene.2012.12.010

[6] J. Brauns and T. Turek, "Alkaline water electrolysis powered by renewable energy: A review," *Processes*, vol. 8, no. 2, 2020.

[7] P. Haug, B. Kreitz, M. Koj, and T. Turek, "Process modelling of an alkaline water electrolyzer," *International Journal of Hydrogen Energy*, vol. 42, no. 24, pp. 15 689–15 707, jun 2017. [Online]. Available: http://dx.doi.org/10.1016/j.ijhydene.2017.05.031https://linkinghub.elsevier.com/retrieve/pii/S0360319917318633

[8] M. Schalenbach, M. Carmo, D. L. Fritz, J. Mergel, and D. Stolten, "Pressurized PEM water electrolysis: Efficiency and gas crossover," *International Journal of Hydrogen Energy*, vol. 38, no. 35, pp. 14 921–14 933, 2013.

[9] V. Schröder, B. Emonts, H. Janßen, and H. P. Schulze, "Explosion limits of hydrogen/oxygen mixtures at initial pressures up to 200 bar," *Chemical Engineering and Technology*, vol. 27, no. 8, pp. 847–851, 2004.

[10] D. M. Santos, C. A. Sequeira, and J. L. Figueiredo, "Hydrogen production by alkaline water electrolysis," *Quim. Nova*, vol. 36, no. 8, pp. 1176–1193, sep 2013. [Online]. Available: http://ieeexplore.ieee.org/document/8125843/

[11] G. J. Hwang, B. M. Gil, and C. H. Ryu, "Preparation of the electrode using NiFe2O4 powder for the alkaline water electrolysis," *Journal of Industrial and Engineering Chemistry*, vol. 48, pp. 242–248, 2017. [Online]. Available: http://dx.doi.org/10.1016/j.jiec.2017.01.011

[12] A. Nidola, "Water electrolysis in alkaline solutions. New electrode materials," *International Journal of Hydrogen Energy*, vol. 9, no. 5, pp. 367–375, 1984.

[13] F. Gutmann and O. J. Murphy, "Electrochemical Splitting of Water." in *Modern Aspects of Electrochemistry*. Texas: Department of Chemistry, Texas A&M University, 1983, no. 15, ch. 1, pp. 1–82.

[14] H. Wendt and G. Kreysa, *Electrochemical engineering: science and technology in chemical and other industries.* Springer Science & Business Media, 1999.

[15] C. Sillen, "The effect of gas bubble evolution on the energy efficiency in water electrolysis," Ph.D. dissertation, Technical University Eindhoven, 1983.

[16] D. Zhang and K. Zeng, "Evaluating the behavior of electrolytic gas bubbles and their effect on the cell voltage in alkaline water electrolysis," *Industrial and Engineering Chemistry Research*, vol. 51, no. 42, pp. 13 825–13 832, 2012.

[17] L. J. Janssen, C. W. Sillen, E. Barendrecht, and S. J. van Stralen, "Bubble behaviour during oxygen and hydrogen evolution at transparent electrodes in KOH solution," *Electrochimica Acta*, vol. 29, no. 5, pp. 633–642, 1984.

[18] V. S. Craig, B. W. Ninham, and R. M. Pashley, "The effect of electrolytes on bubble coalescence in water," *Journal of Physical Chemistry*, vol. 97, no. 39, pp. 10 192–10 197, 1993.

[19] P. Van Der Linde, P. Peñas-López, Á. Moreno Soto, D. Van Der Meer, D. Lohse, H. Gardeniers, and D. Fernández Rivas, "Gas bubble evolution on microstructured silicon substrates," *Energy and Environmental Science*, vol. 11, no. 12, pp. 3452–3462, 2018.

[20] J. Eigeldinger and H. Vogt, "The bubble coverage of gas-evolving electrodes in stagnant electrolytes," *Electrochimica Acta*, vol. 45, pp. 4449–4456, 2000.

[21] R. Bird, W. Stewart, and E. Lightfoot, *Transport Phenomena*, 2nd ed., R. Brid, W. Stewart, and E. Lightfoot, Eds. United States of America: John Wiley & Sons, Inc, 1924.

[22] G. Duhar and C. Colin, "Dynamics of bubble growth and detachment in a viscous shear flow," *Physics of Fluids*, vol. 18, no. 7, 2006.

[23] Y. Li, G. Yang, S. Yu, Z. Kang, J. Mo, B. Han, D. A. Talley, and F. Y. Zhang, "In-situ investigation and modeling of electrochemical reactions with simultaneous oxygen and hydrogen microbubble evolutions in water electrolysis," *International Journal of Hydrogen Energy*, vol. 44, no. 52, pp. 28 283–28 293, 2019. [Online]. Available: https://doi.org/10.1016/j.ijhydene.2019.09.044

[24] K. Buist, *FTV HC5 BERNOULLI (NON IDEAL)*, 2017.

[25] J. J. Jasper, "The Surface Tension of Pure Liquid Compounds," *Journal of Physical and Chemical Reference Data*, vol. 1, no. 4, p. 948, 1972.

[26] H. Matsushima, Y. Fukunaka, and K. Kuribayashi, "Water electrolysis under microgravity. Part II. Description of gas bubble evolution phenomena," *Electrochimica Acta*, vol. 51, no. 20, pp. 4190–4198, 2006.

[27] G. H. Yeoh, S. C. Cheung, J. Y. Tu, and M. K. Ho, "Fundamental consideration of wall heat partition of vertical subcooled boiling flows," *International Journal of Heat and Mass Transfer*, vol. 51, no. 15-16, pp. 3840–3853, 2008.

[28] T. Ziegenhein, "Fluid dynamics of bubbly flows," Ph.D. dissertation, 2016.

[29] B. Guo and A. Ghalambor, "Separation," in *Natural Gas Engineering Handbook*. Elsevier, 2005, ch. 7, pp. 113–141. [Online]. Available: https://linkinghub.elsevier.com/retrieve/pii/B9781933762418500149

[30] M. Stewart and K. Arnold, *Gas-Liquid and Liquid-Liquid separators*, Intergovernmental Panel on Climate Change, Ed. Oxford: Gulf Professional Publishing, 2008. [Online]. Available: https://www.cambridge.org/core/product/identifier/CBO9781107415324A009/type/book{_}part

[31] Shell Global Solutions International, "Gas/Liquid Separators - Type Selection and Design Rules," vol. 2007, p. 88, 2007.

[32] M. Aula, J. Haapakangas, A. Heikkila, and M. Iljana, *Some Environmental Aspects of BF, EAF and BOF*, R. Keisk, Ed. Oulu: University of Oulu, Faculty of Technology, Department of Process and Environmental Engineering, 2012, no. August.

[33] I. Naderipour and J. Khorshidi, "Design of Vertical Gas-Liquid Separator and Examination its Effective Parameters in Sarkhoun & Qeshm Treating Company," *Journal of Basic and Applied Scientific Research*, vol. 2, no. 7, pp. 6986–6994, 2012.

[34] VIADUX, "Chemical Resistance Guide," Tech. Rep.

[35] J. Telleen, A. Sullivan, J. Yee, O. Wang, P. Gunawardane, I. Collins, and J. Davis, "Synthetic Shutter Speed Imaging," *EUROGRAPHICS*, vol. 26, no. 3, pp. 592–598, 2007.

[36] P. Granados Mendoza, "Intensification of the chlor-alkali process using a rotorstator spinning disc membrane electrochemical reactor," Ph.D. dissertation, Eindhoven University of Technology, Eindhoven, 2016.

[37] MathWorks, "Detect and Measure Circular Objects in an Image," 2016. [Online]. Available: http://uk.mathworks.com/help/images/examples/detect-and-measure-circular-objects-in-an-image.html

[38] P. Chandran, S. Bakshi, and D. Chatterjee, "Study on the characteristics of hydrogen bubble formation and its transport during electrolysis of water," *Chemical Engineering Science*, vol. 138, pp. 99–109, 2015. [Online]. Available: http://dx.doi.org/10.1016/j.ces.2015.07.041

[39] Wallevik, O., H. J. Fell, and P. Chladek, "Electrolyser frame concept, method and use." 2017.

[40] J. H. Zheng, *Transport Phenomena*, J. H. Zheng, Ed. Rijeka, Croatia: intechOpen, 1924.

[41] S. Dehaeck, H. Van Parys, A. Hubin, and J. P. Van Beeck, "Laser marked shadowgraphy: A novel optical planar technique for the study of microbubbles and droplets," *Experiments in Fluids*, vol. 47, no. 2, pp. 333–341, 2009.

Appendix

A | Bubble shape

The shape of the bubble is important to determine the motion of the bubbles [28]. During the visualisation the shape of the bubble will be visualised. In this appendix the shape of the bubbles will be discussed based on the theoretical expectation. The shape of the bubbles is correlated by the Grace Diagram on the Reynolds number, the Eotvos number and the Morton number as shown in Figure A.1.

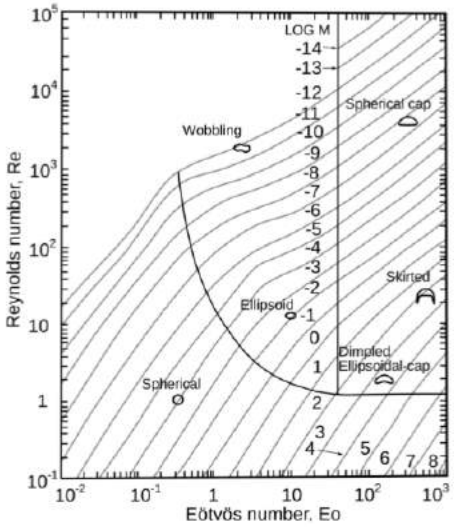

Figure A.1: *Grace Diagram [28]. A map of bubble shapes depending on the Reynolds number, Eotvos number and the Morton number.*

The Reynolds number is defined as follows:

$$Re = \frac{\rho_l v_{rel} d_b}{\mu_l} \tag{A.1}$$

For Reynolds numbers lower than 1 the gas bubbles are always spherical. However the shape of the bubble at higher Reynolds numbers is depending on the Eotvos number and the Morton number. The Eotvos number and the Morton number are defined as shown in Equation A.2 and A.3.

$$E_o = \frac{(\rho_l - \rho_g) g d_b^2}{\sigma} \tag{A.2}$$

$$M = \frac{(\rho_l - \rho_g) g \mu_l^4}{\rho_l^2 \sigma^3} \tag{A.3}$$

B | Cell design

In this appendix the design of the electrochemical cell is shown. The electrochemical cell is printed by a 3D printer with ABS as matarial. The design is shown in Figure B.1. At the bottom the electrolyte enters the electrochemical cell. The electrolyte is equally distributed over the electrode via the inlet device. At the electrode the reaction takes place and via the outlet device the fluid leaves the electrochemical cell. To prevent leakages there is a sealing. Below each part of the cell will be discussed in more detail

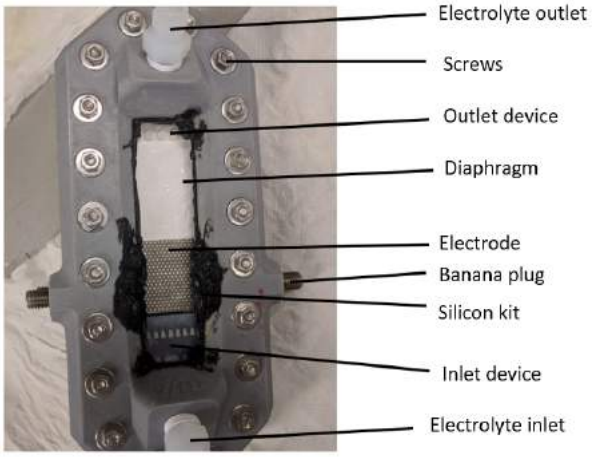

Figure B.1: *Cell design. All the parts of the cell are named.*

- *Diaphragm*
  In this research a ZIRFON PERL UTP 500 diaphragm is used as diaphragm. The diaphragm permeates the OH^- ions, but prevents permeation of the gases. This diaphragm is placed in the middle of the electrochemical cell and separates the anode and cathode side.

- *Inlet device*
  The inlet device is placed on both sides of the cell. The function of the inlet device is to distribute the electrolyte equally over the electrode. During this research the shape of this inlet device is only tested with a floXpress function in SolidWorks. In this simulation it is assumed that the electrolyte behaves like water and the gravity forces are not taken into account. The results are shown in Figure B.2b. To prevent that the main flow only flows through the middle, in the first row of blocks the blocks in the middle are bigger than close to the wall. The second row is added to make the distribution of the flow better. This inlet devices is 3D printed with ABS as material (see Figure B.2a).

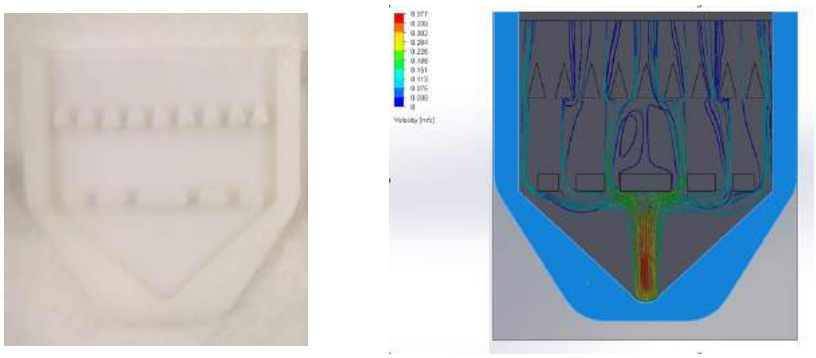

(a) *3D printed inlet device*

(b) Flow simulation

Figure B.2: *Inlet device electrochemical cell.*

- *Electrode and banana plugs*
  The electrode and banana plugs are also placed on both sides of the electrochemical cell. At the electrode the reaction takes place and the banana plugs are used to connect the electrode with the power supply. Round hole staggered perforated Nickel plates are used as electrodes with a hole diameter of 1 mm ($36\frac{holes}{cm^2}$) (see Figure B.3. Before placing the electrode in the electrochemical cell, the electrode is washed with iso-propanol and sequentially with demineralized water. To reach a zero-gap configuration the diaphragm is pressed in between the electrodes. The size of the electrode: Length x Width = $0.03m$ x $0.033m$. The power is supplied to the electrode by connecting the power supply to the banana plugs. When the electrode is placed and the banana plugs are tightened the banana plugs are connected with the electrodes.

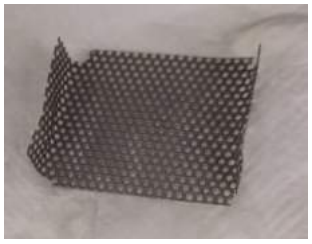

Figure B.3: *A round hole staggered perforated Nickel plate with a hole diameter of 1 mm (*$36\frac{Holes}{cm^2}$.

- *Outlet device*
  The outlet device is also placed on both sides of the electrochemical cell. The design of the outlet device is based on the design used in industry. Since during this research the bubbles are visualised at the outlet device of the elecotrochemical cell, it is opted for a longer distance to follow the bubbles compared to the inlet device of the electrohemical cell.

- *Sealing*
  To prevent leakages of the electrochemical cell sealing is added. This sealing consist of a O-ring (see Figure B.5b), two thin rubber (see Figure B.5a) and Silicon kit. The O-ring is placed only one side of the electrochemical cell and is designed in such a way that maximal 90% of the groove is filled with the rubber and has to be 20% oversized in relation to the groove. The thin rubbers are used to prevent the flow of the oxygen and hydrogen side from mixing. To prevent leakages through the glass window, silicon kit is added. Unfortunately, due to a damaged cell, leaking occurs. After some time this leakages increases that most probably influenced some results of Experiment 3.

  It is found that silicon kit is not a long term solution. This is tested by adding silicon kit on a glass window, which was placed in an electrolyte solution of 30 wt% for at least 2 months. Afterwards,

Figure B.4: *3D printed outlet device based on industrial design.*

the silicon kit was not attached to the window anymore.

(a) *Thin rubber.*

(b) *O-ring.*

Figure B.5: *Sealing. Two different types of sealing which were present in the electrochemical cell. (a) Sealing used to prevent that oxygen and hydrogen bubbles are mixing. (b) Sealing used to prevent leakages.*

In Figure B.6 the assembly of the cell is explained step by step. There are two different cell sides. First, the inlet device, the electrode and the outlet device are placed in each cell side; Then the sealing is placed in both cell sides. For one side this is only the thin rubber and on the other side an o-ring is also included. Sequentially the diaphragm is placed on one side. The cell sides are placed above each other and tightened. In this last step, the diaphragm is pressed between the electrodes. To reach a zero-gap configuration at the end, the banana plugs are tightened.

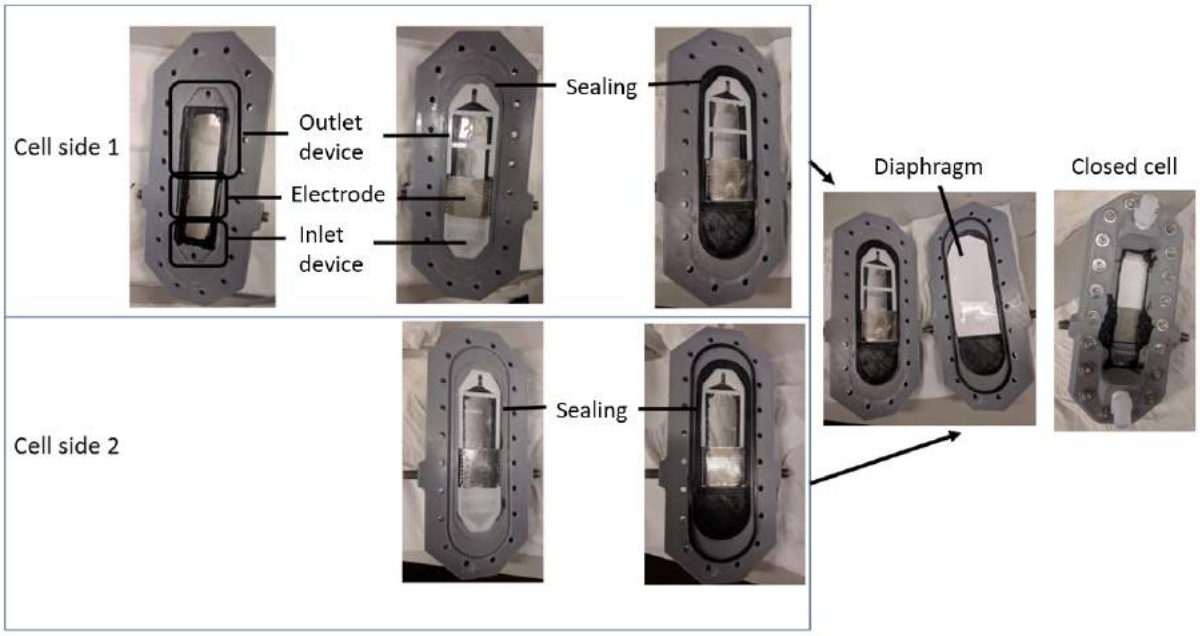

Figure B.6: *Closing the cel step by step.*

C | Visualisation

For the visualisation of the gas bubbles the light source, the type of window, the shutter speed and the camera type matters. Therefore, in this appendix each parameter is discussed.

Light source and light position
The light source is very important to make good pictures of the bubbles. When using front lighting, the position of the light source is relevant to minimise the effect of reflection and shadow, which can influence the measurement [40]. The shadow of a bubble will also be detected as a bubble in the MATLAB script. Therefore, to reduce the effect of the shadow an extra light source could be added. In Figure C.1a a picture is shown with front lighting. Inside the black circle a bubble is present. However, the disadvantage of front lighting is the corresponding shadow shown in the red circle.

In case of back-lighting only the contour of the bubbles is visable. The main disadvantage of back lighting is that the distance between the bubbles and the camera is not exactly known [41]. It shows the contour of each bubble between the camera and the light source and therefore the unfocused bubbles will not be visible on the picture. A result of back-lighting is shown in Figure C.1b . Here a bubble is black circled, but there is no shadow anymore. This makes the detection much easier.

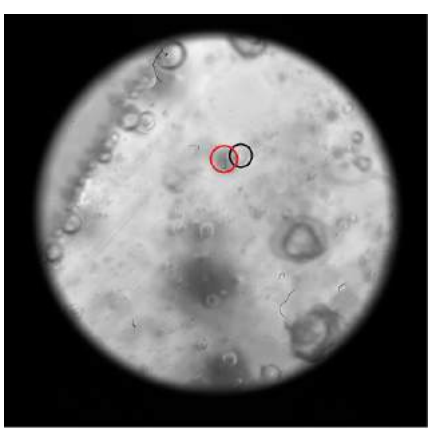

(a) *Front lighting with two light sources*

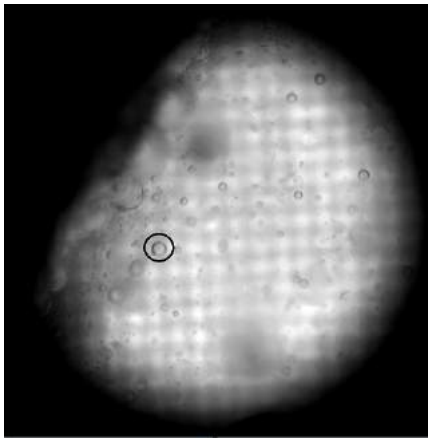

(b) *Back-lighting*

Figure C.1: *Influence of the light source on the bubble detection. (a) is for each bubble also a shadow of the bubble visible, while in (b) this is no problem anymore.*

Window material and depth of the cell
To start, an epoxy window was used in order to make the bubbles visible. However, the epoxy window became less clear over time probably due to corrosion (C.2a). Therefore, the epoxy window was replaced by glass. For this replacement, it was also decided to reduce the depth of the cell from 5 to $2mm$ to reduce the chance for bubbles to be not detected. To attach the glass at the electrochemical cell, Silicone kit is used. In Figure C.2b the result of the glass window is shown. Both pictures in Figure C.2 are at the hydrogen side at $10\frac{A}{m^2}$, an electrolyte close to $5wt\%$, a superficial inlet velocity of $0.02\frac{m}{s}$ and at room temperature.

It could be noticed that the contours of the bubbles became more clear, which makes it easier to detect the bubbles. Furthermore, more bubbles are visual. A reason for this is that the focus of the camera is much better since the depth of the cell is much lower. Furthermore, it was noticed that some bubbles were stuck in between the diaphragm and the glass. The reason for this behavior is not known yet.

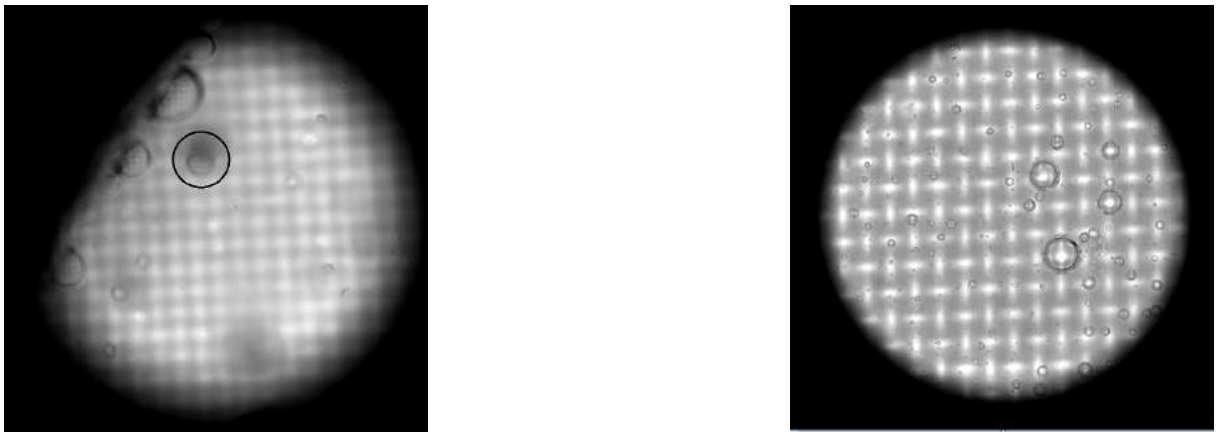

(a) *Epoxy window* (b) *glass window*

Figure C.2: *Influence of the glass window on the visualisation. The contours of the bubbles in (b) are more clear than in (a).*

Shutter speed

The shutter speed of the camera is also important for the visualisation of the bubble size distribution. At a longer shutter speed the pictures of a moving object could be more blurry, than at a shorter shutter speed. [35]. For a shorter shutter speed, more light is necessary to prevent noise. At the TU/e there were different camera's with several shutter speeds available.

The Dino-Lite microscope 'DinoCapture 2.0' the maximum shutter speed was $\frac{1}{30}$ s. It was noticed that a shutter speed of $\frac{1}{30}$ s was much to short to obtain a sharp picture of the moving bubble, as shown in figure C.3a. Only the bubbles which were stuck are clearly visible.

The high speed camera 'FastCam mini AX200' and the Nikon COOLPIX A900 the shutter speed could be much shorter. At a shutter speed of $\frac{1}{1000}s$ the bubbles were not blurry anymore.

(a) $\frac{1}{30}s$ (b) $\frac{1}{1000}s$

Figure C.3: *Influence of the shutter time on the visualisation. In (a) the moving bubbles are more blurry compared to (b).*

Camera type
There were two different types of camera's which could be used (shutter speed $\frac{1}{1000}s$). In Figure C.4 the pictures of the 1mm hole diameter perforated plate with the different camera's are shown.

- FastCam mini AX200: This camera is a high speed camera with 1024 x 1024 pixels, which could go up to 6400 frames per second (fps). This camera could be used with different lenses. Below the different lenses are discussed.
  - Edmund Optics Telecentric Lens 2.0X TML-HP - This lens has a fixed magnification of 2 times and has no zoom option. There are 100 pixels measured per mm. It is decided to use this lens during the research.
  - Zoom 7000 Macro Lenses - This lens has a magnification of 1.1x and a zoom of 6x. However, since the lens has a minimal focal length of 13 cm, there are only 60 pixels per mm. Therefore, it is decided not to use this lens during the research.
  - Nikon af micro nikkor 60mm f/2.8d - This lens has a magnification of 1x and a zoom of 32 x . Due to the zoom function, the number of pixels per mm were not always exact predictable but they were about $115\frac{pixels}{mm}$. Due to uncertainly of the exact number of pixels per mm, it is decided to use 'Edmund Optics Telecentric Lens 2.0X TML-HPs' since it is not a lot of difference in number of pixels which could be measured.
- Nikon COOLPIX A900 - This is a digital photo camera with 35x optical zoom with 21 Megapixels. Due to applying zoom, the focus distance becomes bigger. Due to the zoom function, the number of pixels per mm were not always exact predictable but they were about $100\frac{pixels}{mm}$. Due to uncertainly of the exact number of pixels per mm, it is decided to use 'Fastcam mini AX200' since it is not a lot of difference in number of pixels which could be measured.

(a) *'FastCam mini AX200-Edmund Optics Telecentric Lens 2.0X TML-HP'*

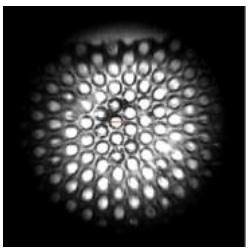

(b) *FastCam mini AX200- Zoom 7000 Macro Lenses*

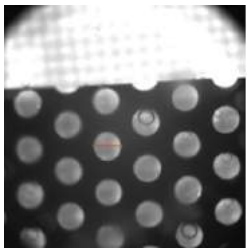

(c) *FastCam mini AX200- Nikon af micro nikkor 60mm f/2.8d*

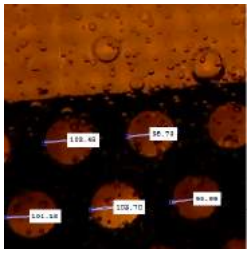

(d) *Nikon COOLPIX A900*

Figure C.4: *Influence of the camera type. (a) has a resolution of* $100\frac{pixels}{mm}$*, (b) has a resolution of* $60\frac{pixels}{mm}$*, (c) has a resolution of* $115\frac{pixels}{mm}$ *and (d) has a resolution of* $100\frac{pixels}{mm}$.

D | Electrolyte change over time

It was noticed that the bubble size distribution changes over time (Figure D.1). This behavior is checked with the conductivity of the electrolyte. The conductivity decreases from 191 to $174\frac{mS}{cm}$ which corresponds to a change in KOH concentration from 5 to $4.5wt\%$.

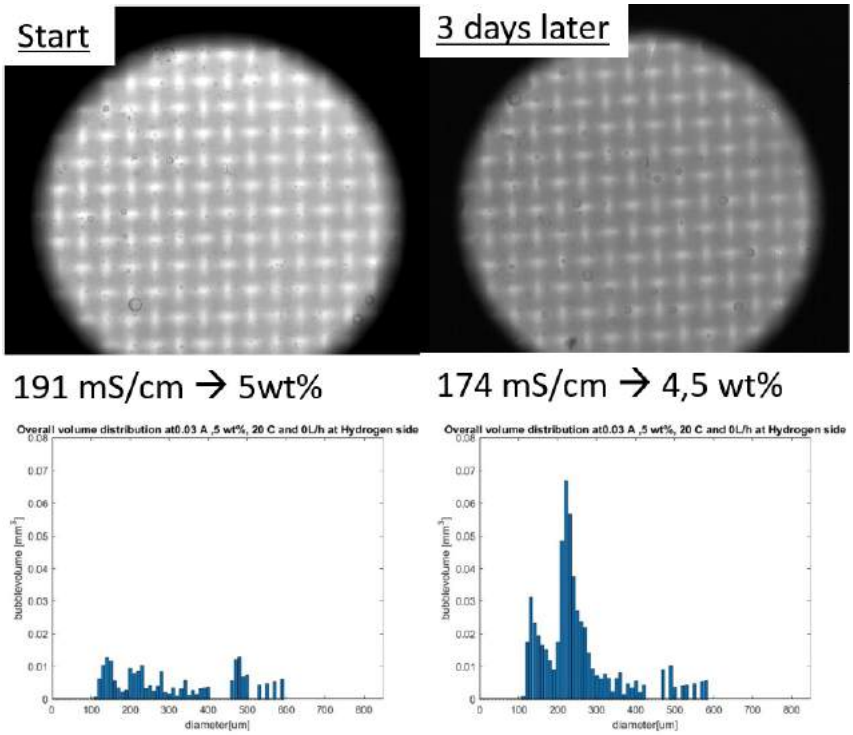

Figure D.1: *Bubble size distribution changed over time. There was more gas volume measured when the electrolyte is already used for 3 days and the conductivity of the electrolyte decreases. This decrease is correlated to a change of KOH concentration from 5 to 4.5 wt%.*

The conductivity could be changed due to the reaction of CO_2 and KOH to form K_2CO_3 and H_2O. It was noticed that the effect of the conductivity change is smaller when Nitrogen is flushed through the system. Possible reasons for the change in bubble size distribution could be:

- At a lower KOH concentration the bubble size distribution is effected a lot. (In the future this could be tested by doing experiments at lower KOH concentrations.)
- Due to the presence of K_2CO_3 the bubble behavior changes. (In the future this could be tested by doing experiments with a K_2CO_3 solution.)

This is not investigated during this research. During this research the electrolyte is renewed after using a solution during 2 days.

E | Matlab script - Bubble detection

```
close all; clc; clear
%% variable parameters_side
%These settings could be different for each set of pictures. So be aware of
%that and check these parameters before running the script .

%Type of gas H for hydrogen and O for oxygen
type_of_gas= 'O';

% parameters electrochemical cell
width_outletdevice= 0.029; %m
depth_outlet= 0.002; %m
length_electrode= 0.033; %m
width_electrode=0.001/0.033; %m

%scale based on lens
distance_in_m=0.001;
distance_in_pixels=100;% add by yourself in this case a magnification of 2
distance_per_pixel_m=distance_in_m/distance_in_pixels;%m per pixel
distance_per_pixel_um= distance_per_pixel_m*10^6; %um per pixel

%% Specify the folder where the files live and specify the conditions.

%Select one folder witht the folders you want to analyse
folder='E:\master project\experiments\single analyses\test'
start_path = fullfile(folder);
if ~exist(start_path, 'dir')
        start_path = matlabroot;
end
% Ask user to confirm the folder, or change it.
uiwait(msgbox('Pick a starting folder on the next window that will come up.'));
topLevelFolder = uigetdir(start_path);
if topLevelFolder == 0
        return;
end

% Get list of all subfolders using genpath.  It will be one long string
% with folders separated by a semicolon.
allSubFolders = genpath(topLevelFolder);
% Let's extract all the folders into individual cells in a cell array.
% That will be easier to use when we need to get the folder name in a loop.
listOfFolderNames = strsplit(allSubFolders, ';');
% Strsplit() seems to give an empty string for the last one.  Get rid of
%any empty folder names.
emptyCells = cellfun(@isempty, listOfFolderNames);
listOfFolderNames = listOfFolderNames(~emptyCells);
numberOfFolders = length(listOfFolderNames);
%analyse each folder separate.
fprintf('The total number of folders to look in is %d\n', numberOfFolders);
for k = 1 : numberOfFolders
        % Get this folder and print it out.
```

```
        thisFolder = listOfFolderNames{k};
        fprintf('Looking inside folder %s\n', thisFolder);

% This if loop prevents that the main folder is analysed.
if size(folder,2)==size(thisFolder,2)==0
% empty arrays
radiustotal = [];
radiustotal_real = [];
centerstotal = [];
centerstotal_real = [];
numberofbubblesperpicturetotal = [];
numberofbubblesperpicturetotal_real = [];
gasvolumepictures=[];
gasvolumepicturetotal=[];
gasfraction = [];
p = [];
fps=[];
volumeflow=[];
temperature=[];
current=[];

%number of pictures analysed, start at 0
number_of_pictures=0;

% Get a list of all files in the folder with the desired file name pattern.
filePattern = fullfile(thisFolder, '*.bmp'); % Change to whatever pattern you need.
theFiles = dir(filePattern);
fullnamefile = fullfile(theFiles(1).name);

%parameters based on file name
namefile = sscanf(fullnamefile,'%d_wt_%g_A_%g_C_%g_Lh_%g_fps_H2side_C001H001S%d.bmp'
    );
fps=namefile(5); %framespersecond
volumeflow =namefile(4); %L/h
temperature =namefile(3); %C
current =namefile(2);%A
concentration= namefile(1); %M
currentdensity = current / (length_electrode* width_electrode);
velocity_outlet =((volumeflow/(60*60*1000))/(width_outletdevice*depth_outlet));%m/s
if velocity_outlet ==0
    velocity_outlet= 0.003831; %m/s
end

%% Specify the window and the timestep of detection and the sensitivity

%calculate the total volume liquid of the picture
rect = [210,210,570,570];%size cutting pictures[x,y,width,height]
lengthpicture= (rect(4))*distance_per_pixel_m; %m
widthpicture= (rect(3))*distance_per_pixel_m; %m
totalvolumepicture= widthpicture*lengthpicture*(depth_outlet);%m3

%calculate the number of frames in between the analysed frames.
necessary_time_in_between_frames = lengthpicture/velocity_outlet;%s
step_frame=fps*necessary_time_in_between_frames;

%Sensitivity of hydrogen
if volumeflow == 0
if current == 0.01
sensitivity = [0.89, 0.88, 0.88, 0.88];
end
if current == 0.03
sensitivity = [0.9, 0.88, 0.88, 0.88];
end
```

```
if current == 0.05
sensitivity = [0.91, 0.88, 0.88, 0.88];
end
if current == 0.07
sensitivity = [0.92, 0.88, 0.88, 0.88];
end
if current == 0.1
sensitivity = [0.92, 0.88, 0.88, 0.88];
end
if current == 0.2
sensitivity = [0.92, 0.88, 0.88, 0.88];
end
end

if volumeflow > 0
  if current == 0.01
sensitivity = [0.89, 0.88, 0.88, 0.88];
end
if current == 0.03
sensitivity = [0.89, 0.88, 0.88, 0.88];
end
if current == 0.05
sensitivity = [0.89, 0.88, 0.88, 0.88];
end
if current == 0.07
sensitivity = [0.89, 0.88, 0.88, 0.88];
end
if current == 0.1
sensitivity = [0.89, 0.88, 0.88, 0.88];
end
if current == 0.2
sensitivity = [0.89, 0.88, 0.88, 0.88];
end
end

%% run the script
for k = 1 : ceil(step_frame) : length(theFiles)
   number_of_pictures=number_of_pictures+1 ;

   %selecting the file
    baseFileName = theFiles(k).name;
    fullFileName = fullfile(theFiles(k).folder, baseFileName);
    fprintf(1, 'Now reading %s\n', fullFileName);

    % reading it in as an image array with imread()
    imageArray = imread(fullFileName);

    %cut the image in part that will be analysed
    imageArray = imcrop(imageArray,rect);

%measures and locates the bubbles at different pixel sizes (if you want to
%get rid of the warning, the pixels has to be higher than 6.
[centers, radii] = imfindcircles(imageArray,[6 16],'ObjectPolarity','dark', '
    Sensitivity',sensitivity(1));
[centers1,radii1] = imfindcircles(imageArray,[10 30],'ObjectPolarity','dark', '
    Sensitivity',sensitivity(2));
[centers2,radii2] = imfindcircles(imageArray,[23 50],'ObjectPolarity','dark', '
    Sensitivity',sensitivity(3));
[centers3,radii3] = imfindcircles(imageArray,[45 70],'ObjectPolarity','dark', '
    Sensitivity', sensitivity(4));

%All bubbles including the bubbles which were stuck
radiuspicture=[radii3;radii2;radii1;radii];
```

```
centerspicture= [centers3;centers2;centers1;centers];
[number_of_bubbles] = size(radiuspicture,1);

%for adjustments
radiuspicture_real=radiuspicture;
centerspicture_real= centerspicture;
[number_of_bubbles_real] = number_of_bubbles;

% prevent bubble detects twice with different radius.takes always the
% biggest bubble
double=[];
if number_of_bubbles_real >0
   for i = 1:number_of_bubbles_real
   double(:,i)=sum(abs(centerspicture_real-centerspicture_real(i,:)),2)<(
       radiuspicture_real(i,:));
   end
   a=find(sum(double,2)>1);
   c=size(a,1);
    if c>0
        d=[];
        e=[];
   for i = 1:c
   d=(find(double(a(i),:)))';
   e(i,1)= radiuspicture_real(a(i))~=max(radiuspicture_real(d));
   end
  radiuspicture_real(a(find(e)),:)=[];
  centerspicture_real(a(find(e)),:)=[];
 number_of_bubbles_real = size(radiuspicture_real,1);
end
end

if number_of_bubbles_real>0
%delete the bubbles which where stuck at the membrane for already 3
%pictures before.
if number_of_pictures>4
    p=[];
    q=[];
    s=[];
for i = 1:number_of_bubbles_real
    % output will be 0 when bubbles are at the same position as the current bubble
    % with a deviation of the radius of the current bubble.

    if sum(numberofbubblesperpicturetotal(1:(number_of_pictures-4)))>0

    %compared to the bubbles 3 pictures before
    s(i,1)=sum(sum(abs(centerstotal(sum(numberofbubblesperpicturetotal(1:...
    (number_of_pictures-4))):sum(numberofbubblesperpicturetotal(1:...
    (number_of_pictures-3))),:)-centerspicture_real(i,:)),2)<=radiuspicture_real(i))
        <1;
    else
        s=1;
    end

    %compared to the bubbles 2 pictures before
    if sum(numberofbubblesperpicturetotal(1:(number_of_pictures-3)))>0
p(i,1)=sum(sum(abs(centerstotal(sum(numberofbubblesperpicturetotal(1:...
    (number_of_pictures-3))):sum(numberofbubblesperpicturetotal(1:...
    (number_of_pictures-2))),:)-centerspicture_real(i,:)),2)<=radiuspicture_real(i))
        <1;
    else
        p=1;
    end
    %compared to the bubbles 1 picture before
```

```
    if sum(numberofbubblesperpicturetotal(1:(number_of_pictures-2)))>0
q(i,1)=sum(sum(abs(centerstotal(sum(numberofbubblesperpicturetotal(1:...
    (number_of_pictures-2))):sum(numberofbubblesperpicturetotal(1:...
    (number_of_pictures-1))),:)-centerspicture_real(i,:)),2)<=radiuspicture_real(i))
        <1;

z= (s+p+q)>1; %output is 0 when bubbles in at least 2 pictures the bubbles were
    stuck
    else
        z = 1;
    end
end

%Delete the bubbles which were stuck
radiuspicture_real = nonzeros(radiuspicture_real.*z);
centerspicture_real = centerspicture_real.*z;
centerspicture_real(centerspicture_real(:,1)==0,:) = [];
[number_of_bubbles_real] = size(radiuspicture_real,1);

else
%rewrite to real values
radiuspicture_real = radiuspicture_real;
centerspicture_real = centerspicture_real;
[number_of_bubbles_real] = size(radiuspicture_real,1);

end

else
%rewrite to real values
radiuspicture_real = radiuspicture_real;
centerspicture_real = centerspicture_real;
[number_of_bubbles_real] = size(radiuspicture_real,1);

end


gasvolumepicture =(radiuspicture_real*distance_per_pixel_m).^3*pi*4/3;
gasfraction(number_of_pictures,1) = sum(gasvolumepicture)/totalvolumepicture;
gasvolumepictures(number_of_pictures,1) = sum(gasvolumepicture);
if number_of_bubbles>0

%draw the measured bubbles
%Show the image twice
if number_of_pictures < 20
f1(1)=figure(1);
imshow(imageArray);
fullsavefile=strrep(fullnamefile, '.bmp','.jpg');
filename = ['picture_' num2str(number_of_pictures) '_' num2str(fullsavefile)];
saveas(f1,filename,'jpg')

f2= figure(2);
imshow(imageArray)
viscircles(centerspicture_real,radiuspicture_real);
filename = ['picture_detected_' num2str(number_of_pictures) '_' num2str(fullsavefile
    )];
saveas(f2,filename,'jpg')

%make a bar diagram radius bubble size distribution
f3=figure(3);
title(['Bubble size distribution of picture number ' num2str(number_of_pictures) 'at
    ' num2str(current) ' A ,' ...
num2str(concentration) ' M, ' num2str(temperature) ' C and ' ...
num2str(volumeflow) 'L/h at the ' num2str(type_of_gas) '2 side']);
```

```
number_of_same_diameter=accumarray(round(radiuspicture_real.*2),1);
diameter_lowtohigh= 1:size(number_of_same_diameter,1);
bar(diameter_lowtohigh,number_of_same_diameter);
xlabel('diameter[pixels]');
ylabel('number of bubbles');
filename = ['picture bubble size distribution_' num2str(number_of_pictures) '_'
    num2str(fullsavefile)];
saveas(f3,filename,'jpg')

end

else
  if number_of_pictures < 20
    f1(1)=figure(1);
    imshow(imageArray);
    fullsavefile=strrep(fullnamefile, '.bmp','.jpg');
    filename = ['picture_' num2str(number_of_pictures) '_' num2str(fullsavefile)];
    saveas(f1,filename,'jpg')

  end
end

%output of the loops.
%The radiustotal,centerstotal,numberofbubblesperpicturetotal are the values
%without deleting the bubbles which were stuck or counted double.
%The radiustotal_real,centerstotal_real,numberofbubblesperpicturetotal_real
%are the values with deleting the bubbles which were stuck or
% counted double.
radiustotal = [radiustotal;radiuspicture]; %pixels
gasvolumepicturetotal = [gasvolumepicturetotal;sum(gasvolumepicture)];%m3
radiustotal_real= [radiustotal_real;radiuspicture_real];%pixels
centerstotal = [centerstotal;centerspicture];%pixels
centerstotal_real = [centerstotal_real;centerspicture_real];%pixels
numberofbubblesperpicturetotal= [numberofbubblesperpicturetotal;number_of_bubbles];
numberofbubblesperpicturetotal_real= [numberofbubblesperpicturetotal_real;
    number_of_bubbles_real];

end
%make an overall bubble size distribution in bar diagram with the radius
%versus the number of bubbles.
%does not take into account the first 4 pictures because then alot of
%bubbles are counted double.
if sum(numberofbubblesperpicturetotal_real(1:4))>0
number_of_same_diameter= accumarray(round(radiustotal_real(sum(
    numberofbubblesperpicturetotal_real(1:4)):end).*2),1)./(number_of_pictures-4);
diameter_lowtohigh= 1:10:(size(number_of_same_diameter,1)*distance_per_pixel_um);
else
number_of_same_diameter= accumarray(round(radiustotal_real.*2),1)./(
    number_of_pictures);
diameter_lowtohigh= 1:10:(size(number_of_same_diameter,1)*distance_per_pixel_um);
end

%making a table
numberpicturesarray=repelem([1:number_of_pictures], [
    numberofbubblesperpicturetotal_real])';
T = array2table([numberpicturesarray,radiustotal_real, centerstotal_real(:,1),
    centerstotal_real(:,2),gasvolumepicturetotal(numberpicturesarray)*10^9],'
    VariableName',{'numberpicture';'radiustotal'; 'centerstotalx';'centerstotaly';'
    gasvolumepicture'} );
fullsavefile = strrep(fullnamefile,'.bmp','.dat');
writetable(T,fullsavefile);


```

```
346 end
347 end
```

F | Check time step at flow condition

To determine the time step of the bubble rising velocity at flow conditions, the bubbles are tracked manually. In Figure F.1 the results of the rising are shown. The difference between the experimental and theoretical data would be the liquid rising velocity. In this case a superficial velocity of $0.015\frac{m}{s}$ is found which is almost 3 times lower than the inlet superficial velocity. In Figure F.2 the influence of the time steps is shown. At the time step of 0.16 s some smaller bubbles will be detected twice. However, this seems to have less effect on the bubble size distribution. Therefore, during this research the smallest time step is used.

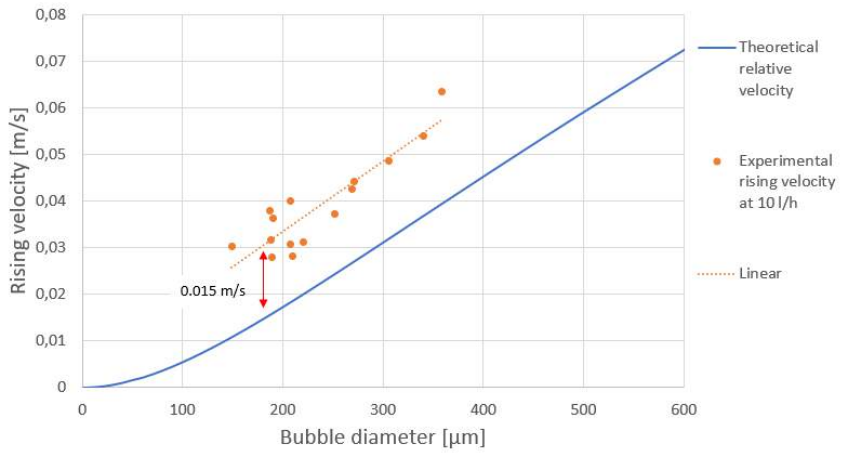

Figure F.1: *Bubble rising velocity at an superficial inlet velocity of* $0.048\frac{m}{s}$ *over the bubble diameter at* $20°C$ *and* $20wt\%$.

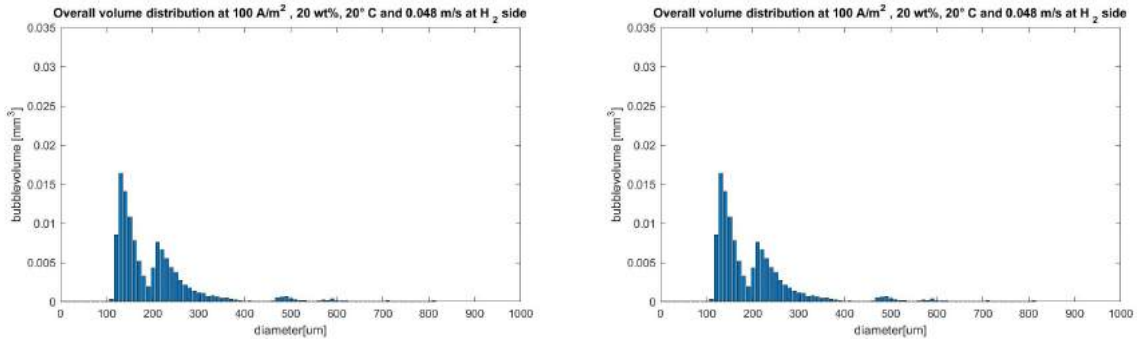

(a) *Time step of 0.16 s (so 8 frames)*

(b) *Time step of 0.48 s (so 24 frames.)*

Figure F.2: *Influence time step of on the bubble size distribution.*

G Detection and analysing bubble size distribution

In this appendix first the bubble detection of the MATLAB script is checked with the bubble detection by hand. Afterwards, an example is given of how the pictures are converted into bubble size distribution. The method of getting the pictures is discussed in Appendix C. The bubbles are detected with the MATLAB script which is described in Appendix E.

In Figure results of analysing the bubble size distribution by hand and by the MATLAB script is shown. It is shown that the MATLAB script measurements are close to the measurements by hand. In some cases the bubble size is over estimated a bit in the MATLAB script. However, in this research the bubble sizes are determined by the MATLAB script.

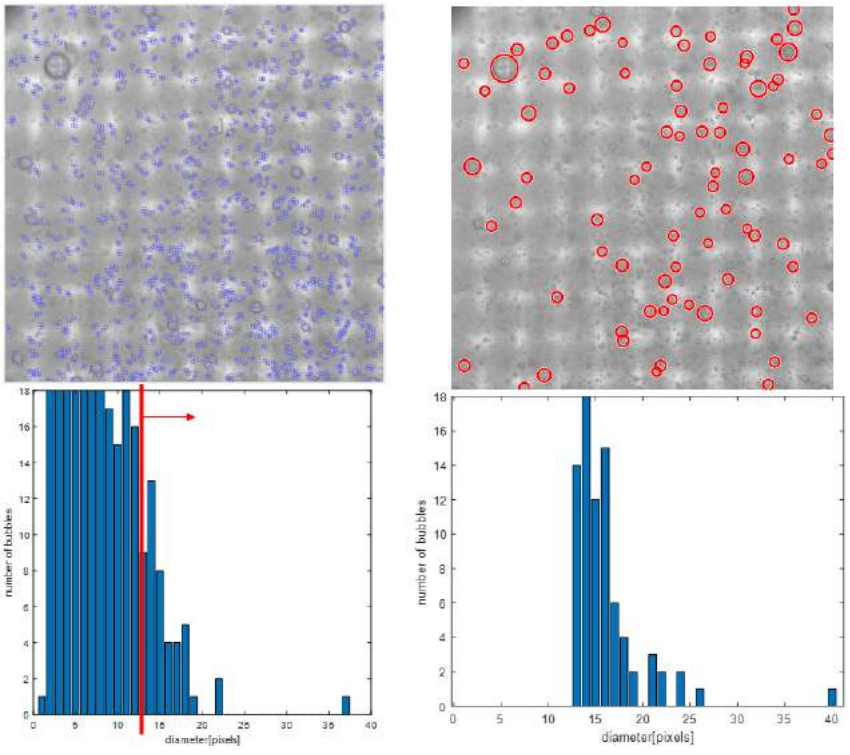

Figure G.1: *Bubble size distribution based on the detection by hand and the detection by the MATLAB script.*

In Figure G.2 a few results of the bubble detection are shown. Only bubbles with a minimum diameter of $120\mu m$ are detected. In Figure G.2a to G.2d the detection of all bubbles, both moving and not moving, is shown. These pictures are not used for the bubble size distribution. The rest of the pictures, in which only the moving bubbles are detected, are used to determine the bubble size distribution (the three pictures rule as discussed in 3.2.1). In Figure G.2e to G.2h only a few detections are shown. An appropriate time step between pictures is chosen to prevent that (two analysed) pictures (partly) overlap.

The total number of bubbles per diameter is divided by the number of analysed pictures. The results of this is shown in Figure G.3a. In a picture the number of bubbles depends on the value of current density and the liquid velocity. To be able to compare the varies results more easily, the graphs are normalized. Normalization means two steps:

- First, the bubble size distribution based on the number of bubbles is converted to a bubble size distribution based on volume (see Figure G.3b). This is done since bigger bubbles have a bigger volume compared to the smaller bubbles.
- Second, the volume per diameter is divided by the total volume per picture. (see Figure G.3c)

The result is a normalized bubble size distribution based on volume.

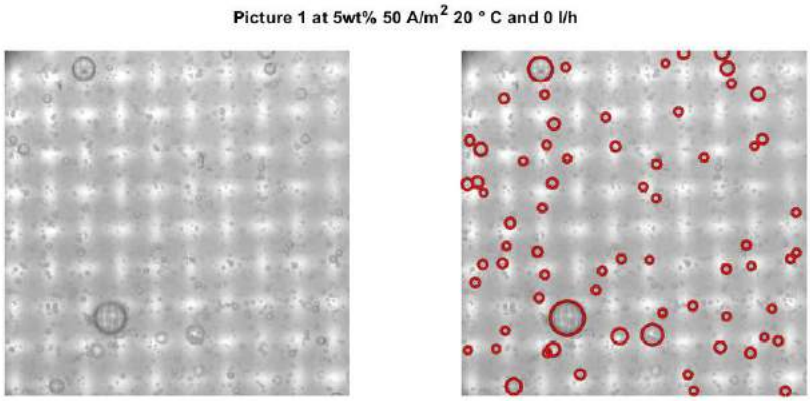

(a) *Picture 1*

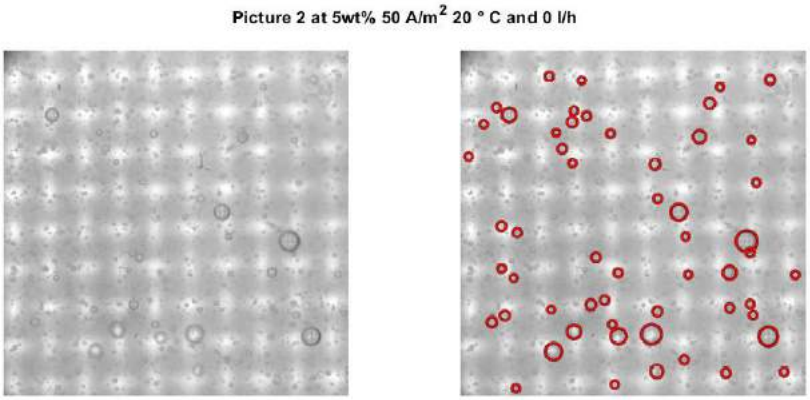

(b) *Picture 2*

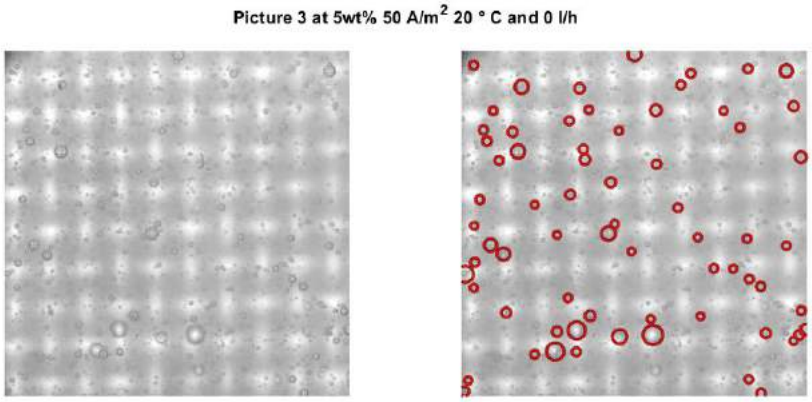

(c) *Picture 3*

Figure G.2: *Bubble detection. The first 4 pictures all bubbles were detected, while in the last 4 pictures only the moving bubbles are detected.*

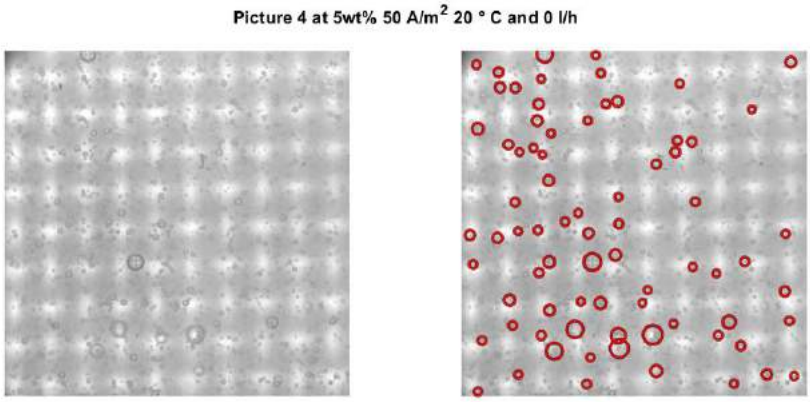

(d) *Picture 4*

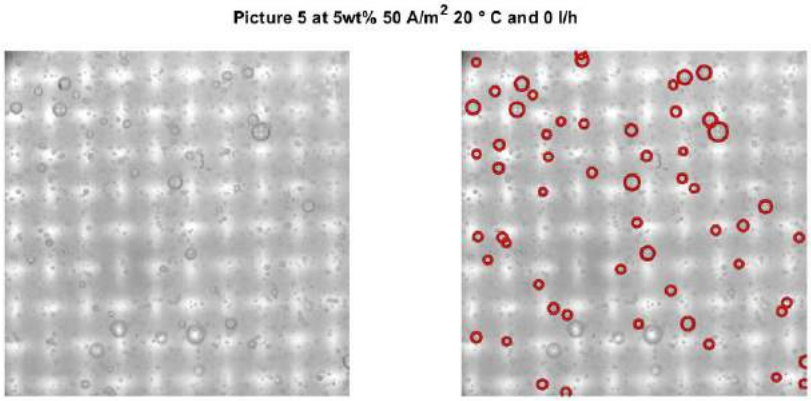

(e) *Picture 5*

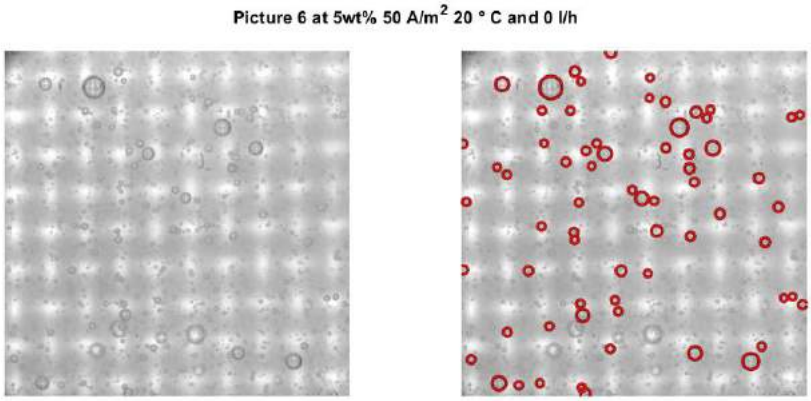

(f) *Picture 6*

Figure G.2: *Bubble detection. The first 4 pictures all bubbles were detected, while in the last 4 pictures only the moving bubbles are detected.*

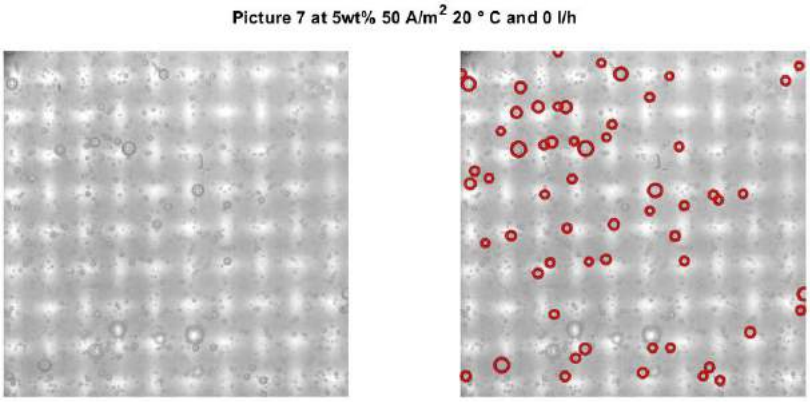

(g) *Picture 7*

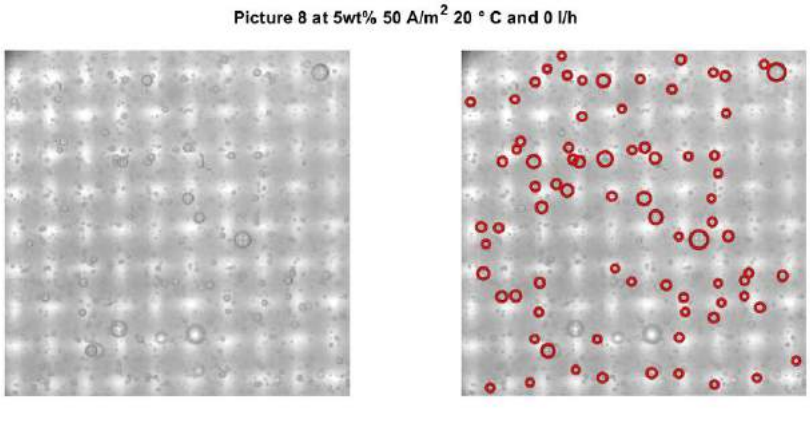

(h) *Picture 8*

Figure G.2: *Bubble detection. The first 4 pictures all bubbles were detected, while in the last 4 pictures only the moving bubbles are detected.*

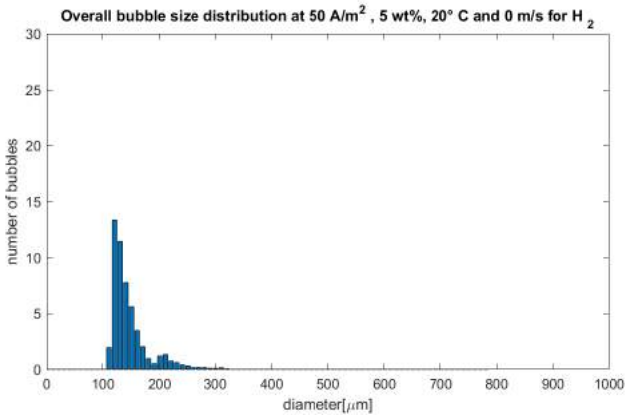

(a) *Bubble size distribution based on number of bubbles.*

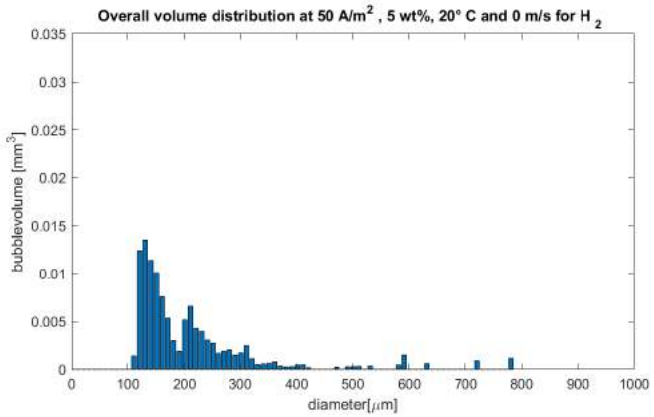

(b) *Bubble size distribution based on volume.*

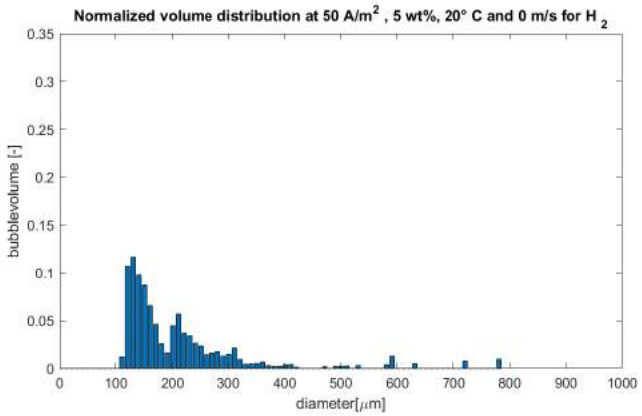

(c) *Normalized based on volume.*

Figure G.3: *Bubble size distributions based on the number of bubbles and the bubble volume.*

H | Current density limitations

The bubble detection has a limitation in the height of the current density. At a current density of $30\frac{A}{m^2}$ for hydrogen and a current density of $50\frac{A}{m^2}$ for oxygen the distribution is reproducible. At lower current density the distribution is not constant since the gas fraction is too low (see Figure H.1 and Figure H.2)

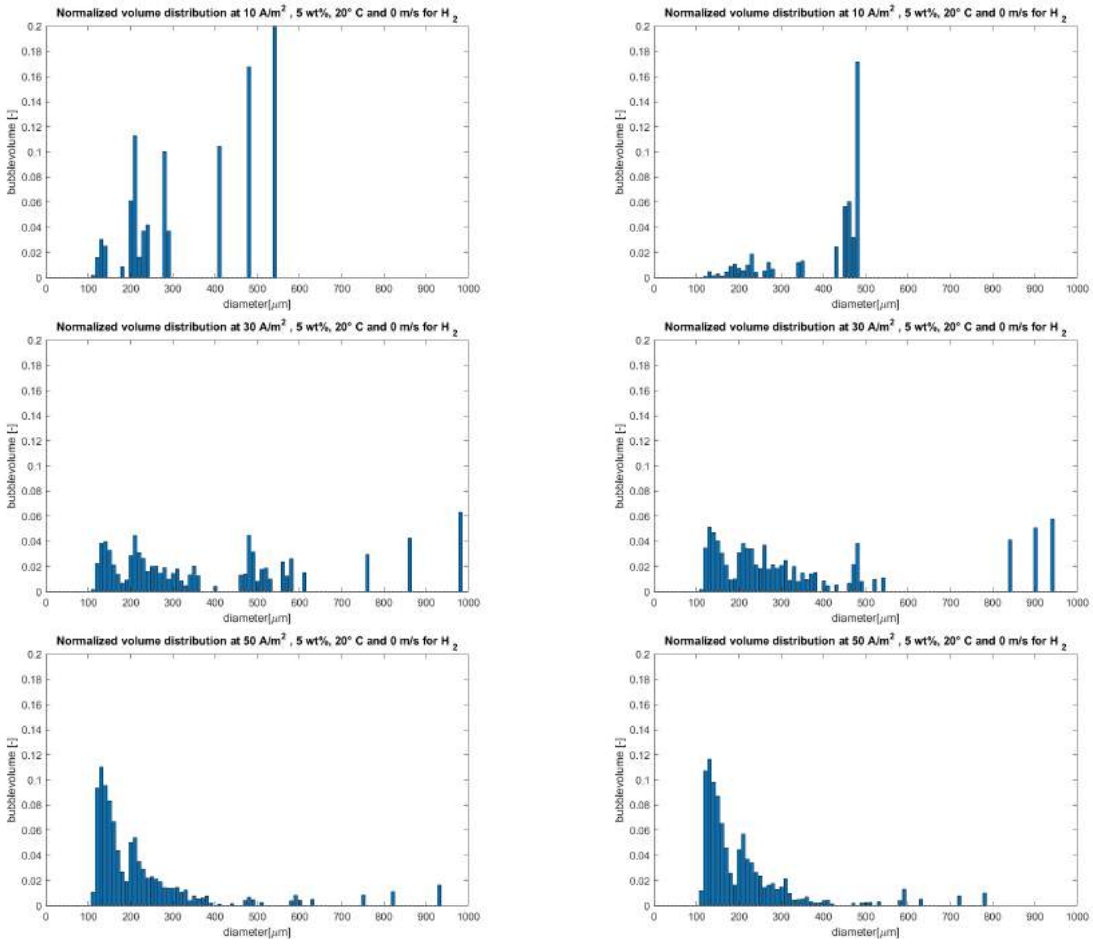

Figure H.1: *Limited reproducibility at low current densities for the hydrogen bubbles. The graphs are normalized and shown at different current densities.*

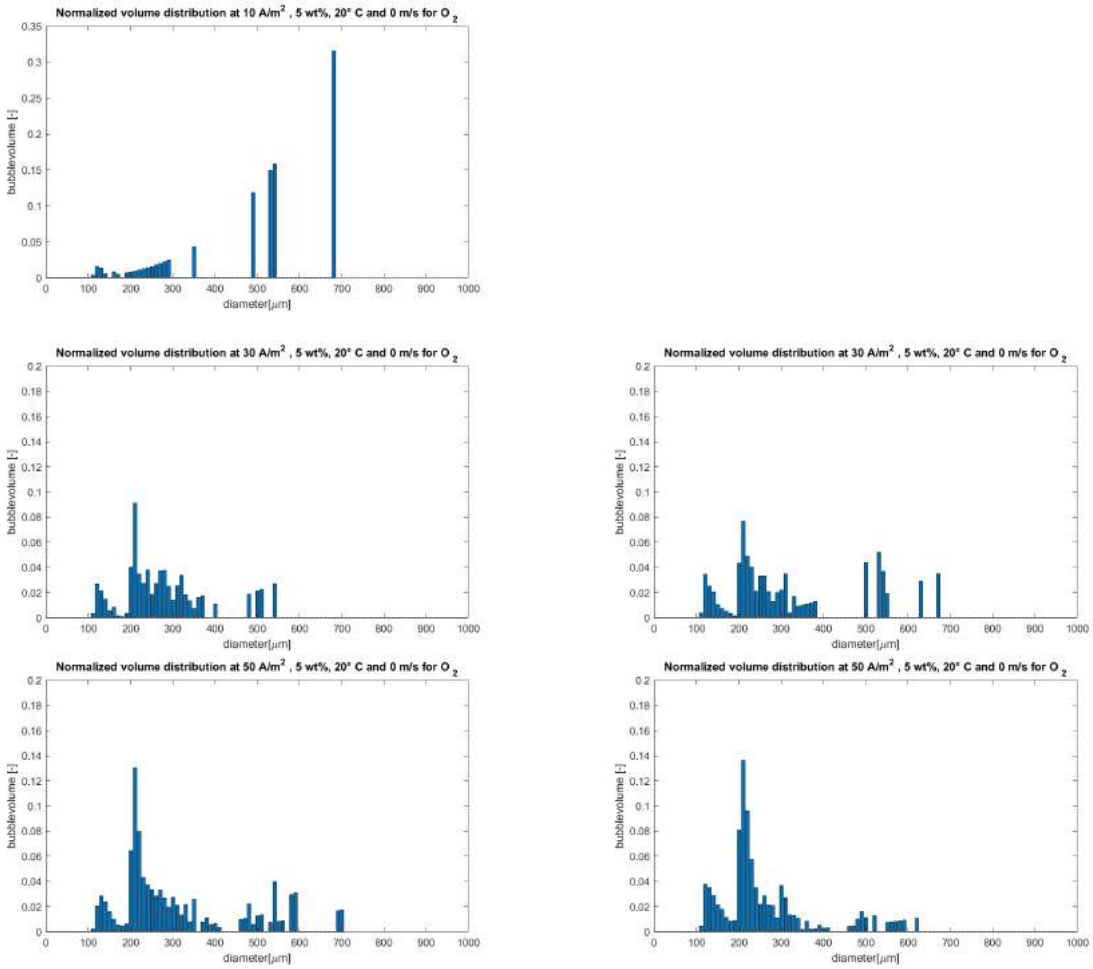

Figure H.2: *Limited reproducibility at low current densities for the oxygen bubbles. The graphs are normalized and shown at different current densities.*

At higher current densities, the bubble detection becomes less reliable. In Figure H.3 the bubble detection is shown at $50\frac{A}{m^2}$. Most of the bubbles were detected correctly. For $100\frac{A}{m^2}$ the bubble detection became already critical (see Figure H.4). In the Figure H.5 most of the bubbles are not detected due to the large amount of bubbles which were present.

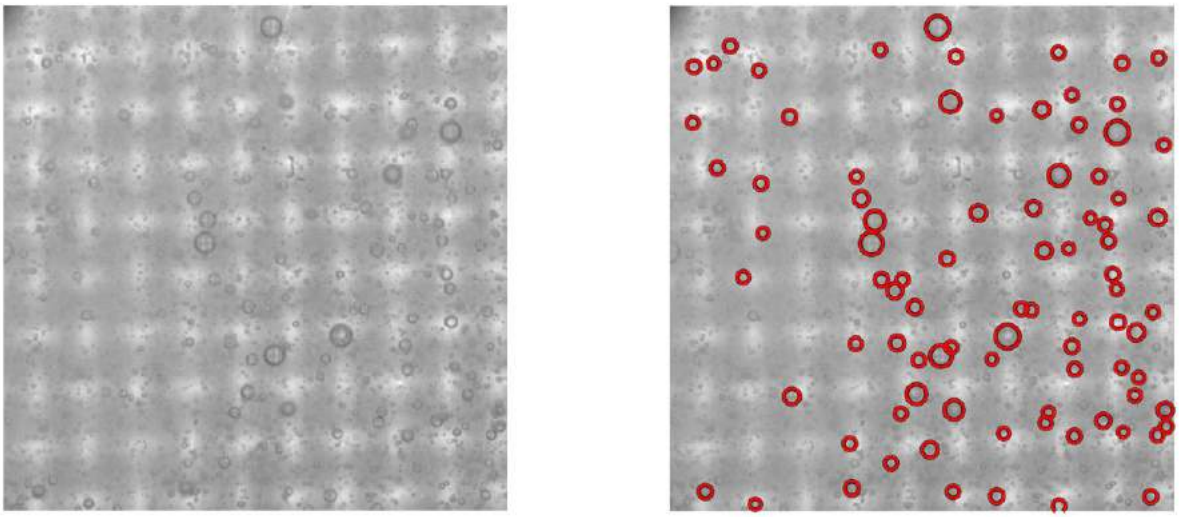

Figure H.3: *Bubble detection at* $50\frac{A}{m^2}$

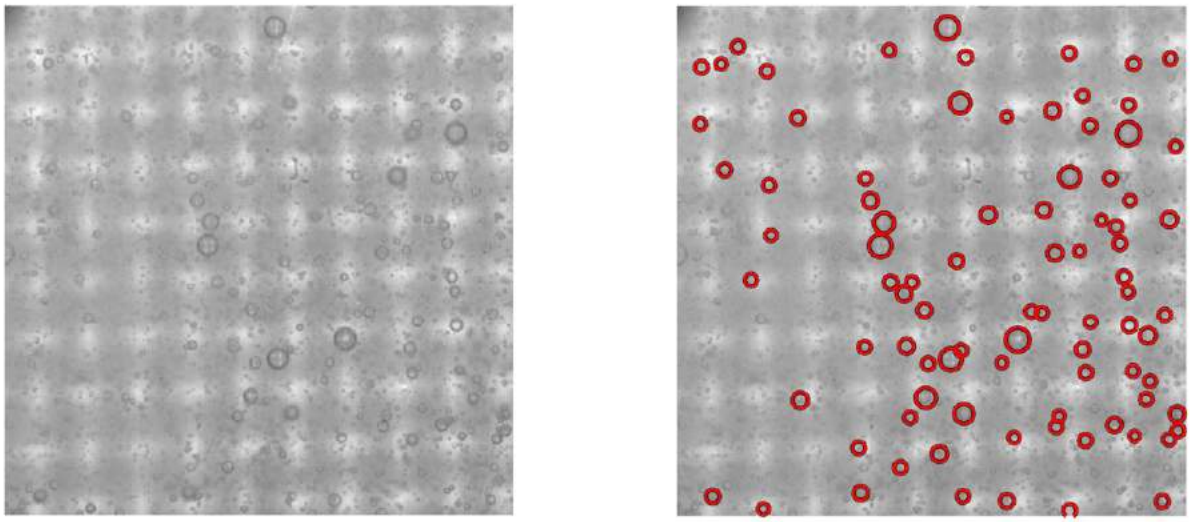

Figure H.4: *Bubble detection at* $100\frac{A}{m^2}$

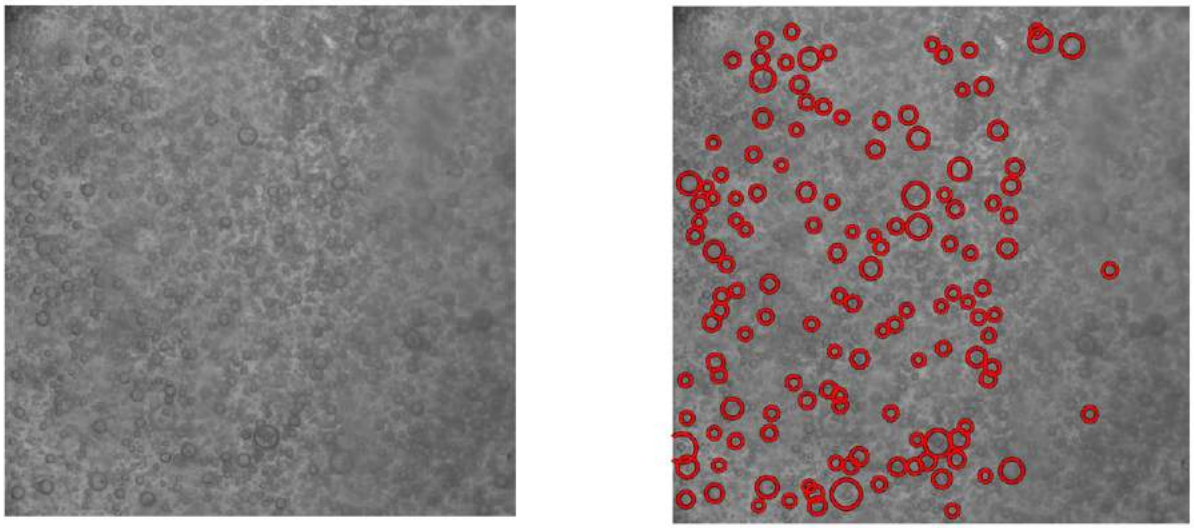

Figure H.5: *Bubble detection at* $500\frac{A}{m^2}$

I Overview experiments bubble size distribution

In this appendix an overview is given of the experiments which were done to determine the bubble size distribution. For each experiment the minimum activated time of the diaphragm and if the results of the experiments are included in this research for determining the bubble size distribution is shown. The overview is shown in Figure I.1 and in Figure I.2.

A few experiments are missing. There are several reasons for this:

- In Experiment 1 the range of the current densities were not yet know since the bubble behavior was different than expected. Therefore, not at all the used conditions the experiments were met.
- Some files became corrupted, so, as a result the pictures could not be analysed anymore.

Moreover, it could be noticed that a few experiments are excluded form this research. The reason for this are summed below:

- There is a lower limitation of current density at $30\frac{A}{m^2}$ for the hydrogen side and $50\frac{A}{m^2}$ for the oxygen side. The limitation is caused by a too low gas volume to find a correlation
- There is an upper limitation of current density at $100\frac{A}{m^2}$ for the hydrogen side and $200\frac{A}{m^2}$ for the oxygen side. The upper limit is caused by the difficulty of analysing because of the relatively high gas volume.
- Only the test with an activation of 3 or 5 days are included in this research. Because at a lower activation time it was noticed that the measured gas fraction was lower.
- An increase in leakages of the cell results in a lower measured gas volume. Therefore, the following results are excluded: 'Experiment 3 20wt%, 20 °C, no flow for O_2' and 'Experiment 3 5wt% for O_2'.

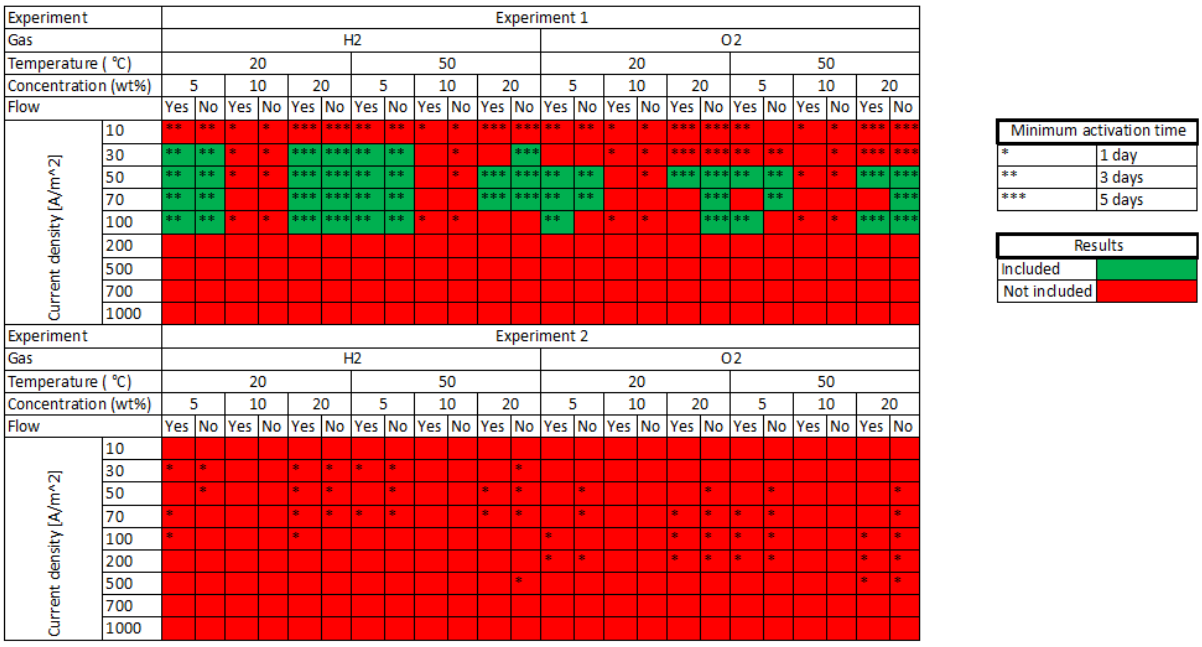

Figure I.1: *Overview experiments 1 and 2. The minimum activation time of the diaphragm and if the results are used for the bubble size distribution are indicated.*

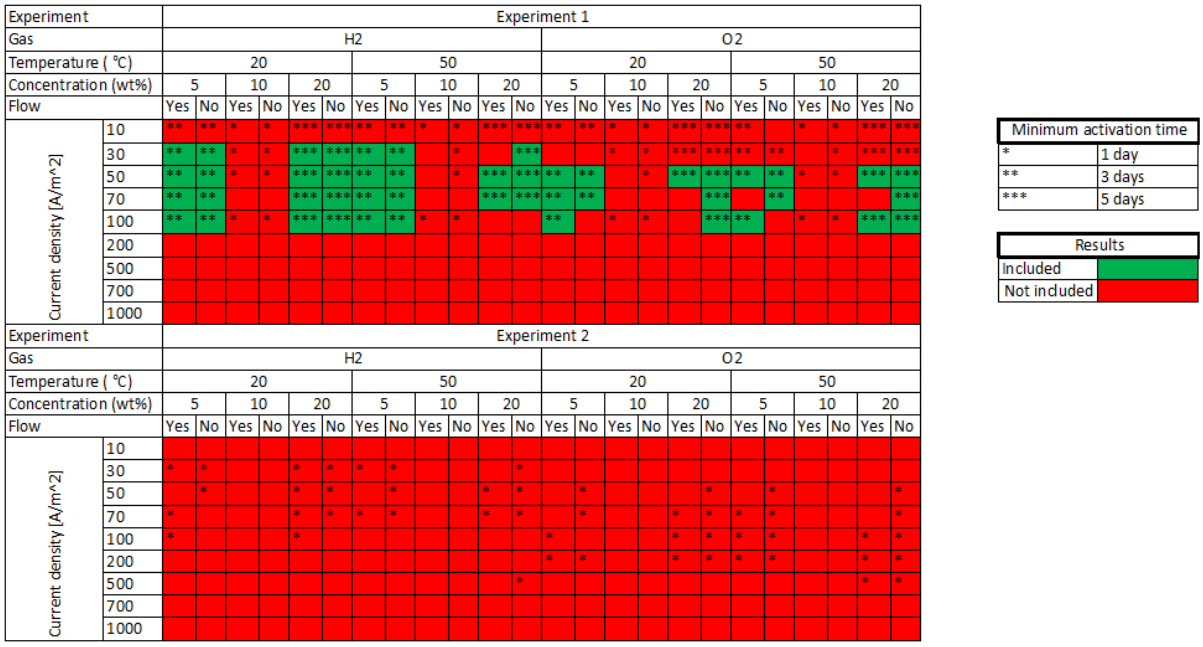

Figure I.2: *Overview experiments 3 and 4. The minimum activation time of the diaphragm and if the results are used for the bubble size distribution are indicated.*

J Influence of activation of diaphragm on the gas fraction

The experiments for determining the bubble size distribution are done in triplicate. The gas fraction gives an indication of the reliability of the results. According to the gas production, the gas fraction should in a linear way and should be almost equal for the different temperatures and concentrations. The gas fraction is determined based on the bubble size distribution of bubbles with a bubble diameter larger than $120\mu m$. In Figure J.1 the correlation between the gas fraction and current density is shown for the different experiments.

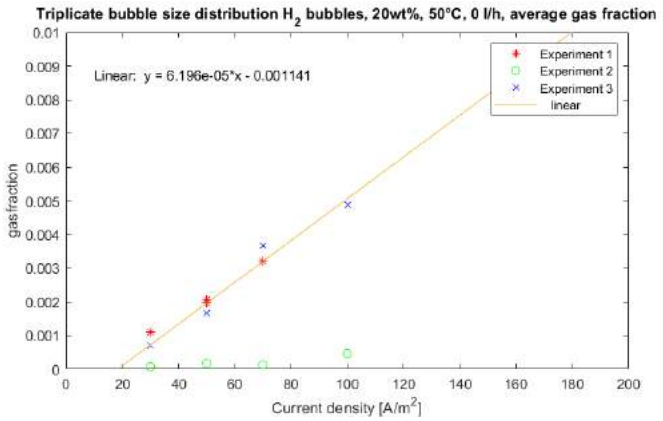

Figure J.1: *Triplicate results of the gas fraction. Experiment 1 and 3 seem to have a similar linear correlation between current density and gas fraction. Experiment 2 shows a complete different relation.*

In Experiment 2 the gas fraction is lower compared to Experiment 1 and Experiment 3. Therefore, the results of the Experiment 2 are not used.

A possible reason for measuring a lower gas fraction could be that not all of the bigger bubbles are detected. Therefore, the gas fraction is analysed for different time steps in between the analysed pictures (1 and $1.5s$). The gas volume did not change a lot with the different time steps. However, it was noticed that the gas volume in the bubbles with a bubble diameter above $400\mu m$ varied in Experiment 2 more than the in other experiments. This could indicate that there is a larger amount of bigger bubbles which were not measured. In Appendix K the results of the different time steps are shown.

During the experiments it was noticed that in Experiment 2 more bubbles were stuck to the diaphragm compared to the other experiments. When a bubble is attached to the diaphragm it grows. A possible reason for the different behavior at the diaphragm is that the diaphragm was not fully activated. The diaphragm has to be soaked in the electrolyte for a while so that it could become active.

This same phenomenon is found for some results at Experiment 1. Here, the experiment was split in different days:

- At the day that the diaphragm became activated, the experiments at 10 wt% are done.

- After 3 days that the diaphragm was activated, the experiments at 5wt% are done.
- After 5 days that the diaphragm was activated, the experiments at 20 wt% are done.

In Figure J.2 the gas volume fraction of the first experiment at different concentration is shown.

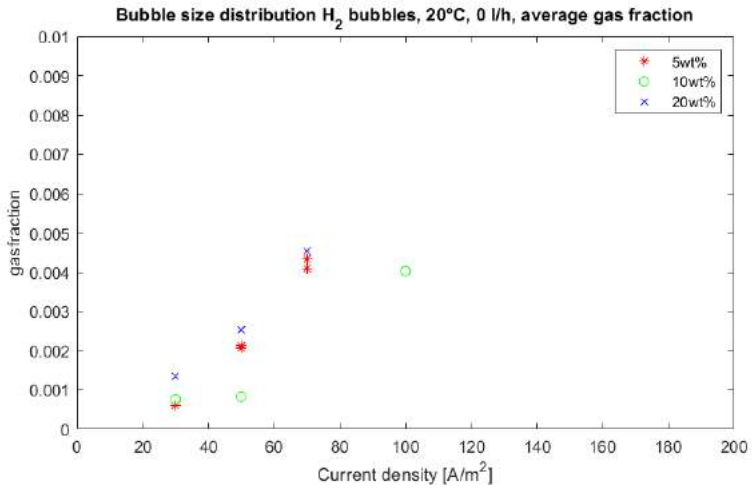

Figure J.2: *Volume fraction at different concentrations.*

The results of 5 and 20 wt% are comparable while the result of 10 wt% is totally different. Again, a reason could be the activation of the diaphragm.

The difference between an activated and not activated diaphragm is not yet explained in the literature. A possible explanation for this behavior could be that the adherence forces are different. Therefore only tests with an minimal activation of 3 days are included in this research.

K Influence time step in between the pictures

In Appendix J it was noticed that the gas fraction of Experiment 1 and 3 were comparable to each other, while the gas fraction of Experiment 2 differs a lot from Experiment 1 and 3. A possible cause for this could be the time step. Therefore, MATLAB has analysed the pictures with two different time steps (1 and $1.5s$). Again the results show no difference between Experiment 1 and 3 (see Figure K.1, Figure K.2, Figure K.3 and Figure K.4) and again Experiment 2 gave complete different results at the bigger gas bubbles ($> 400\mu m$) (see Figure K.6 and Figure K.6). This confirms that the different results of experiment 2 were the result of the wrong activation time of the diaphragm.

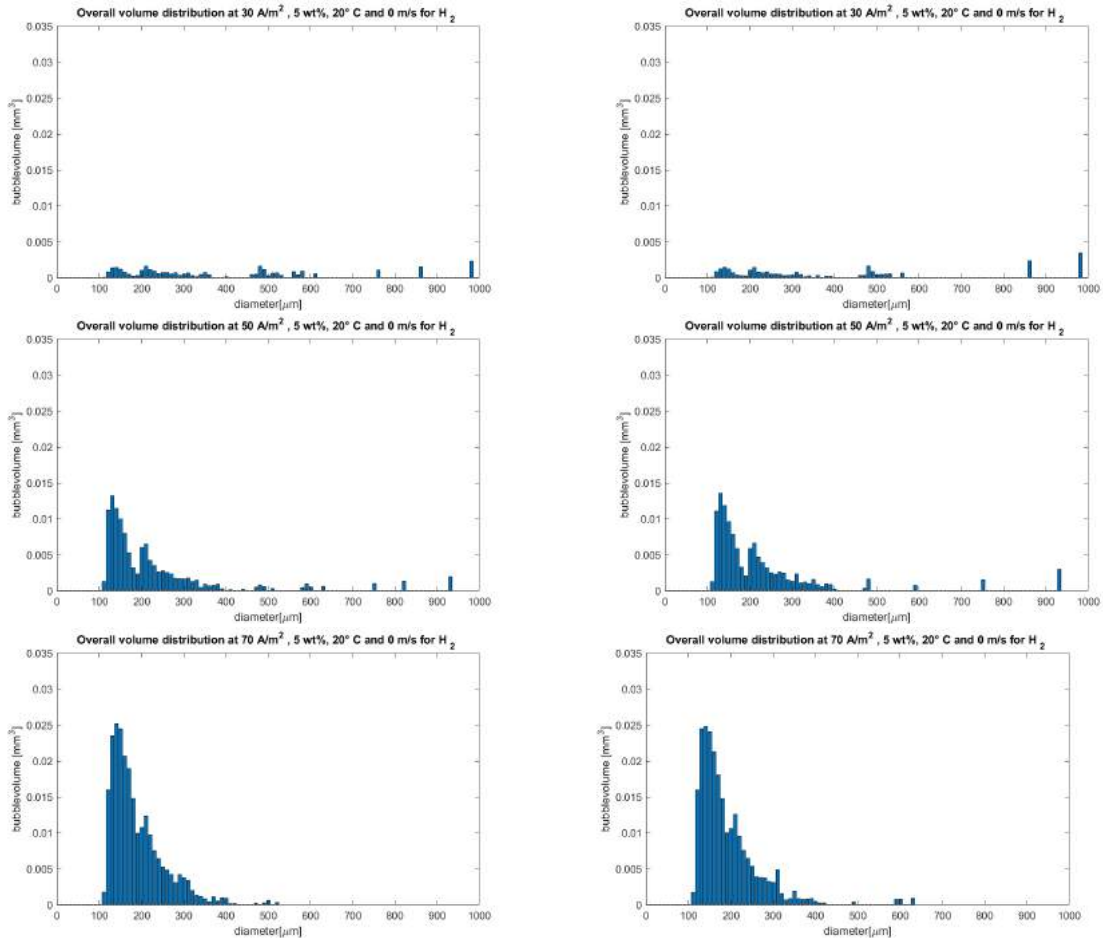

Figure K.1: *Influence of a different time step in between the pictures on the bubble volume of Experiment 1 on the hydrogen side. On the left side the bubble size distribution at a time step of* $1s$ *is shown, while on the right side a time step of* $1.5s$ *is shown. At the top the results at a current density of* $10\frac{A}{m^2}$ *are shown, followed by* $30\frac{A}{m^2}$ *and* $50\frac{A}{m^2}$.

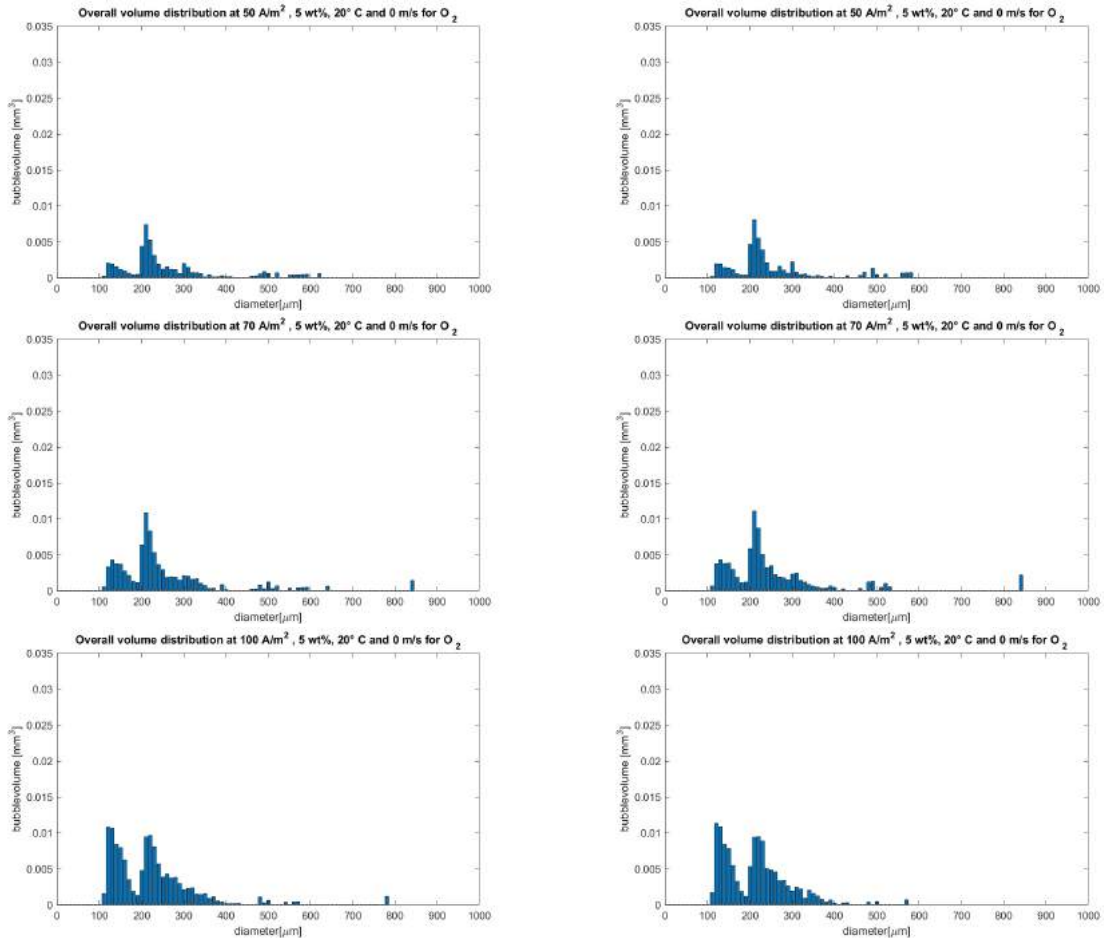

Figure K.2: *Influence of a different time step in between the pictures on the bubble volume of Experiment 1 on the oxygen side. On the left side the bubble size distribution at a time step of* $1s$ *is shown, while on the right side a time step of* $1.5s$ *is shown. At the top the results at a current density of* $10\frac{A}{m^2}$ *are shown, followed by* $30\frac{A}{m^2}$ *and* $50\frac{A}{m^2}$.

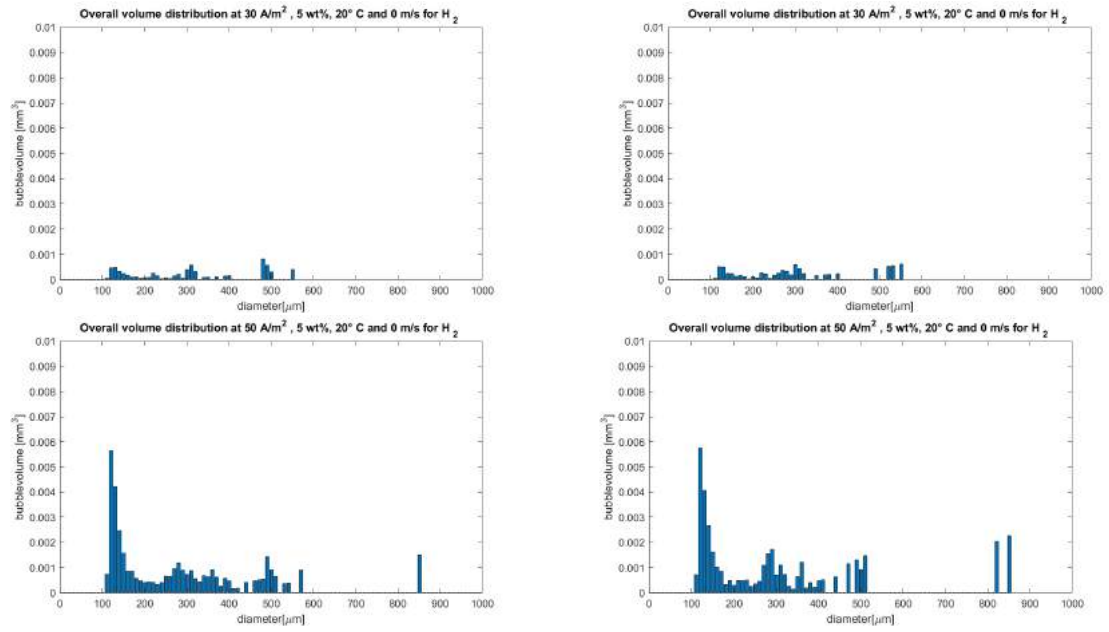

Figure K.3: *Influence of a different time step in between the pictures on the bubble volume of Experiment 2 on the hydrogen side. On the left side the bubble size distribution at a time step of* $1s$ *is shown, while on the right side a time step of* $1.5s$ *is shown. At the top the results at a current density of* $10\frac{A}{m^2}$ *are shown, followed by* $30\frac{A}{m^2}$.

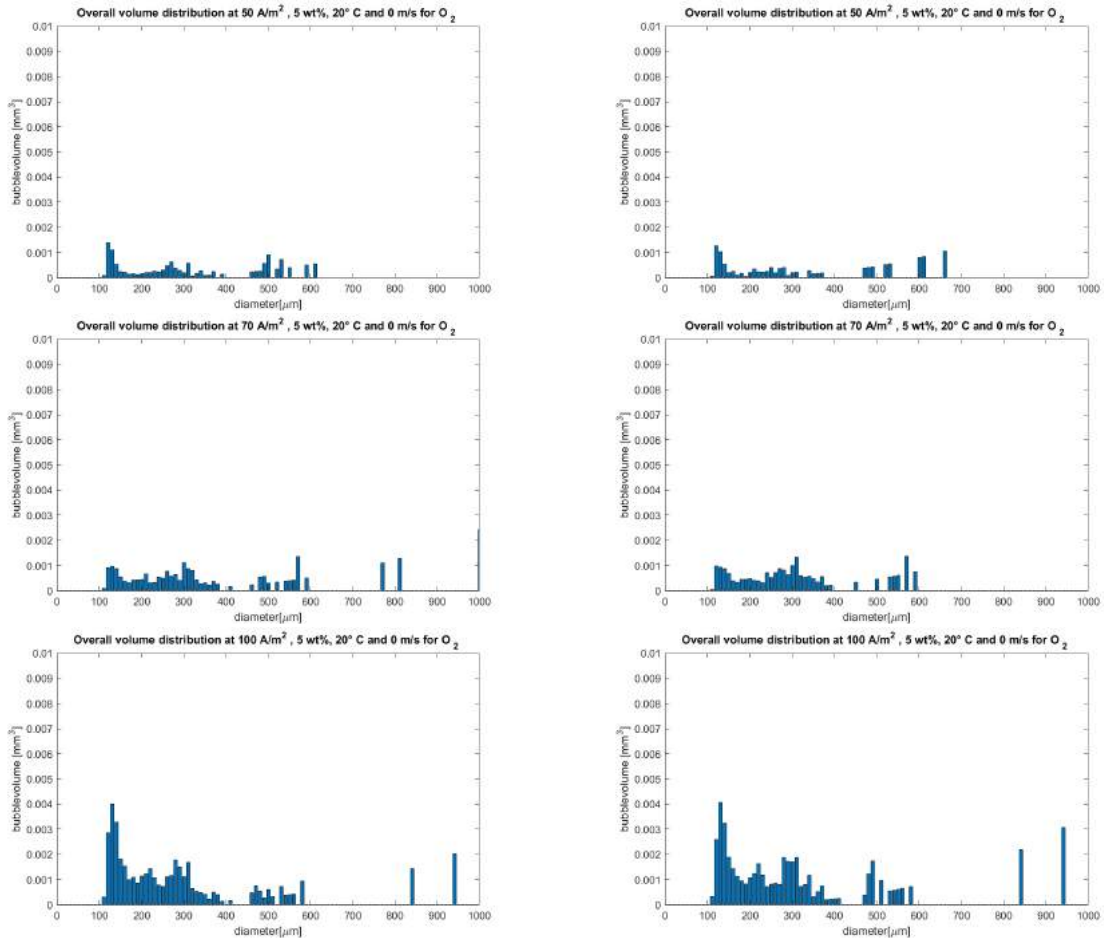

Figure K.4: *Influence of a different time step in between the pictures on the bubble volume of Experiment 2 on the oxygen side. On the left side the bubble size distribution at a time step of* $1s$ *is shown, while on the right side a time step of* $1.5s$ *is shown. At the top the results at a current density of* $10\frac{A}{m^2}$ *are shown, followed by* $30\frac{A}{m^2}$ *and* $50\frac{A}{m^2}$.

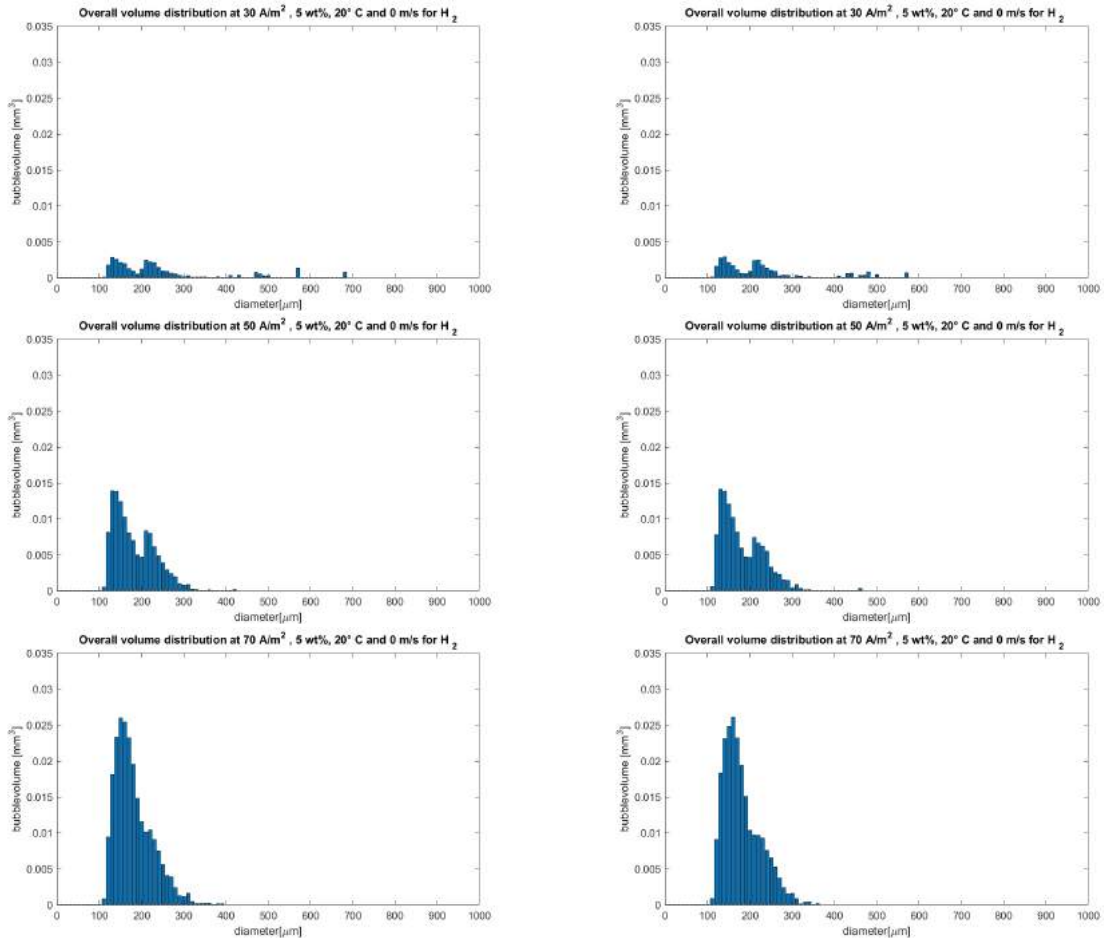

Figure K.5: *Influence of a different time step in between the pictures on the bubble volume of Experiment 3 on the hydrogen side. On the left side the bubble size distribution at a time step of* $1s$ *is shown, while on the right side a time step of* $1.5s$ *is shown. At the top the results at a current density of* $10\frac{A}{m^2}$ *are shown, followed by* $30\frac{A}{m^2}$ *and* $50\frac{A}{m^2}$.

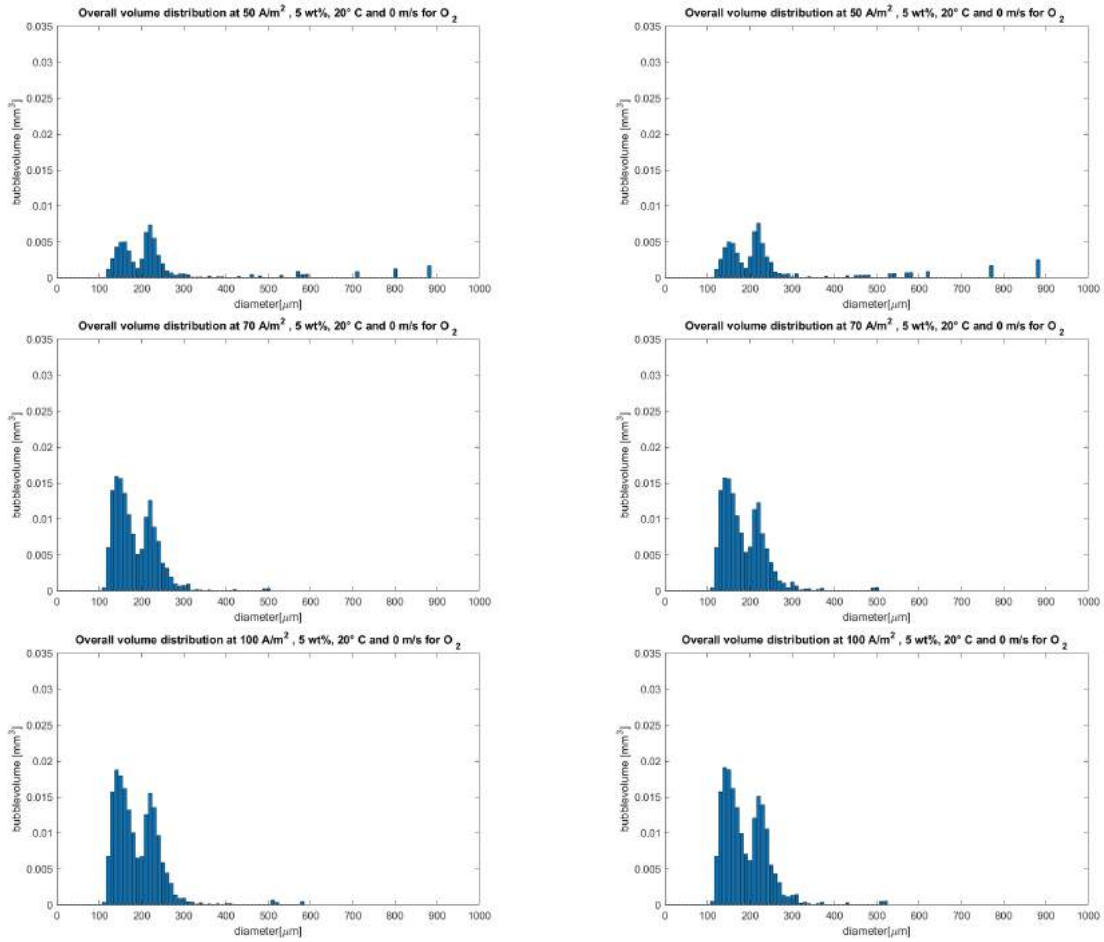

Figure K.6: *Influence of a different time step in between the pictures on the bubble volume of Experiment 3 on the oxygen side. On the left side the bubble size distribution at a time step of* $1s$ *is shown, while on the right side a time step of* $1.5s$ *is shown. At the top the results at a current density of* $10\frac{A}{m^2}$ *are shown, followed by* $30\frac{A}{m^2}$ *and* $50\frac{A}{m^2}$.

L Influence of the increase in leakages on measured gas volume

Based on the reaction ratio it is expected that the gas volume of hydrogen is twice as high as oxygen. This is a good indication for checking if the results on the oxygen side are correct (Figure L.1). Most of the measurements are between a ratio of 1.5 and 3. For 'Experiment 3 5wt% 50 °C' and 'Experiment 3 20wt% 20 °C' a ratio of 4 or higher is found. For both experiments there was a real leakage at the electrochemical cell, this explain the difference in H_2/O_2 ratio. Therefore, these results are excluded.

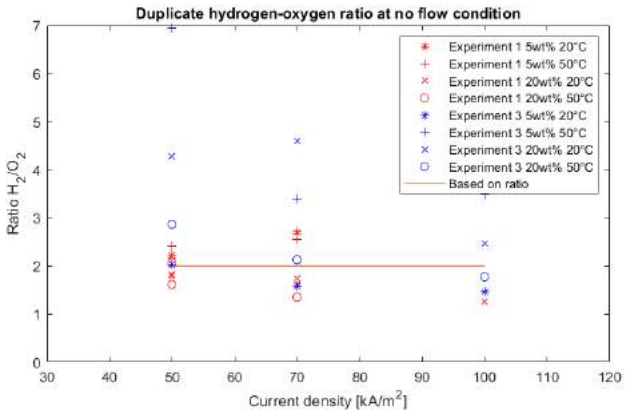

Figure L.1: *Duplicate results of ratio of hydrogen over oxygen at different current density. According to the reaction ratio, a ratio of 2 is expected.*

M Normalized bubble size distributions

The normalized bubble size distribution is obtained based on the gas volume. It is found that always one volume peak is at a bubble diameter between 120 and $200\mu m$ and one volume peak is at a bubble diameter between 200 and $400\mu m$. In this appendix all the graphs are shown:

- Duplicated experiment for the H_2 bubbles at 20°C, 5 wt%, no flow condition (see Figure M.1).
- Duplicated experiment for the H_2 bubbles at 50°C, 5 wt%, no flow condition (see Figure M.2).
- Duplicated experiment for the H_2 bubbles at 20°C, 20 wt%, no flow condition (see Figure M.3).
- Duplicated experiment for the H_2 bubbles at 50°C, 20 wt%, no flow condition (see Figure M.4).
- Duplicated experiment for the O_2 bubbles at 20°C, 5 wt%, no flow condition (see Figure M.5)
- Experiment for the O_2 bubbles at 50°C, 5 wt%, no flow condition (see Figure M.6)
- Experiment for the O_2 bubbles at 20°C, 20 wt%, no flow condition (see Figure M.7)
- Duplicated experiment for the O_2 bubbles at 50°C, 20 wt%, no flow condition (see Figure M.8)
- Duplicated experiment for the H_2 bubbles at 20°C, 5 wt%, $0.048\frac{m}{s}$ electrolyte flow (see Figure M.9).
- Duplicated experiment for the H_2 bubbles at 50°C, 5 wt%, $0.048\frac{m}{s}$ electrolyte flow (see Figure M.10).
- Duplicated experiment for the O_2 bubbles at 20°C, 5 wt%, $0.048\frac{m}{s}$ electrolyte flow (see Figure M.11)
- Duplicated experiment for the O_2 bubbles at 50°C, 5 wt%, $0.048\frac{m}{s}$ electrolyte flow (see Figure M.12)
- Experiment for the H_2 bubbles at 20 and 50°C, 20 wt%, $0.048\frac{m}{s}$ electrolyte flow (see Figure M.13)
- Experiment for the O_2 bubbles at 20 and 50°C, 20 wt%, $0.048\frac{m}{s}$ electrolyte flow (see Figure M.14)

In Figure M.1 the effect of current density on the normalized bubble size distribution of hydrogen bubbles at $20°C$, 5wt% and no flow conditions is shown in duplicate. It is shown that the reproducibility of the normalized bubble size distribution increases at an increasing current density. At low current densities, 30 and $50\frac{A}{m^2}$, a bimodal distribution is obtained with one volume peak with a bubble diameter between 120 and $200\mu m$ and one volume peak with a bubble diameter between 200 and $400\mu m$. At an increase in current density, the volume peak of the bubbles with a bubble diameter between 120 and $200\mu m$ is increasing at at a current density of $100\frac{A}{m^2}$ the bimodal distribution turns in an unimodal distribution.

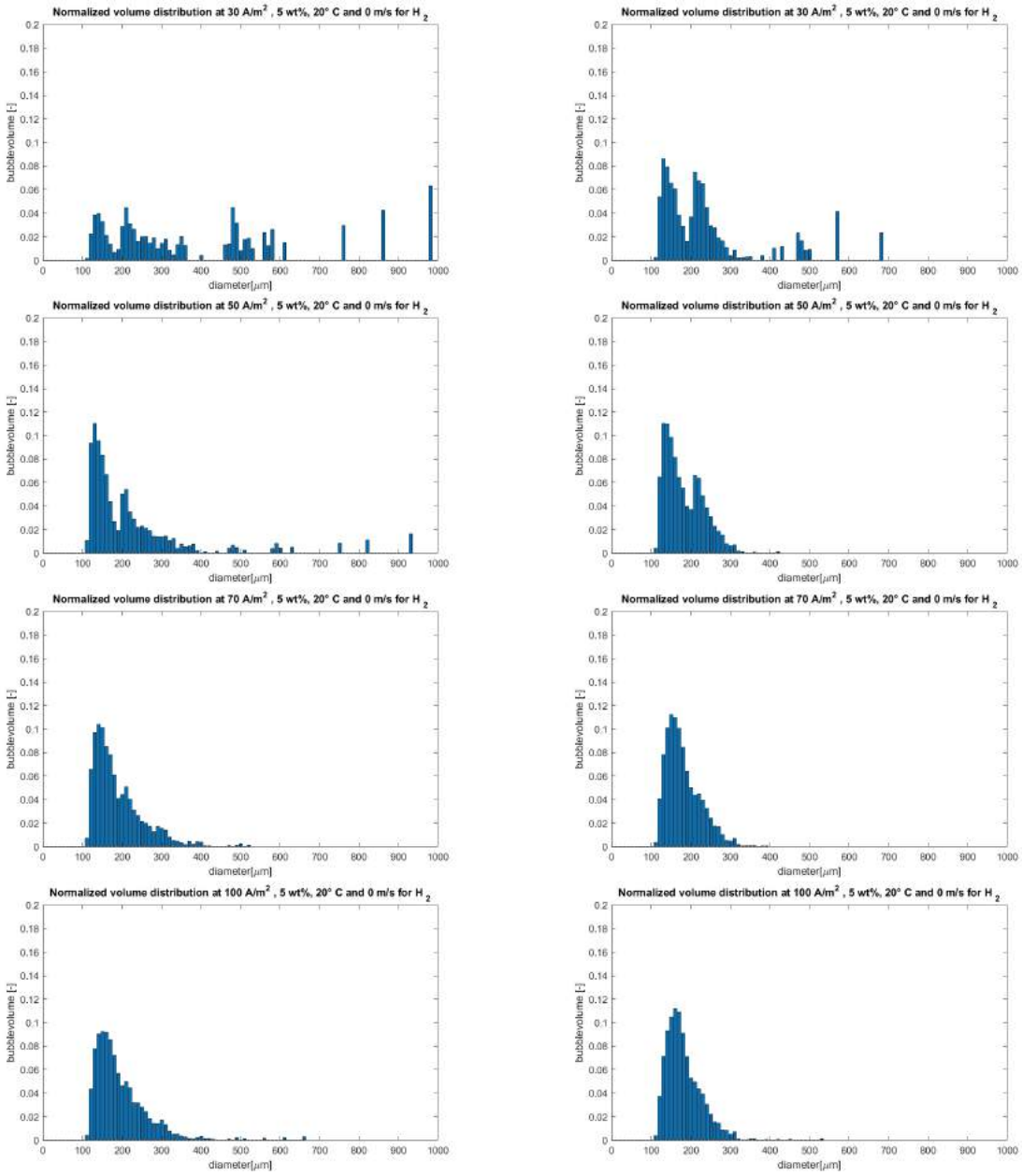

Figure M.1: *The normalized bubble size distributions over different current densities for the hydrogen bubbles at 20 °C, 5 wt% and no flow conditions in duplicate. In the left the results of Experiment 1 are shown and in the right the results of Experiment 3 are shown.*

In Figure M.2 the effect of current density on the normalized bubble size distribution of hydrogen bubbles at $50°C$, 5wt% and no flow conditions is shown in duplicate. These results are quite similar to the results at 20 °C, which were shown in Figure M.1. It shows that the reproducibility of the normalized bubble size distribution increases at an increasing current density. At low current densities, 30 and $50\frac{A}{m^2}$, a bimodal distribution is obtained with one volume peak with a bubble diameter between 120 and $200\mu m$ and one volume peak with a bubble diameter between 200 and $400\mu m$. At an increase in current density, the volume peak of the bubbles with a bubble diameter between 120 and $200\mu m$ is increasing at at a current density of $100\frac{A}{m^2}$ the bimodal distribution turns in an unimodal distribution.

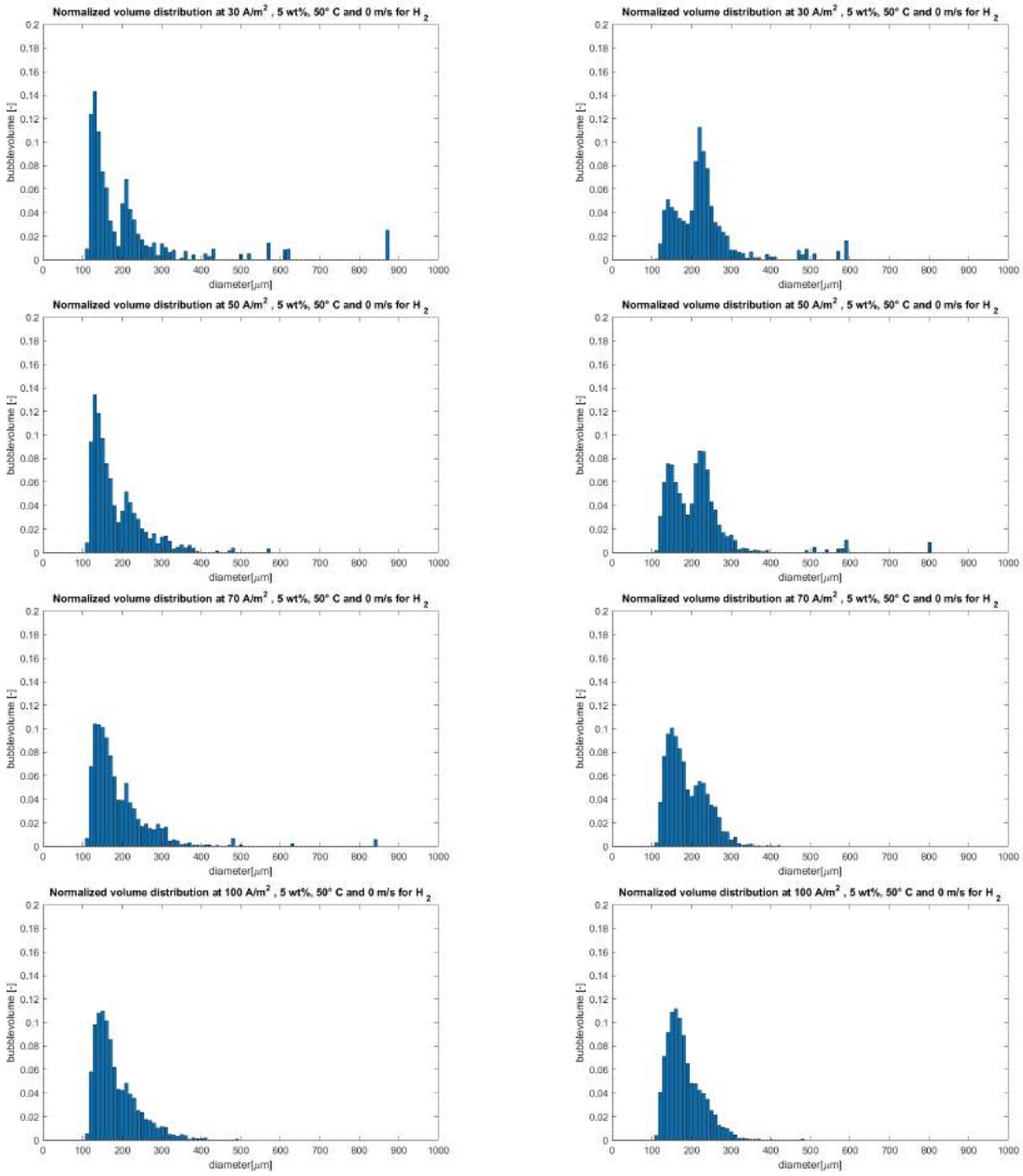

Figure M.2: *The normalized bubble size distributions over different current densities for the hydrogen bubbles at 50 °C, 5 wt% and no flow conditions in duplicate. In the left the results of Experiment 1 are shown and in the right the results of Experiment 3 are shown.*

In Figure M.3 the effect of current density on the normalized bubble size distribution of hydrogen bubbles at $20°C$, 20wt% and no flow conditions is shown in duplicate. There results are quite similar to the results at 5 wt%, which were shown in Figure M.1. However, at 5wt% the distribution turns at $100\frac{A}{m^2}$ into a unimodal while at 20wt% the distribution already turns in a unimodal distribution at a current density of $70\frac{A}{m^2}$. An possible explaination for this would be that the coalescence takes place more easily at lower KOH concentrations. Due to an increased chance on coalescence, the bubbles can grow more easily in the electrode-diaphragm gap and in the electrode hole and so a higher current density is needed to reach a unimodal distribution.

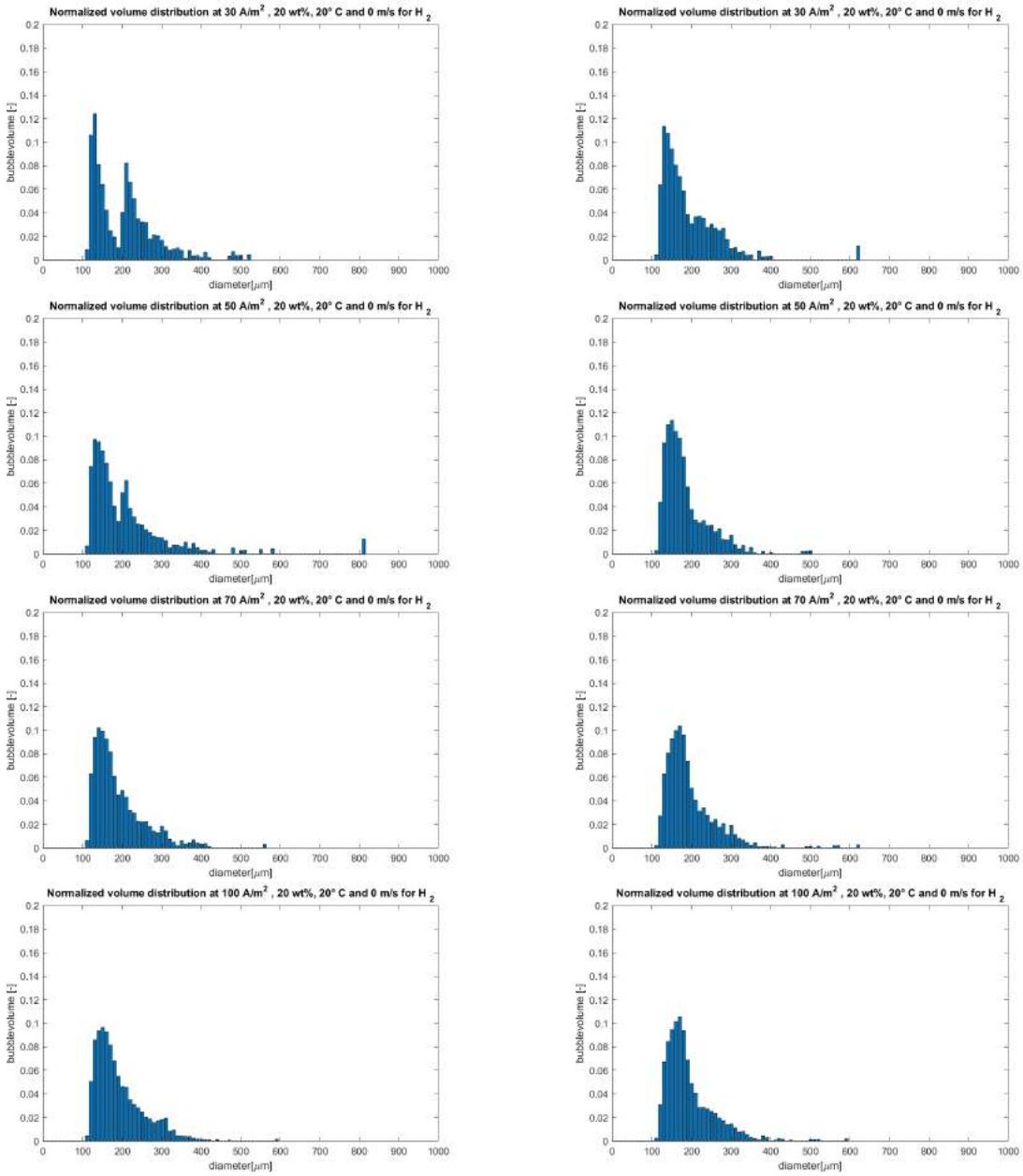

Figure M.3: *The normalized bubble size distributions over different current densities for the hydrogen bubbles at 20 °C, 20 wt% and no flow conditions in duplicate. In the left the results of Experiment 1 are shown and in the right the results of Experiment 3 are shown.*

In Figure M.4 the effect of current density on the normalized bubble size distribution of hydrogen bubbles at $50°C$, 20wt% and no flow conditions is shown in duplicate. These results are comparable to the results at $20°C$ which were shown in Figure M.3.

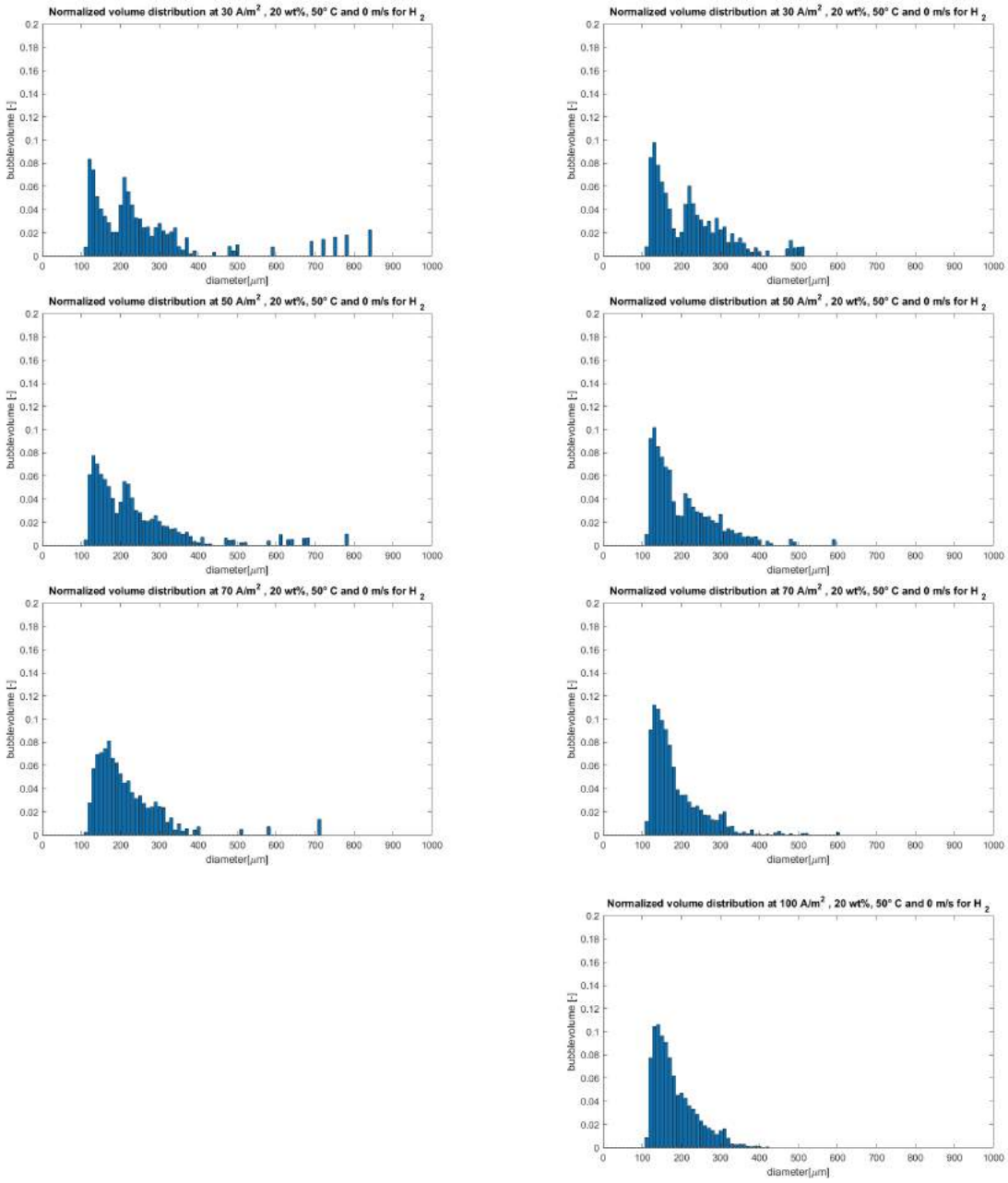

Figure M.4: *The normalized bubble size distributions over different current densities for the hydrogen bubbles at 50 °C, 20 wt% and no flow conditions in duplicate. In the left the results of Experiment 1 are shown and in the right the results of Experiment 3 are shown.*

In Figure M.5 the effect of current density on the normalized bubble size distribution of oxygen bubbles at $20°C$, 5wt% and no flow conditions is shown in duplicate. It could be noticed that the distributions of Experiment 1 are quite different form the results from Experiment 3. However, by comparing the results of Experiment 3 with the results for the hydrogen bubbles (see Figure M.1), it is noticed that the first peak is more narrow compared to the first peak of the hydrogen bubble size distributions. This is in contrast to the literature, because in literature it was also found that the hydrogen bubbles were measured more constant than the oxygen bubbles [17].

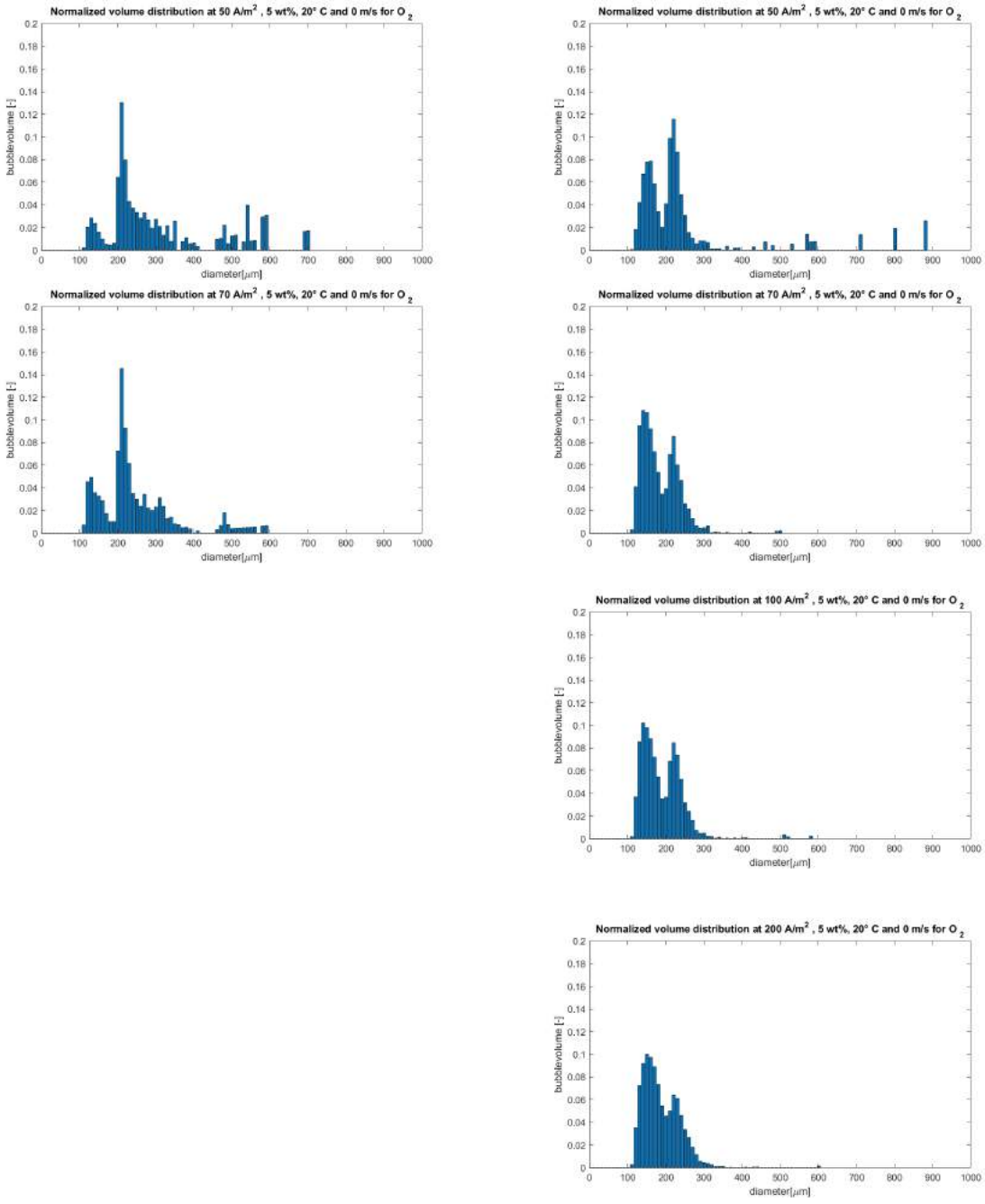

Figure M.5: *The normalized bubble size distributions over different current densities for the oxygen bubbles at 20 °C, 5 wt% and no flow conditions in duplicate. In the left the results of Experiment 1 are shown and in the right the results of Experiment 3 are shown.*

In Figure M.6 the effect of current density on the normalized bubble size distribution of oxygen bubbles at $50°C$, 5wt% and no flow conditions is shown of Experiment 1. These results are quite similar to the results of Experiment 1 at $20°C$ which were shown in Figure M.5.

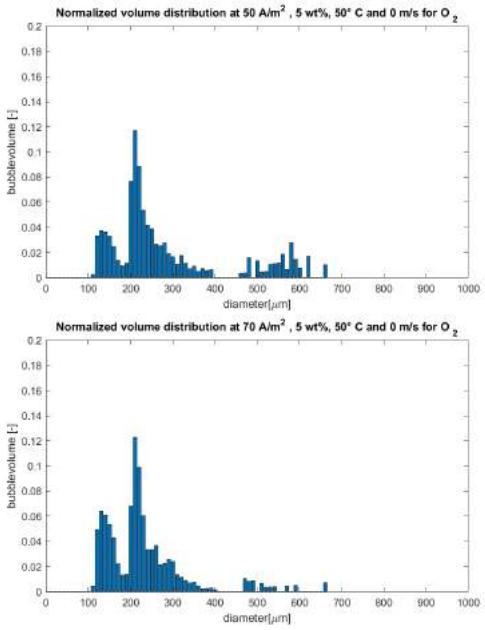

Figure M.6: *The normalized bubble size distributions over different current densities for the oxygen bubbles at 50 °C, 5 wt% and no flow conditions. The results of Experiment 1 are shown.*

In Figure M.7 the effect of current density on the normalized bubble size distribution of oxygen bubbles at $20°C$, 20 wt% and no flow conditions is shown of Experiment 1. Compared to the bubble size distributions of the hydrogen bubbles (see Figure M.3), the bubble size distribution does not become unimodal in this case, while this is happening for the hydrogen bubbles. This could come due to the difference in coalescence behavior for the hydrogen and oxygen bubbles, as found in literature [17]. Moreover, it could be note that the first peak of the hydrogen bubble bubble size distribution is wider compared with the first peak of the oxygen bubble size distribution.

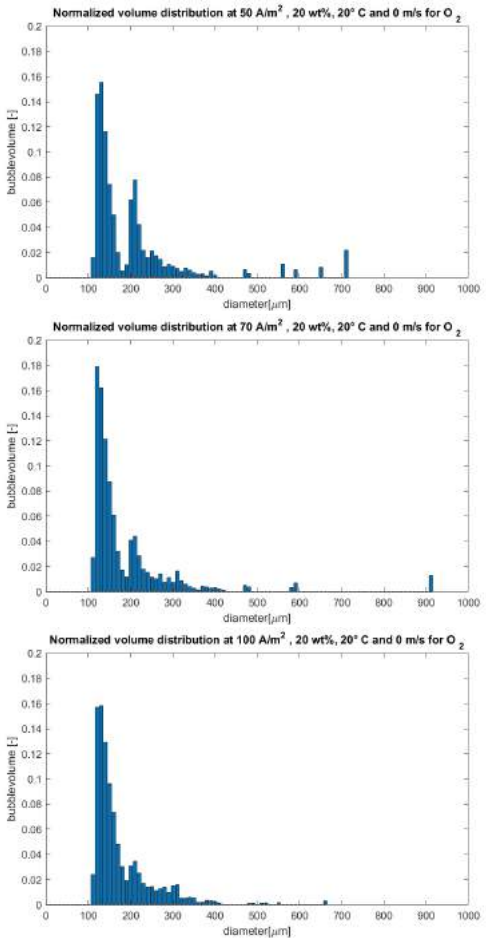

Figure M.7: *The normalized bubble size distributions over different current densities for the oxygen bubbles at 20 °C, 20 wt% and no flow conditions. The results of Experiment 1 are shown.*

In Figure M.8 the effect of current density on the normalized bubble size distribution of oxygen bubbles at $50°C$, 20 wt% and no flow conditions is shown in duplicate. It could be noticed that the first peak of Experiment 1 is sharper than the first peak of Experiment 3. However, since for the oxygen bubbles in the (already showed) results the first peak is more narrow, it is expected that the first results are more reliable. Compared to the bubble size distributions of the hydrogen bubbles (see Figure M.4, the bubble size distribution become unimodal (probably) at a current density of $100\frac{A}{m^2}$, while this is happening for the hydrogen bubbles already at $70\frac{A}{m^2}$. Again, this could come due to the difference in coalescence behavior for the hydrogen and oxygen bubbles.

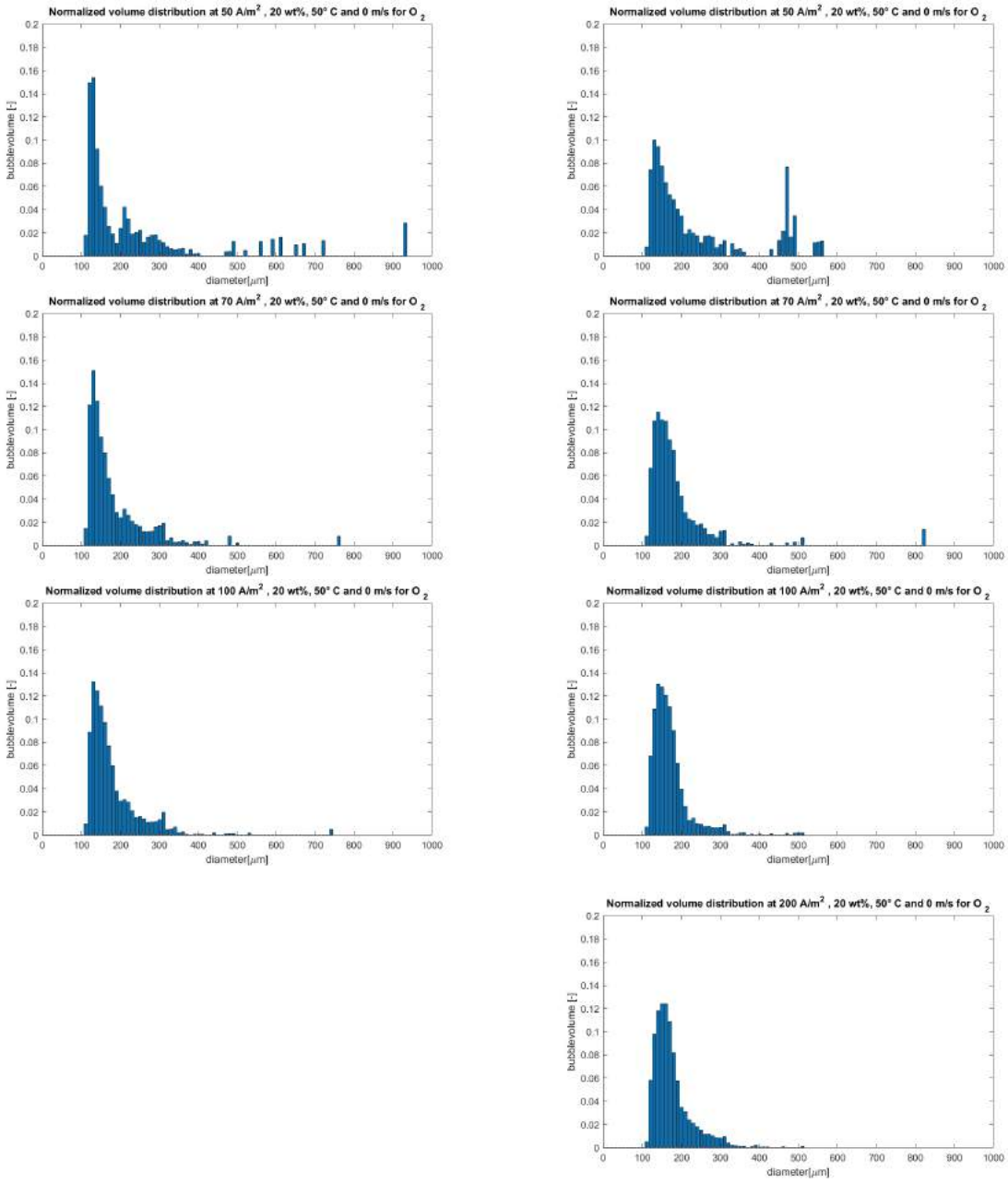

Figure M.8: *The normalized bubble size distributions over different current densities for the oxygen bubbles at 50 °C, 20 wt% and no flow conditions in duplicate. In the left the results of Experiment 1 are shown and in the right the results of Experiment 3 are shown.*

In Figure M.9 to Figure M.14 the affects of current density on the normalized bubble size distribution at a superficial inlet velocity of $0.048\frac{A}{m^2}$ are shown. It is found that these results are less reproducible compared with the no flow condition. Moreover, based on this bubble size distributions, it seems that bubbles in a flow conditions are bigger than bubbles in a no flow condition. This is contrary to the expectation. A possible explanation could be the limiting bubble detection for small bubbles. The video footage shows that there are smaller bubbles, however those cannot be measured by the MATLAB script or by hand due to the lack of resolution.

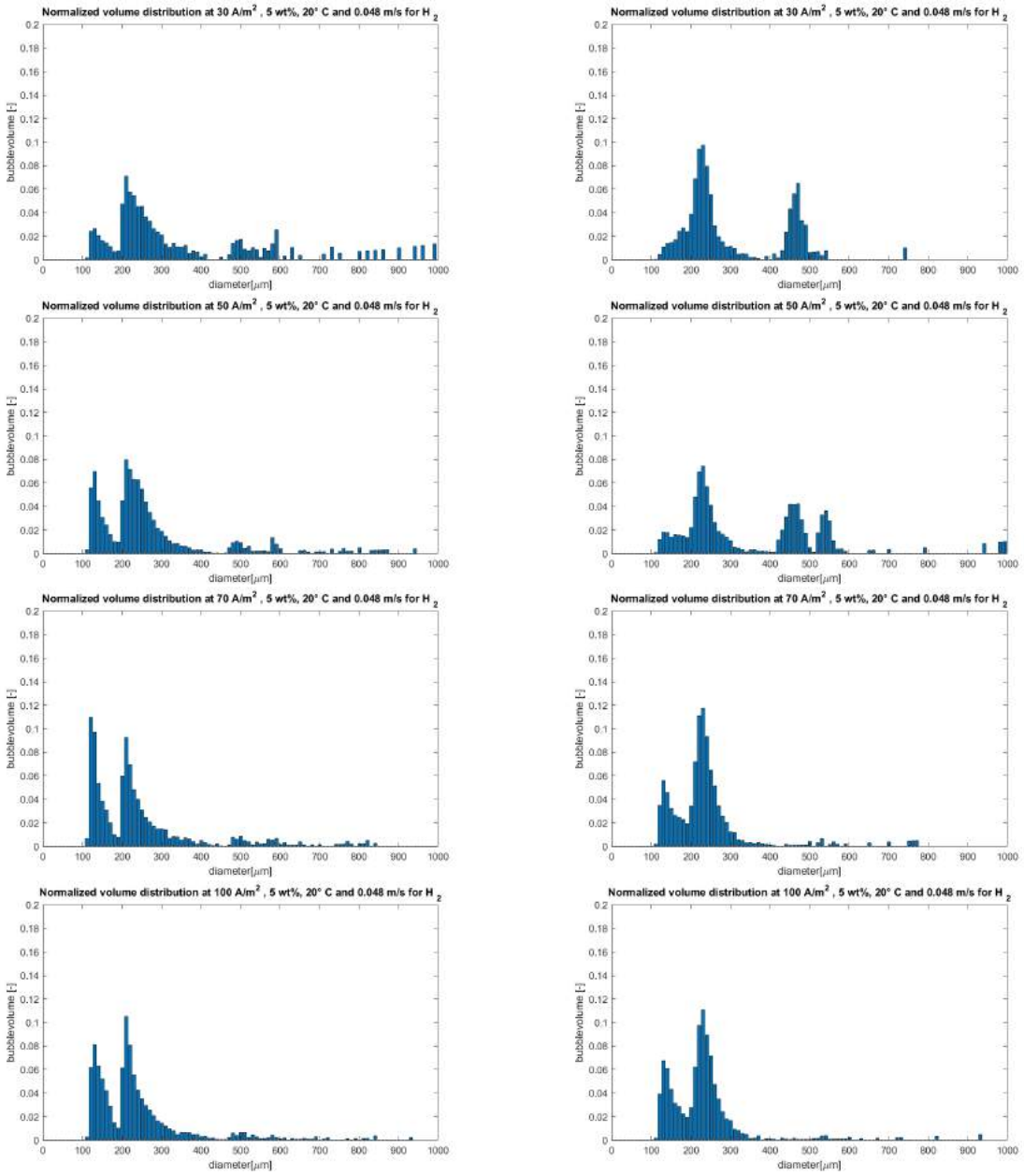

Figure M.9: *The normalized bubble size distributions over different current densities for the hydrogen bubbles at 20 °C, 5 wt% and* $0.048\frac{m}{s}$ *electrolyte flow in duplicate. In the left the results of Experiment 1 are shown and in the right the results of Experiment 3 are shown.*

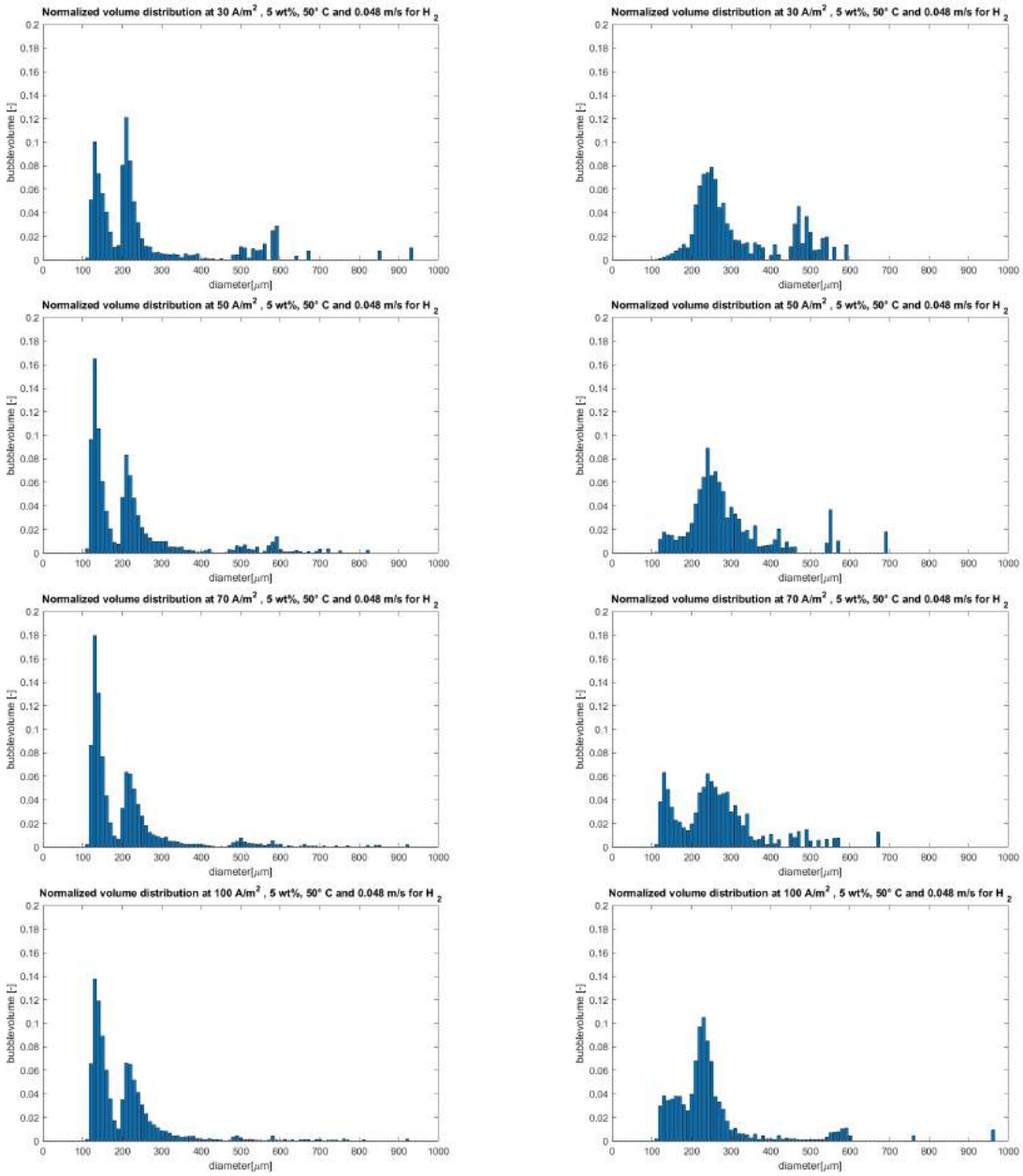

Figure M.10: *The normalized bubble size distributions over different current densities for the hydrogen bubbles at 50 °C, 5 wt% and* $0.048\frac{m}{s}$ *electrolyte flow in duplicate. In the left the results of Experiment 1 are shown and in the right the results of Experiment 3 are shown.*

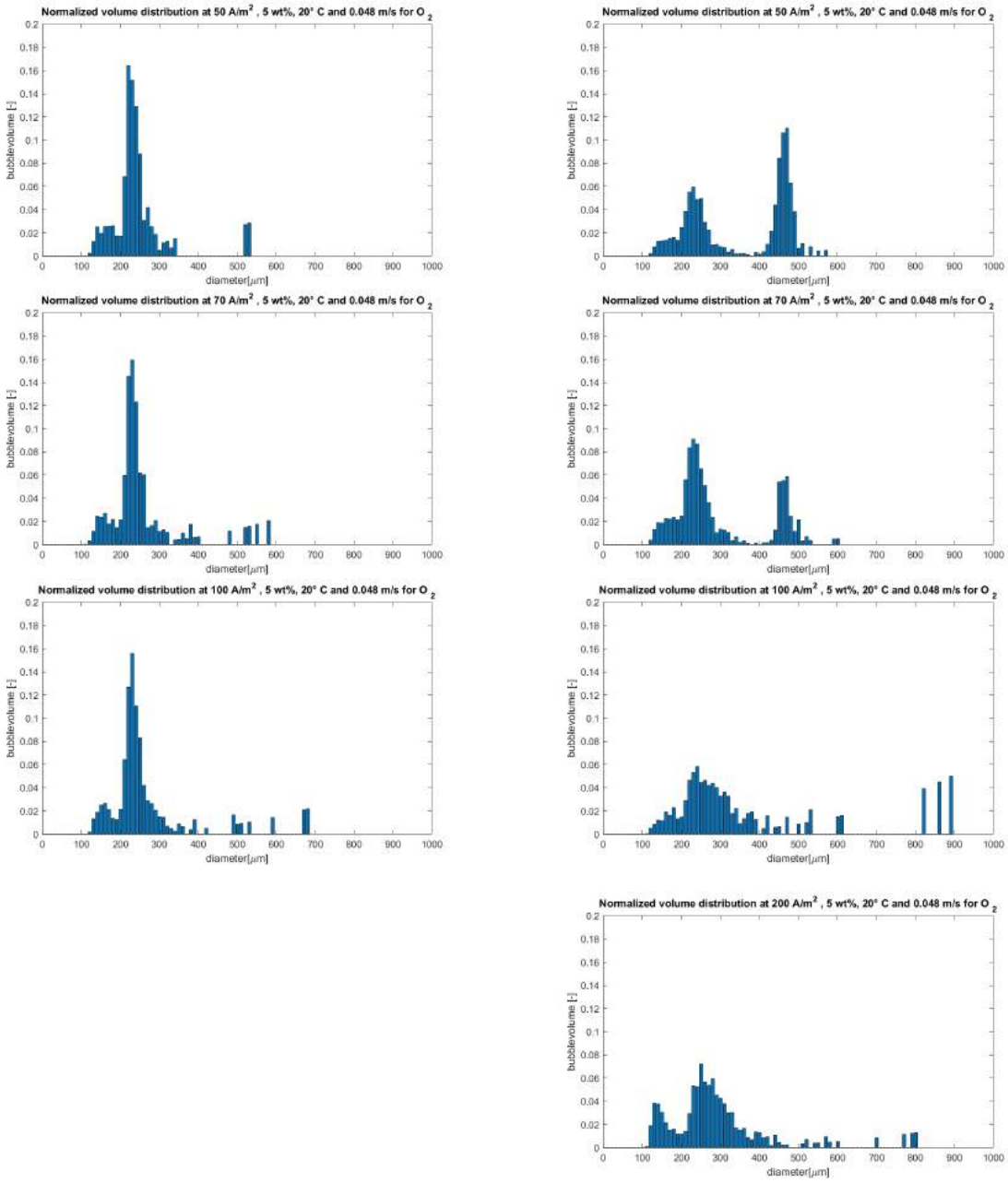

Figure M.11: *The normalized bubble size distributions over different current densities for the oxygen bubbles at 20 °C, 5 wt% and* $0.048\frac{m}{s}$ *electrolyte flow in duplicate. In the left the results of Experiment 1 are shown and in the right the results of Experiment 3 are shown.*

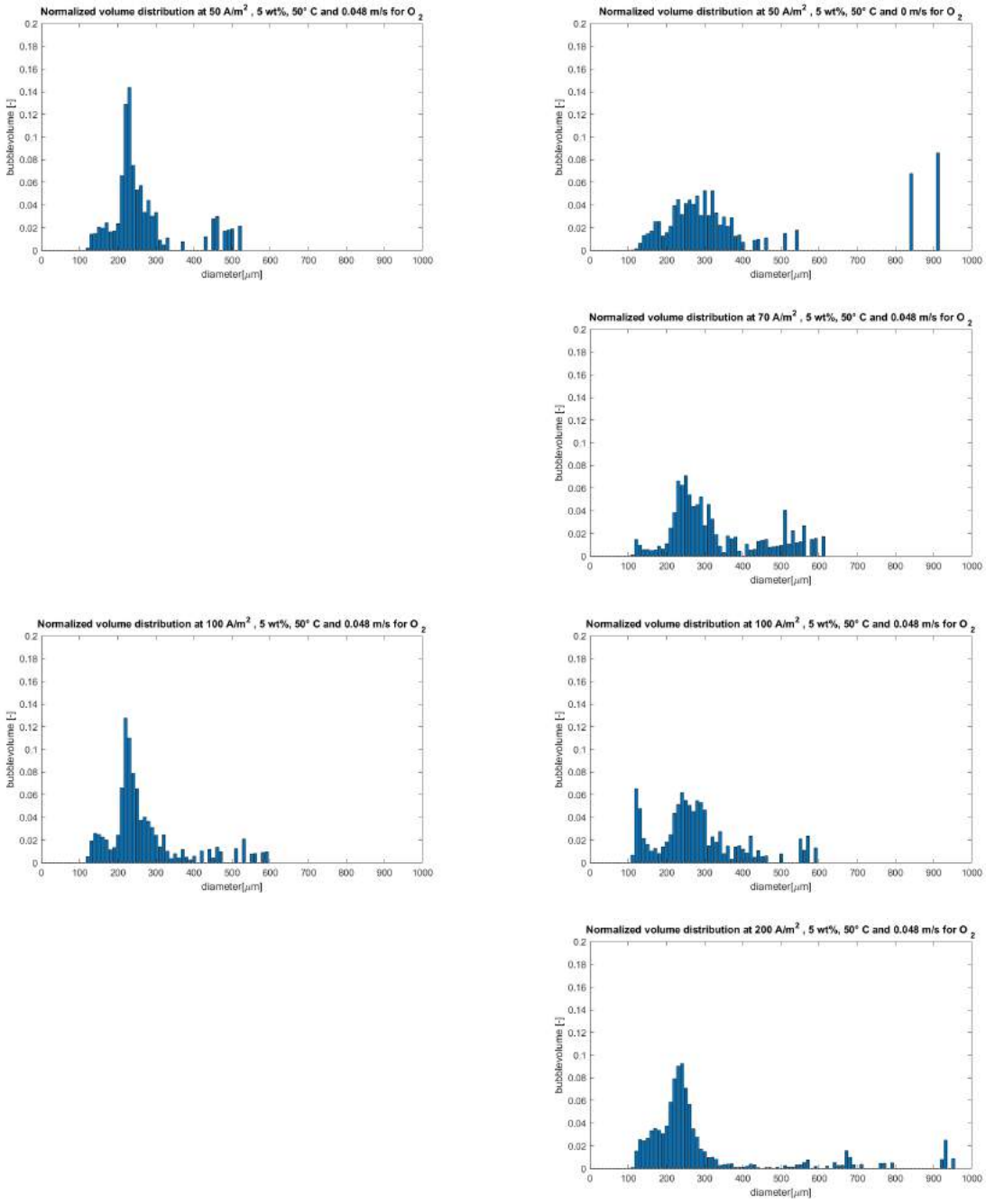

Figure M.12: *The normalized bubble size distributions over different current densities for the oxygen bubbles at 50 °C, 5 wt% and* $0.048\frac{m}{s}$ *electrolyte flow in duplicate. In the left the results of Experiment 1 are shown and in the right the results of Experiment 3 are shown.*

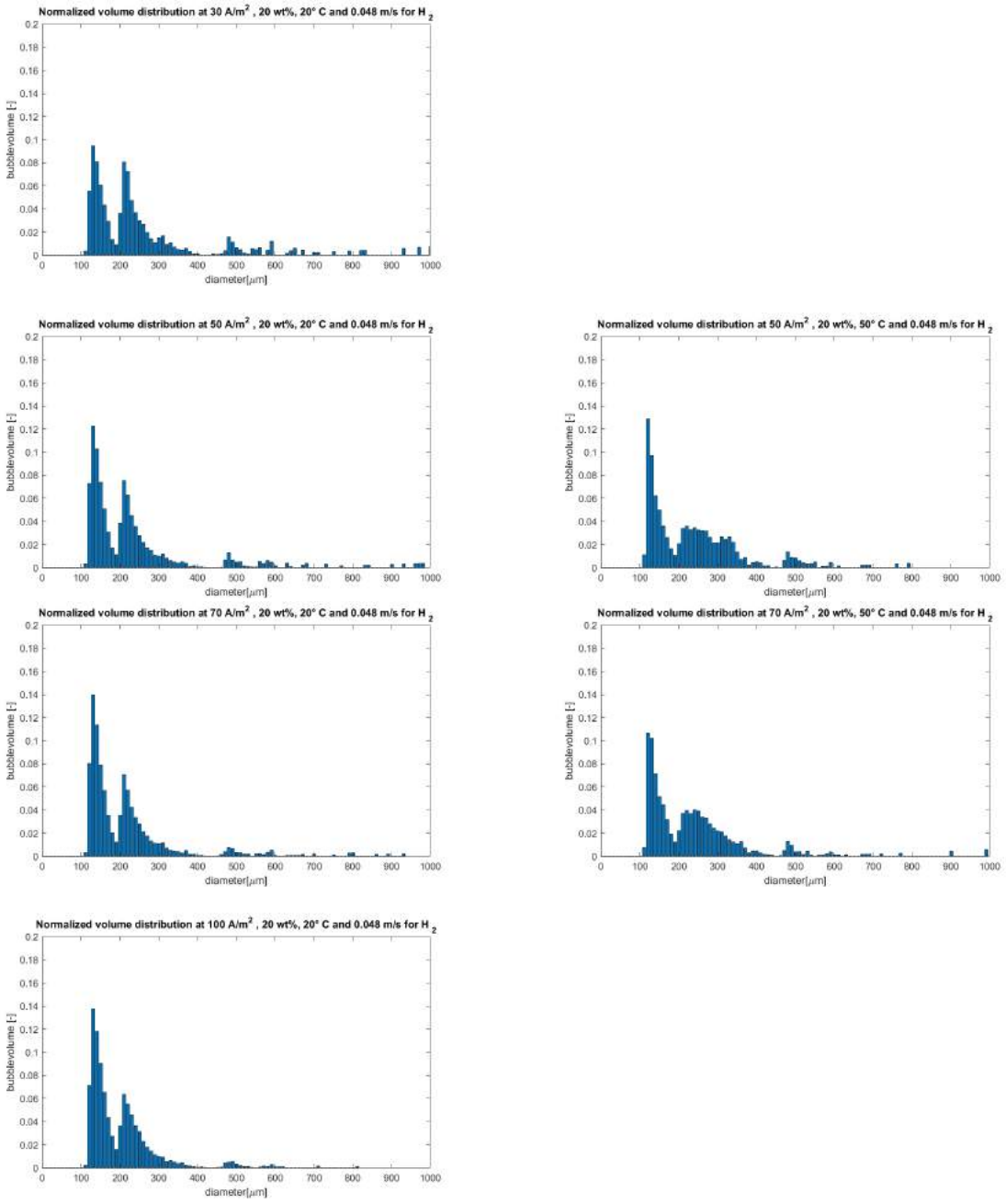

Figure M.13: *The normalized bubble size distributions over different current densities for the hydrogen bubbles at 20 wt% and* $0.048\frac{m}{s}$ *electrolyte flow. In the left the results of Experiment 1 at 20 °C are shown while in the right the results at 50 °C are shown.*

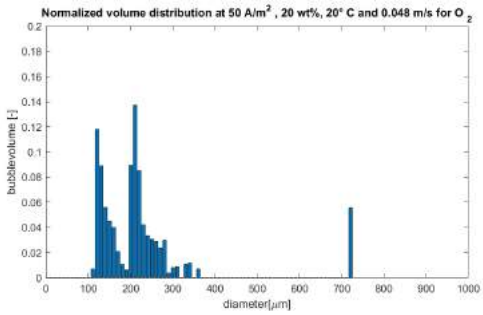

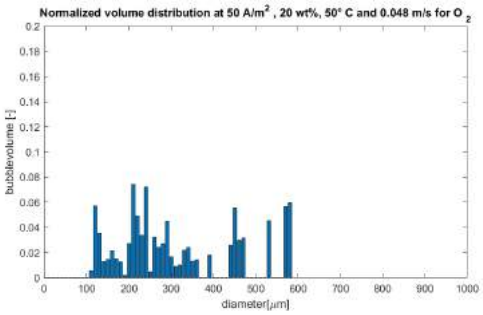

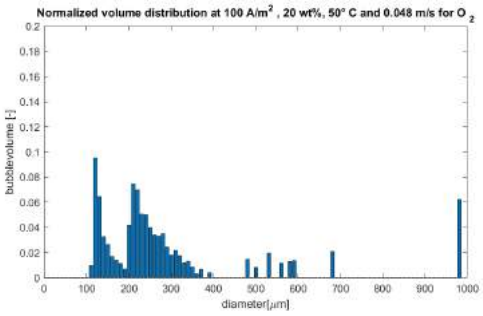

Figure M.14: *The normalized bubble size distributions over different current densities for the oxygen bubbles at 20 wt% and* $0.048\frac{m}{s}$ *electrolyte flow. In the left the results of Experiment 1 at 20 °C are shown while in the right the results at 50 °C are shown.*

N | Distribution fitting

To better describe the distribution, a Binormal and a Poisson distribution are tested. Since the bubbles with a bubble diameter larger than $400\mu m$ are not constantly measured, these are neglected with the distribution fitting.

In Figure N.1 the first peak is fitted with the Poisson distribution. The fitting seems to be good. However, the fitting of the first peak is hard since the first peak begins at $120\mu m$ and $120\mu m$ is the minimum diameter which could be measured by the MATLAB script. In the case that there are also smaller bubbles present, this Poisson distribution is not correct anymore.

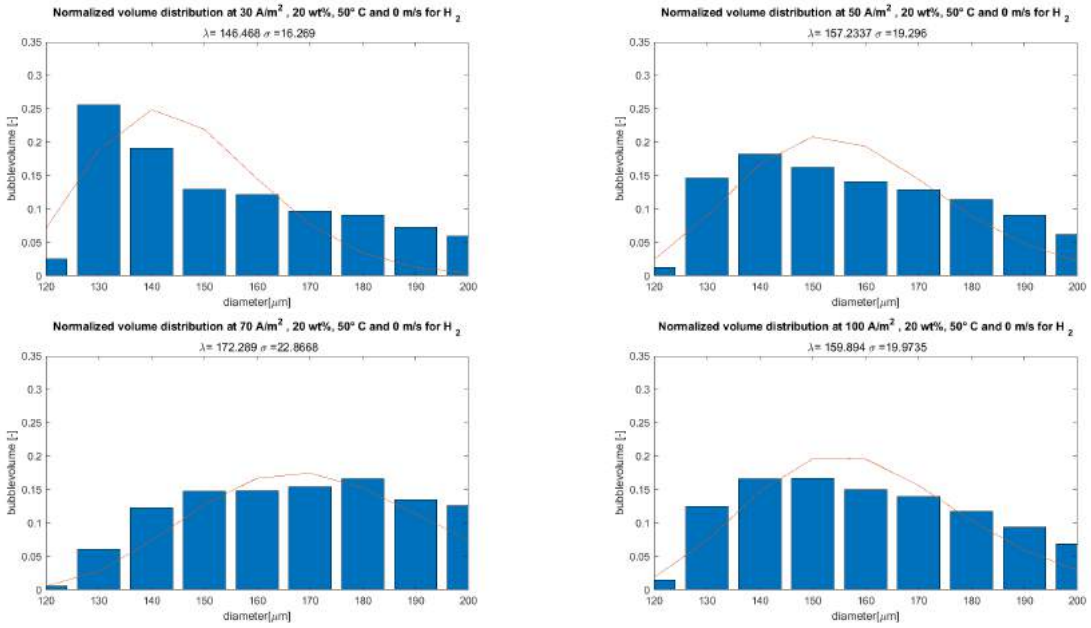

Figure N.1: *Poisson distribution fitting on the first peak for the hydrogen bubbles at different current densities.*

The Poisson distribution is also tested for the second peak, which is shown in Figure N.2. This peak does not seem to fit to the Poisson distribution, since the distribution does not cover the results of a bubble diameter higher than $300\mu m$.

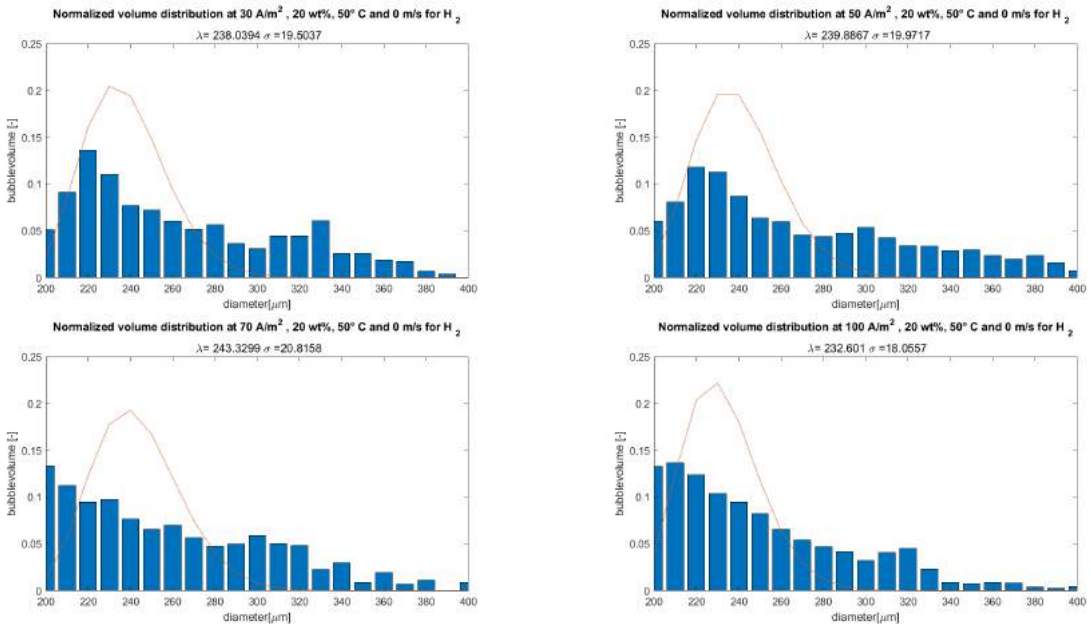

Figure N.2: *Poisson distribution fitting on the second peak for the hydrogen bubbles at different current densities.*

The Binormal distribution is also tested and shown in Figure N.3. This model covers all the bubble diameters, but does not take into account the mode value. Therefore, the binormal distribution is hard to use.

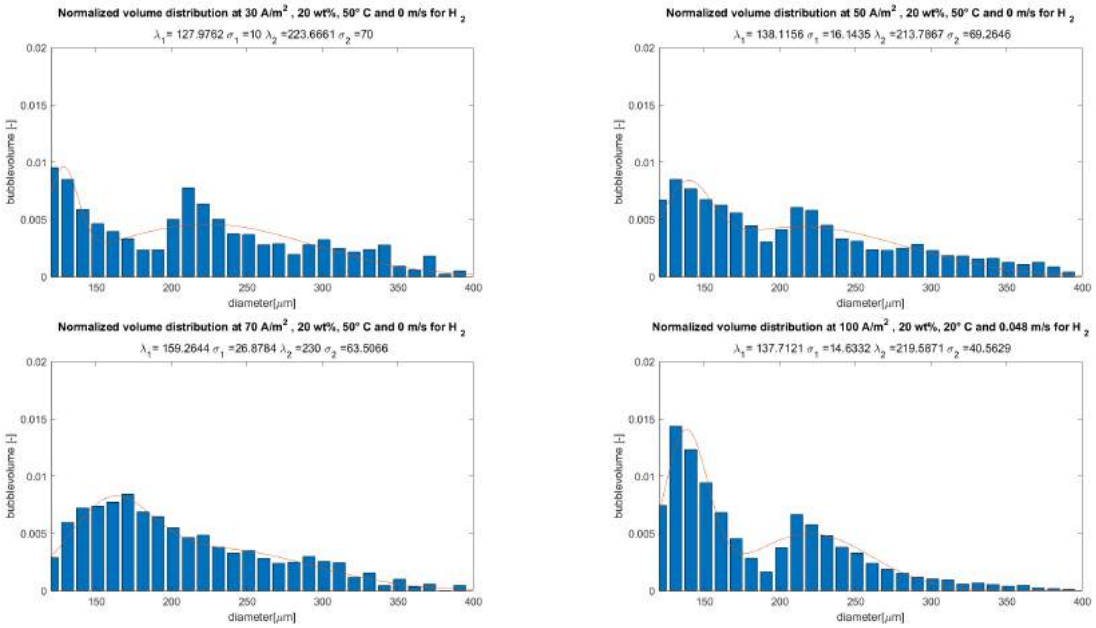

Figure N.3: *Binormal distribution fitting for the hydrogen bubbles at different current densities.*

O | Higher current densities

In this project the bubble size distribution is determined at a current density of 30 to $100\frac{A}{m^2}$ for the hydrogen bubbles and at a current density of 50 to $200\frac{A}{m^2}$ for the oxygen bubbles. At higher current density the bubble detection was poor. However, in this appendix the results are shown at a higher current density with a poor bubble detection. In Figure O.1 the normalized bubble size distribution of the hydrogen bubbles are shown. It can be noted that for the 100 and $500\frac{A}{m^2}$ a comparable distribution is found. However, for the bubble size distributions at 700 and $1000\frac{A}{m^2}$ seem to change. However, since the bubble detection is poor, no conclusion from these results could be made. Comparable results are obtained on the oxygen side (O.2).

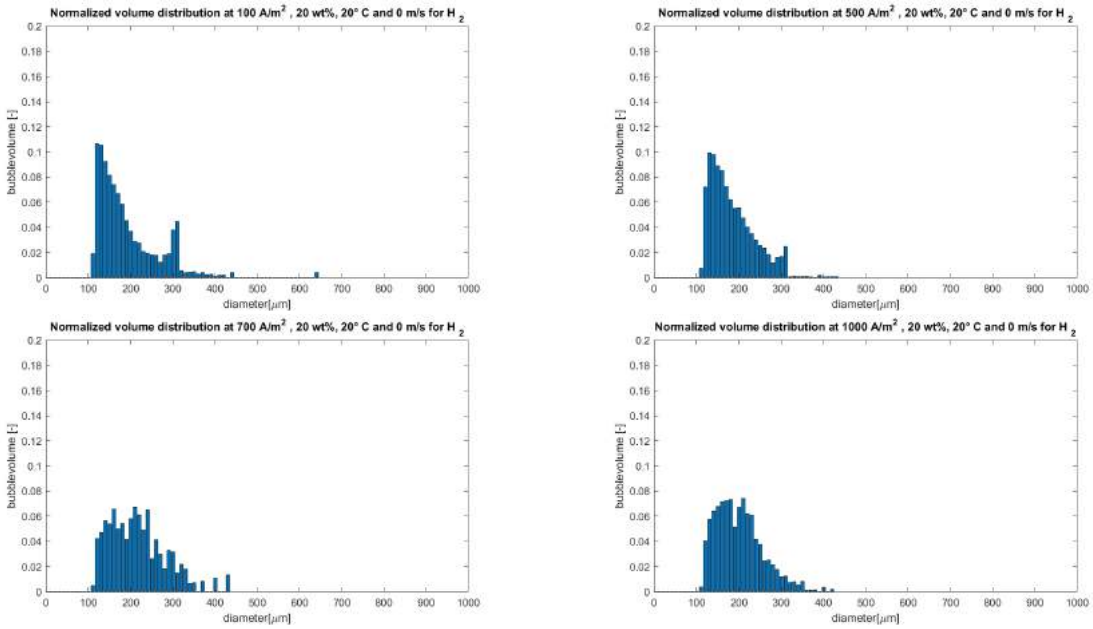

Figure O.1: *The normalized bubble size distribution at different current densities for hydrogen bubbles at 20 wt% KOH, 20 °C and no flow condition.*

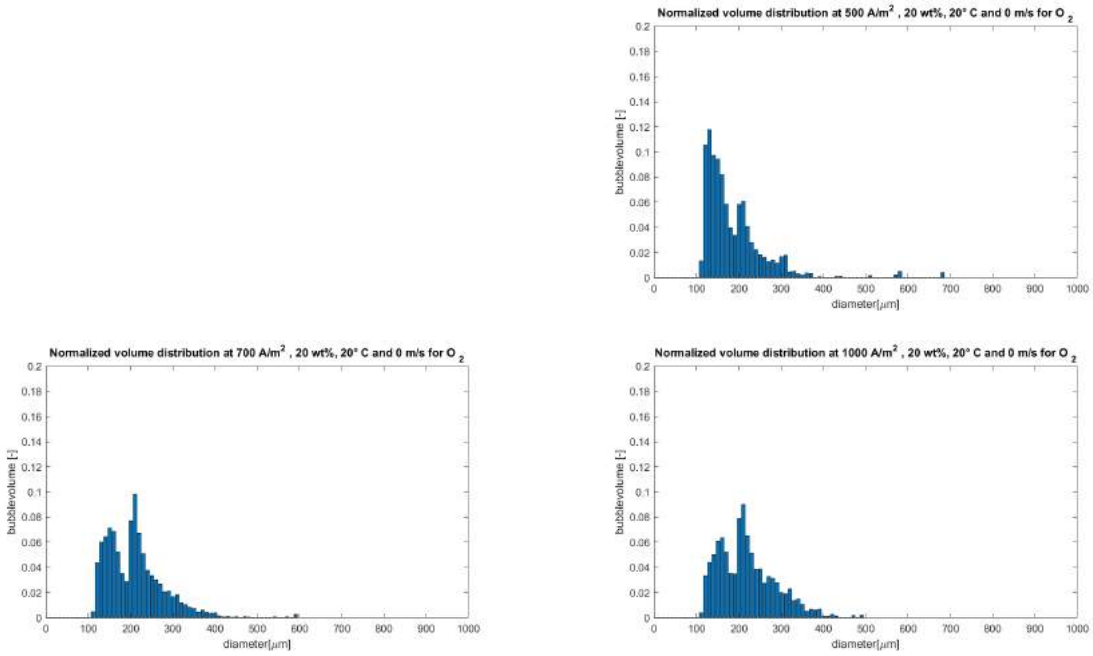

Figure O.2: *The normalized bubble size distribution at different current densities for oxygen bubbles at 20 wt% KOH, 20 °C and no flow condition.*

P | Bubble rising velocity

The theoretical bubble rising velocity is compared with the experimental bubble rising velocity (see Figure P.1 and Figure P.2). It is found that the theoretical rising velocity matches relatively well with the experimental rising velocity.

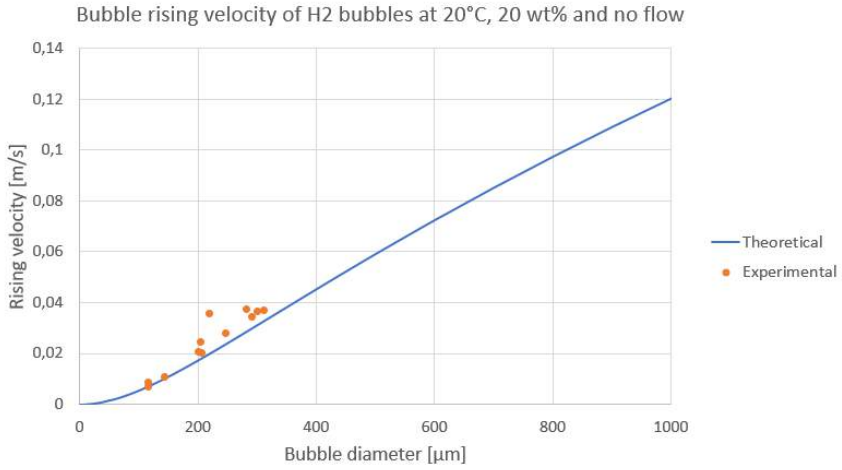

Figure P.1: *The theoretical bubble rising velocity compared to the experimental rising velocity at 20 °C, 20 wt% and no flow condition.*

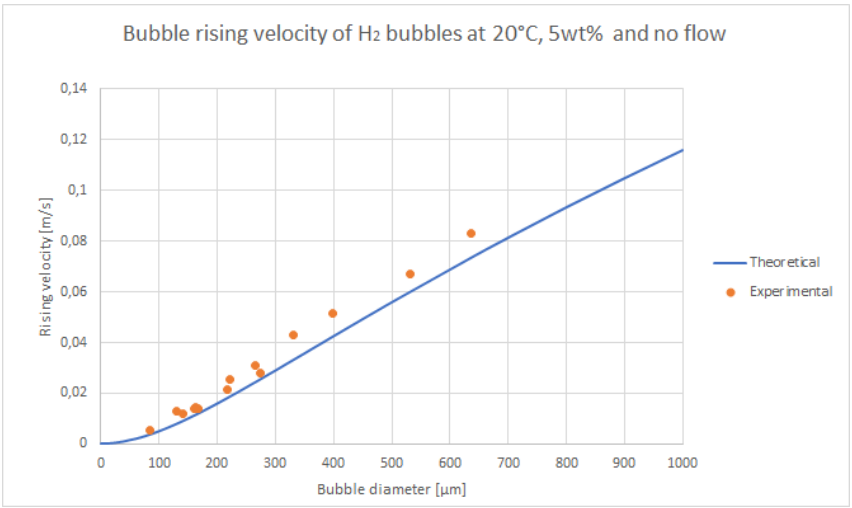

Figure P.2: *The theoretical bubble rising velocity compared to the experimental rising velocity at 20 °C, 5 wt% and no flow condition.*

Q Influence of the outlet device on the bubble size distribution.

The bubble size distribution is measured before and after the barrier of the outlet device. In this appendix the effect is shown on the barrier at the outlet device on the normalized bubble size distribution (Figure Q.1). It is found that more gas volume between 120 and 200μm are measured before compared to after the barrier of the outlet device.

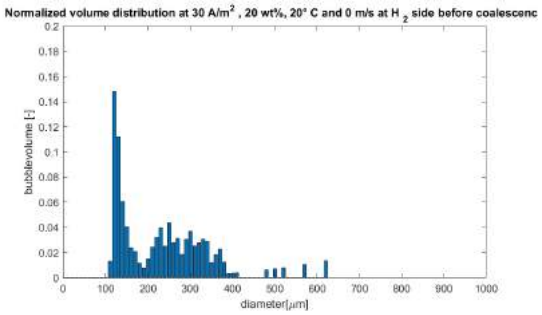

(a) *Before the outlet device*

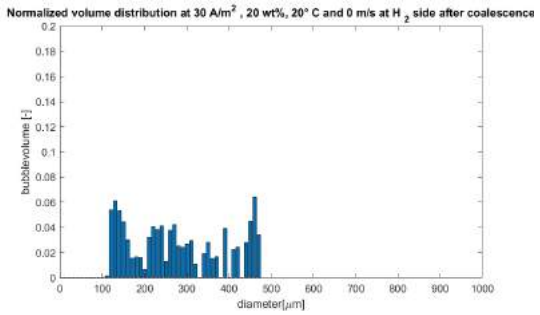

(b) *After the outlet device*

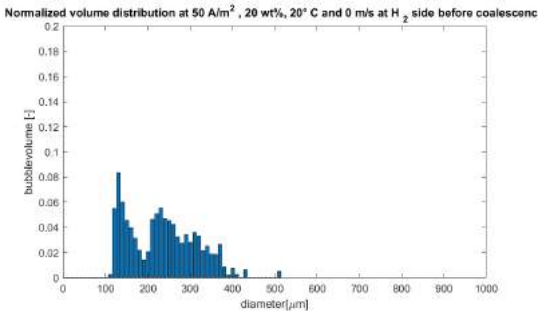

(c) Before the outlet device

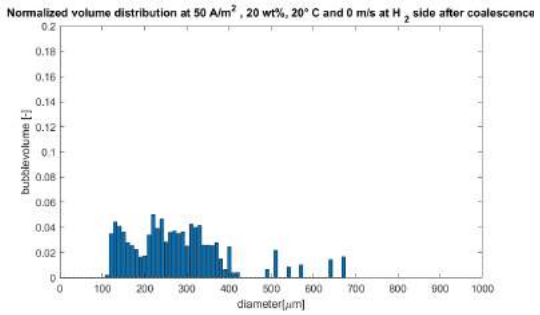

(d) After the outlet device

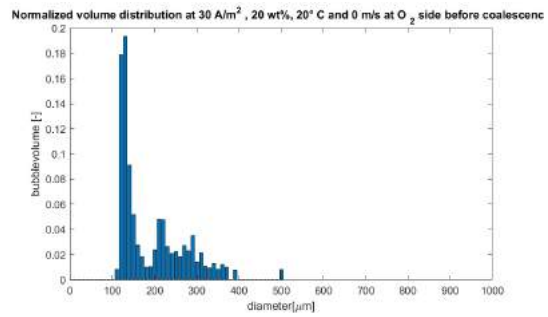

(e) Before the outlet device

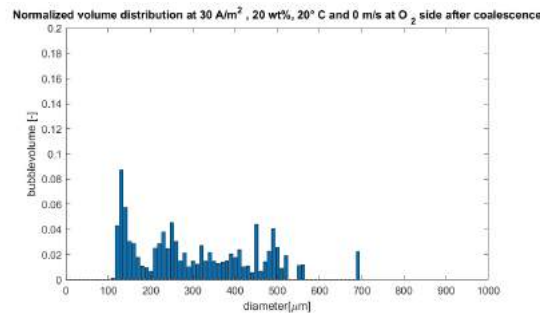

(f) After the outlet device

Figure Q.1: *Effect of barrier in the outlet device on the bubble size distribution. (a) to (d) are for the hydrogen bubbles while (e) to (h) are for the oxygen bubbles.* Continued on next page

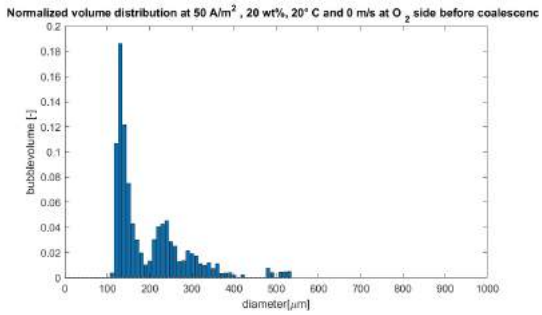

(g) Before the outlet device

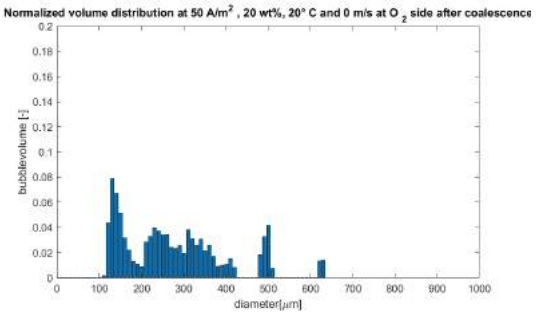

(h) After the outlet device

Figure Q.1: *Effect of barrier in the outlet device on the bubble size distribution. (a) to (d) are for the hydrogen bubbles while (e) to (h) are for the oxygen bubbles.*